Abstract

This thesis describes the newly established techniques for measuring the effective longitudinal piezoelectric coefficient $d_{33}^{'}$ and effective transverse piezoelectric coefficient $e_{31,f}$ of sol-gel derived lead zirconate titanate (PZT) ceramic films. The effects of excess lead, annealing temperature, poling field and poling time on the piezoelectric properties of the PZT films have been studied. The depolarization phenomenon of films has been investigated and explained based on the concept of the Preisach model.

Sol-gel derived PZT films of thickness 1 μm and 2 μm were deposited on Pt/Ti/SiO_2/Si substrates by the multiple-spin-coating technique. The films were dense, crack-free, and well crystallized having single perovskite phase and nontextured polycrystalline structure.

The newly established techniques for measuring $d_{33}^{'}$ and $e_{31,f}$ were based on the converse and direct piezoelectric effects, respectively. For the $d_{33}^{'}$ measurement, the single beam laser interferometry technique was employed, and the substrate bending was effectively suppressed by gluing the substrate on a large and rigid platform with mounting wax. For the $e_{31,f}$ measurement, a new cantilever deflection technique was applied. A rectangular sample (film/substrate) was bent dynamically in such a way that a longitudinal strain was generated along the length of the sample and an ac current was induced on the surface. Both the $d_{33}^{'}$ and $e_{31,f}$ measurements were verified to be free from systematic errors, and the corresponding uncertainties were about 7% and 10%, respectively.

The effects of excess lead, annealing temperature, poling field and poling time on the observed $d_{33}^{'}$ and $e_{31,f}$ values of PZT films were then investigated. The optimum amount of excess lead and optimum annealing temperature for preparing PZT films with the best piezoelectric properties were 10% and 650°C, respectively. The poling time required for switching the domain was very fast, less than 20 seconds, and was almost

independent of the poling field. The PZT films of different thicknesses had almost the same (saturated) values of $d_{33}^{'}$ and $e_{31,f}$, but the required poling field for the 1-μm film was larger than that for the 2-μm film (16 MV/m vs 10 MV/m). A fully polarized PZT film with 10% excess lead and annealed at 650°C for 1 hour had the observed $d_{33}^{'}$ and $e_{31,f}$ values of 90 pm/V and 8.8 C/m^2, respectively.

A polarized PZT film was completely depolarized by the application of ac fields of diminishing amplitude. The amplitude of the ac fields was decreased from 19.5 MV/m to 0.2 MV/m in 8 steps. The observed $d_{33}^{'}$ and $e_{31,f}$ values of the film decreased after each step, and ended up with almost the same values as an as-deposited film. This depolarization phenomenon was explained based on the concept of the Preisach model. The results also revealed that there existed a distribution of coercive fields in the Preisach dipolar units (micro-domains), and that, because of the interaction field between the dipolar units, the magnitudes of the switch-up and switch-down fields of each dipolar unit were not necessarily the same.

Acknowledgement

I would like to take this opportunity to express my appreciation to my supervisors Dr. K. W. Kwok and Prof. H. L. W. Chan for their excellent guidance and constant encouragement during these two years. I would like to thank Prof. C. L. Choy for his invaluable suggestions in my work.

I would like to thank Mr. S. U. Adikary, Mr. C. P. Chong, Mr. K. H. Lam, Miss S. T. Lau, Mr. K. Li, Mr. Y. T. Or, Mr. K. W. Tang and Dr. B. Wang in the Department of Applied Physics for discussions, suggestions and technical supports during my work and the preparation of this thesis.

I gratefully acknowledge the technical support provided by the Material Research Centre (MRC) of the Hong Kong Polytechnic University. The last but not least, I would like to thank my parents for their understanding and constant support.

List of Figures

List of Tables

Table of Contents

Chapter One

Introduction

1.1 Background

The piezoelectric effect was discovered by Pierre Curie and Jacques Curie in 1880 [Jaffe and Cook, 1971, p. 1]. The piezoelectric effect or piezoelectricity is an interaction between the electrical and mechanical systems. The (direct) piezoelectric effect is manifested by the change of the electric polarization under the application of a mechanical stress, and is quantified with a piezoelectric coefficient d_{ip}^{E} which is defined as [Damjanovic, 1998]

$$d_{ip}^{E} = \left.\frac{\partial D_i}{\partial T_p}\right|_{E} \tag{1.1}$$

where D is the electric displacement, E is the electric field and T is the stress, $i = 1, 2, 3$ and $p = 1, 2, \ldots, 6$. In 1881, a year after the discovery of the direct piezoelectric effect, Lippmann predicted the existence of the converse effect from a thermodynamic approach [Ikeda, 1990, p. 1]. The converse piezoelectric effect is manifested by the induction of the strain under the application of an electric field, and is quantified with a piezoelectric coefficient d_{pi}^{T} which is defined as [Damjanovic, 1998]

$$d_{pi}^{T} = \left.\frac{\partial S_p}{\partial E_i}\right|_{T} \tag{1.2}$$

where E is the electric field, T is the stress, S is the elastic strain, $i = 1, 2, 3$ and $p = 1, 2, \ldots,$

6. It was also shown that the piezoelectric coefficients d_{ip}^{E} and d_{pi}^{T} were thermodynamically identical [Ikeda, 1990, p. 1; Damjanovic, 1998], i.e.

$$d_{ip}^{E} = d_{pi}^{T} \tag{1.3}$$

Before the end of the same year, the Curie brothers verified the prediction of Lippmann and also showed that the piezoelectric coefficients d_{ip}^{E} and d_{pi}^{T} of quartz had the same value [Ikeda, 1990, p. 1].

Rochelle salt was the firstly reported crystal exhibiting piezoelectric property, as found by Pockels in Göttingen in 1894 [Jaffe and Cook, 1971]. Then, a number of piezoelectric materials had been discovered. Around 1943, anomalous dielectric properties of barium titanate ($BaTiO_3$) were reported at almost the same time by Wainer and Salmon in the United States [Wainer *et al.*, 1942 and 1943], by Wul and Goldman in Russia [Wul and Goldman, 1945], and by Miyake in Japan [Miyake, 1946]. The crystal was identified as a piezoelectric material later in the subsequent years. In early 1950's, another important piezoelectric material, lead zirconate titanate (PZT), was discovered [Jaffe *et al.*, 1954].

A number of ceramics have been categorized into the perovskite family, such as barium titanate ($BaTiO_3$), lead titanate ($PbTiO_3$) and lead zirconate titanate ($Pb(Zr,Ti)O_3$). The perovskite structure ABO_3 of a large cation (A) on the corners, a small cation (B) in the body centre, and oxygen in the centre of the faces (Figure 1.1) [Damjanovic, 1998]. Most of these materials undergo a structural phase transition from a high-temperature non-ferroelectric (or paraelectric) phase into a low-temperature ferroelectric phase, which

exhibits hysteresis behavior of polarization under influence of electric field. This transition temperature is defined as Curie point, T_C [Lines *et al.*, 1979]. These materials have cubic structure in paraelectric phase and tetragonal structure in ferroelectric phase (Figure 1.1). However, not all the ceramics with the perovskite structure are ferroelectric, for example, lead zirconate ($PbZrO_3$) and lead hafnate ($PbHfO_3$) are anti-ferroelectric.

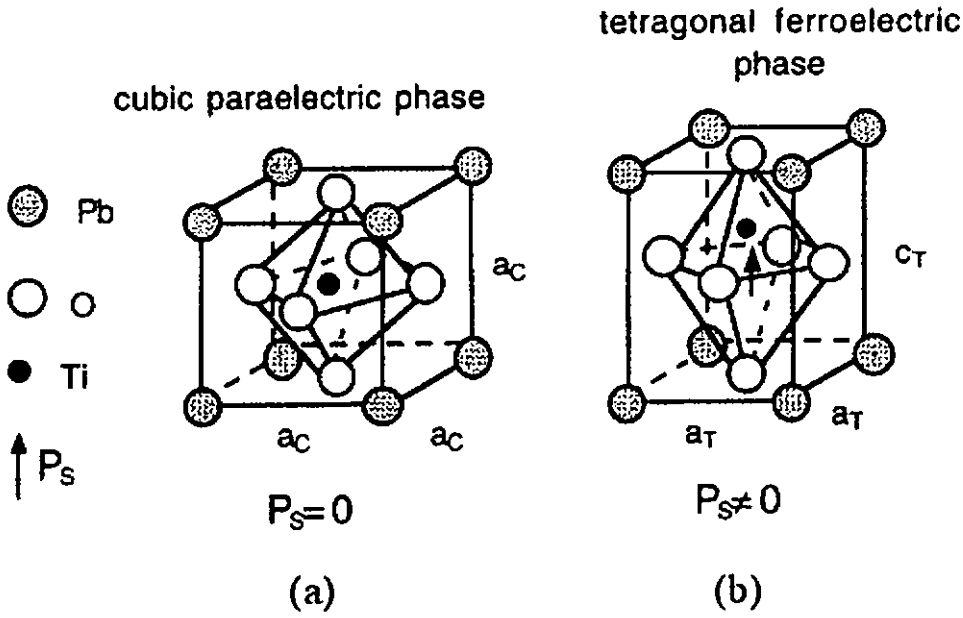

Fig. 1.1 The perovskite structure ABO, showed a cubic structure in paraelectric phase (a) and a tetragonal structure in ferroelectric phase (b) [Damjanovic, 1998].

Nowadays, piezoelectric ceramics have been widely used in a number of applications, such as piezoelectric transformers, piezoelectric lighters, acoustic emission detectors, and medical ultrasonic transducers. The properties, especially the piezoelectric properties, of the active materials play an important role in the design of devices. Miniaturization is the important trend of the modern devices, of which the size is usually in micron or even in sub-micron range. Therefore, property characterization of the

piezoelectric materials in the thin film form becomes important and has attracted an increasing interest.

1.2 Piezoelectric Ceramic Thin Films

1.2.1 Piezoelectric Coefficients

Since the piezoelectric coefficients for the direct piezoelectric effect and the converse piezoelectric effect are thermodynamically identical (Equation 1.3), d_{pi} is usually used to denote the piezoelectric coefficient for both the direct and converse piezoelectric effects. Practically, the piezoelectric samples are polarized along their thickness direction which is denoted as $\hat{3}$. The longitudinal piezoelectric coefficient d_{33} is then a measure of the electric displacement induced along $\hat{3}$ direction by the application of an external stress along the same direction (direct effect), or is a measure of the strain induced along $\hat{3}$ direction by the application of an electric field along the same direction (converse effect). Similarly, the transverse piezoelectric coefficient d_{31} is a measure of the electric displacement induced along $\hat{3}$ direction by the application of an external stress along $\hat{1}$ direction, or is a measure of the strain induced along $\hat{1}$ direction by the application of an electric field along $\hat{3}$ direction.

Besides the longitudinal piezoelectric coefficient d_{33} and transverse piezoelectric coefficient d_{31}, the piezoelectric (voltage) coefficient g_{33} is another useful parameter, which is defined as the ratio of the electric field induced across the sample, i.e. along $\hat{3}$

direction, to the external stress applied along the same direction. g_{33} is related to d_{33} by the dielectric constant ε_r ($g_{33} \sim d_{33}/\varepsilon_o\varepsilon_r$, where ε_o is the permittivity of free space). Different material properties are considered in designing various micro-electromechanical systems (MEMS). Ferroelectric materials with large d_{33} value is desirable for applications involving motion or vibration, e.g. actuators and piezoelectric motors; while materials with large g_{33} value is usually used for applications involving response to mechanical stress, e.g. acoustic emission detectors and hydrophones. As shown in Table 1.1, PZT ceramic with a Zr/Ti mole ratio of 52/48 has the largest piezoelectric coefficient and piezoelectric (voltage) coefficient as compared with $BaTiO_3$ and $PbTiO_3$. For this reason, PZT is the most commonly used material for MEMS applications.

Table 1.1 Piezoelectric coefficient and piezoelectric (voltage) coefficient of $BaTiO_3$, $PbTiO_3$ and $Pb(Zr_{0.52}Ti_{0.48})O_3$.

Properties	**$BaTiO_3$** [Xu, 1991, p. 107]	**$PbTiO_3$** [Xu, 1991, p. 108]	**$Pb(Zr_{0.52}Ti_{0.48})O_3$** [Jaffe and Cook, 1971, p. 146]
d_{33} (pC/N)	190	56	223
d_{31} (pC/N)	-79	-6.8	-93.5
g_{33} (10^{-3}Vm/N)	11.4	33	34.5

1.2.2 Lead Zirconate Titanate (PZT) Ceramics

Lead zirconate titanate (PZT) ceramics have attracted considerable research interest because of their good piezoelectric properties. In 1954, excellent piezoelectric performance was found in a PZT ceramic with a Zr/Ti mole ratio of about 55/45 by Bernard Jaffe [Jaffe, 1955]. After this important discovery, a large number of works had been carried out to study this material.

PZT or $Pb(Zr_{1-x}Ti_x)O_3$ is a solid solution of ferroelectric lead titanate ($PbTiO_3$) and antiferroelectric lead zirconate ($PbZrO_3$), as shown in Figure 1.2. PZT belongs to the perovskite family, with Pb located at the A-site of the perovskite structure ABO_3 (Figure 1.1) and Zr and Ti randomly distributed over the B-site. At high temperatures, $Pb(Zr_{1-x}Ti_x)O_3$ (for all x) has a cubic structure and is in paraelectric phase. As temperature decreases, titanium-rich PZT ($x > 0.47$) transforms into a tetragonal structure, while zirconate-rich PZT ($x < 0.05$) transforms into an orthorhombic structure. For PZT with $0.05 < x < 0.47$, the phase transformation is more complex. As temperature decreases, the structure transforms to a high-temperature rhombohedral structure and then becomes a low-temperature rhombohedral structure around room temperature. Both the tetragonal and rhombohedral structures are ferroelectric. The boundary separating the tetragonal and rhombohedral phases is called morphotropic phase boundary (MPB), which is near the Zr/Ti ratio of 52/48 at room temperature, as shown in Figure 1.2.

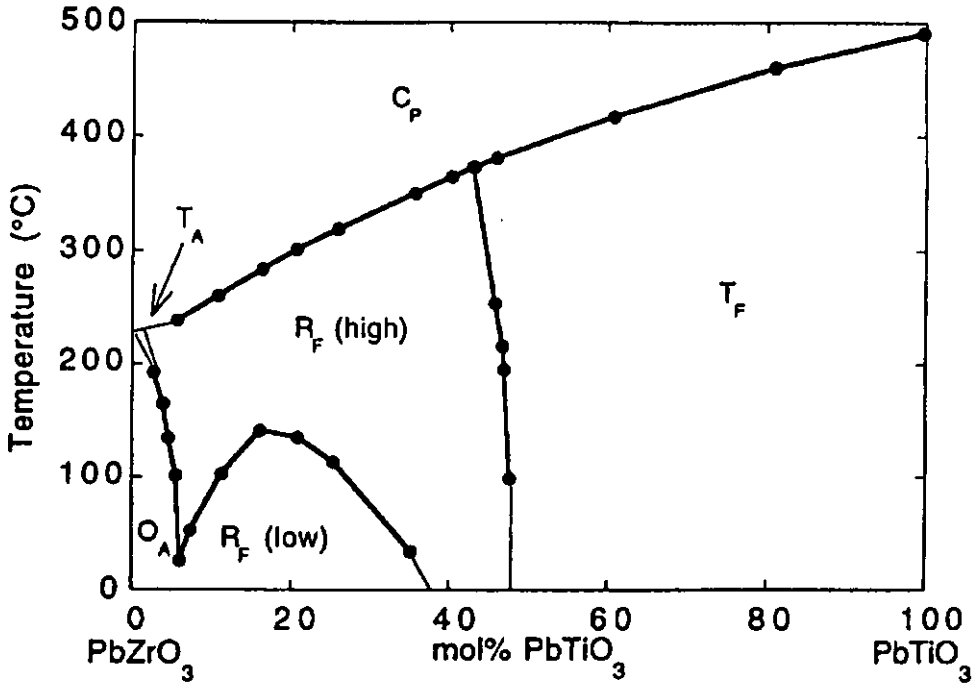

Fig. 1.2 Phase diagram of $Pb(Zr_{1-x}Ti_x)O_3$ solid solution showing the morphotropic phase boundary in the middle of the diagram which separates the tetragonal and rhombohedral ferroelectric phases. C, T, R and O denote the cubic, tetragonal, rhombohedral and orthorhombic phases, respectively, while the subscripts A and F denote the antiferroelectric and ferroelectric phases, respectively [Jaffe and Cook, 1971, p. 136].

It has been shown that PZT ceramics with compositions near the morphotropic phase boundary have the largest piezoelectric coefficients, remanent polarization, electromechanical coupling factor and dielectric constant (Figures 1.3 – 1.5). For example, the d_{33} and $-d_{31}$ values of a PZT ceramic with composition at the MPB are about 200 pC/N and 100 pC/N, respectively (Figure 1.3).

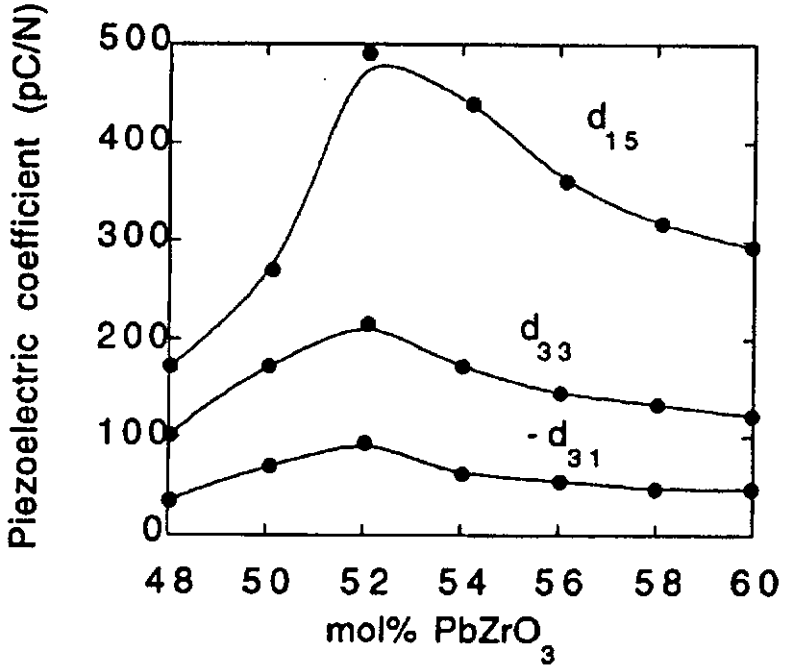

Fig. 1.3 Variations of the piezoelectric coefficient d_{ij} with composition of PZT near the morphotropic phase boundary [Jaffe and Cook, 1971, p. 143].

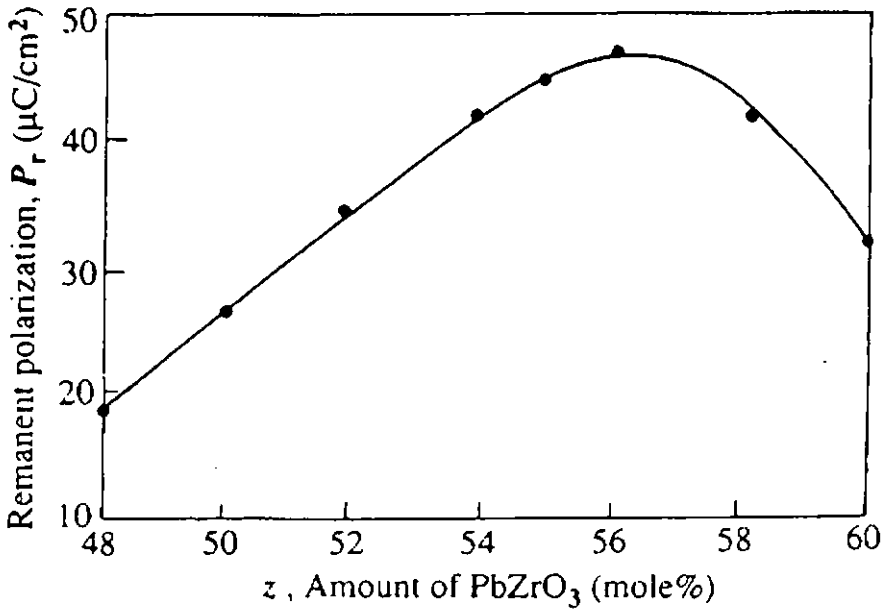

Fig. 1.4 Variation of the remanent polarization P_r with composition of PZT near the morphotropic phase boundary [Jaffe and Cook, 1971, p. 147].

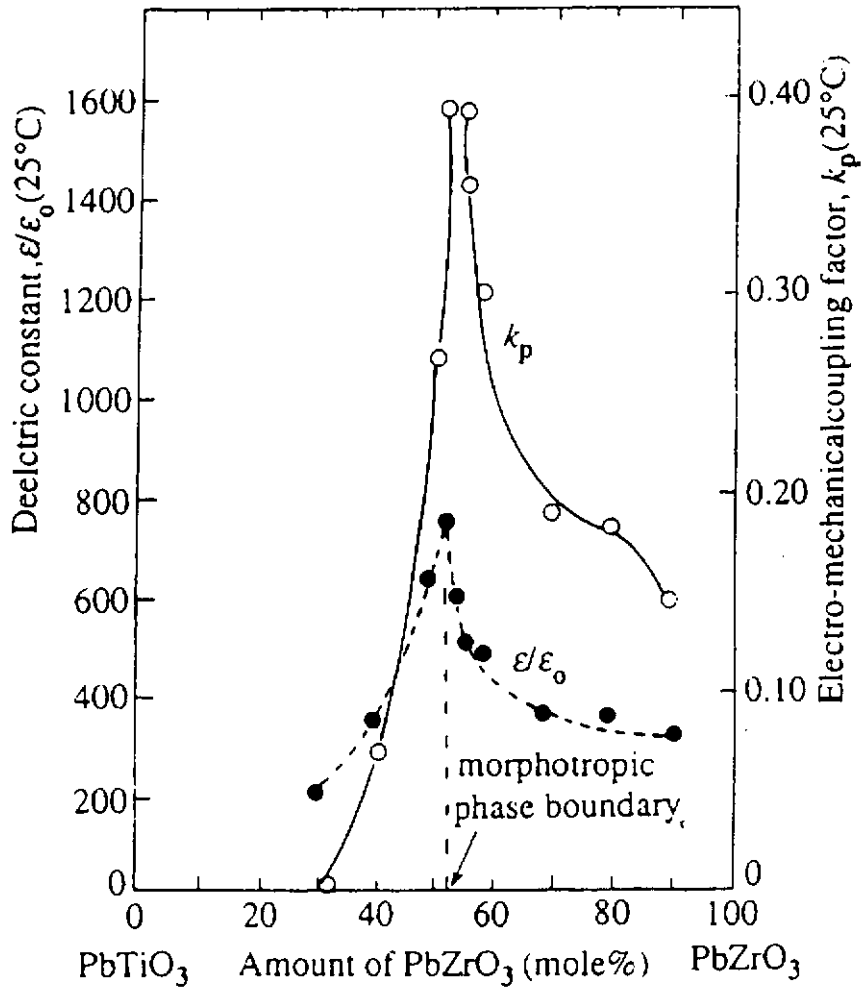

Fig. 1.5 Variations of the dielectric constant $\varepsilon/\varepsilon_o$ and electromechanical coupling factor k_p with composition of PZT at room temperature [Jaffe *et al.*, 1954].

1.2.3 PZT Thin Films

Since miniaturization is the major trend in the development of MEMS devices, the functional materials must be in the form of thin film, of which the thickness is usually in micron or sub-micron range. Most of the MEMS devices are functioning owing to the vibration of a membrane or the deflection of a cantilever, so the longitudinal piezoelectric

coefficient d_{33} and the transverse piezoelectric coefficient d_{31} of ceramic thin films become essential in designing and developing the micro-devices. To date, there is still not enough knowledge or information to derive precisely the thin-film properties from the known bulk-ceramic properties. Therefore, characterization of the thin film properties is necessary and has attracted a lot of research interest recently.

In 1995, Chen *et al.* studied the dielectric and piezoelectric properties of PZT films as a function of composition [Chen *et al.*, 1995]. The PZT thin film was prepared by the sol-gel method and was 1 μm thick. The mole percentage of titanium ranged from 20% to 80%. They showed that the PZT film with about 48 mole % of PT had the largest dielectric constant, effective longitudinal piezoelectric coefficient and remanent polarization, as shown in Figures 1.6 – 1.8. This agreed with the results for the bulk PZT ceramics [Berlincourt *et al.*, 1960; Jaffe and Cook, 1971].

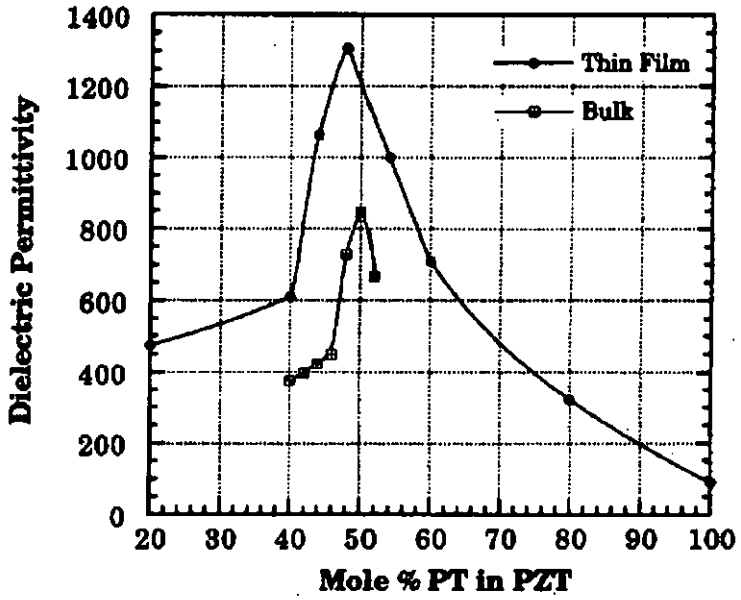

Fig. 1.6 The dielectric constant vs. composition in the $PbZrO_3$ –$PbTiO_3$ solid solution system [Chen *et al.*, 1995]. The data for bulk ceramics were quoted from the work of Berlincourt *et al.* [Berlincourt D. A., Cmolik C., and Jaffe H., "Proc. IRE" 48 (1960) 220].

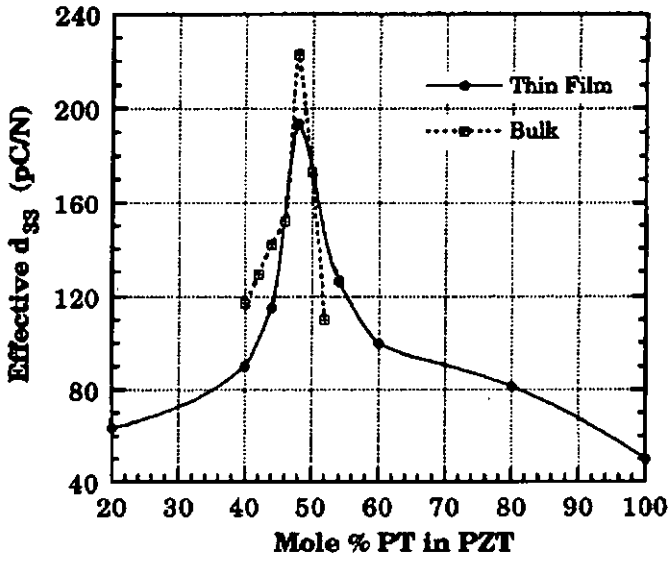

Fig. 1.7 The effective d_{33} as a function of composition in the $PbZrO_3$ –$PbTiO_3$ solid solution system [Chen *et al.*, 1995].

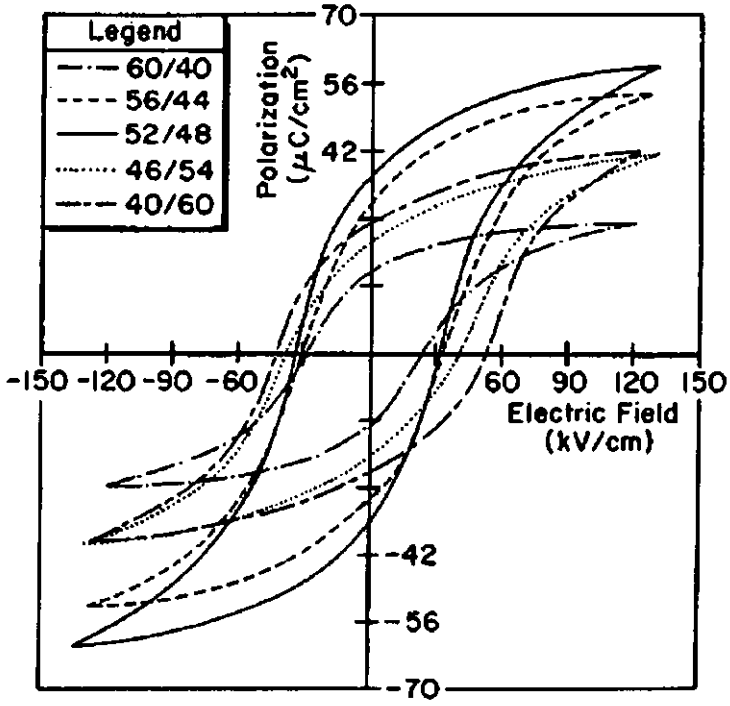

Fig. 1.8 Ferroelectric Polarization hysteresis loops of 1 μm thick PZT films with different compositions near the MPB. [Chen *et al.*, 1995].

1.2.4 Techniques for Deposition of Ceramic Thin Film

In order to prepare the sample in the form of thin film, a number of deposition techniques have been developed, such as pulsed laser deposition (PLD), magnetron sputtering, metal organic chemical vapor deposition (MOCVD), sol-gel process, etc.

Pulsed laser deposition (PLD) – An intense energy pulse is deposited on a source material to a certain depth. As a consequence, an explosive evaporation of a thin layer of the source material occurs [Smith *et al.*, 1995, Chapter 8]. Then the vapor of the source

material is directed and sticked to the substrate in the chamber by pressure gradient between the target and the substrate. Heater is installed beneath the substrate holder. The substrate holder is heated to a certain temperature, which depends on the material to be deposited, so the material can crystallize on the substrate. The schematic diagram of PLD is shown in Figure 1.9. The depth of the layer of the explosive source material is determined either by the optical absorption or by the thermal diffusion length. For the purpose of evaporating the source material by a pulse laser, the energy must be high enough for heating up the material to a very high temperature. This heating may involve the heat of fusion consumed in melting the material. Although an UV laser is not a unique choice for the pulsed laser deposition, it is commonly used in most of the applications because of the short wavelength and high energy of each photon. However, the efficiency of pulsed laser deposition can be reduced either by the reflection of the pulse energy from the surface or by the absorption by the vapor cloud formed over the source material.

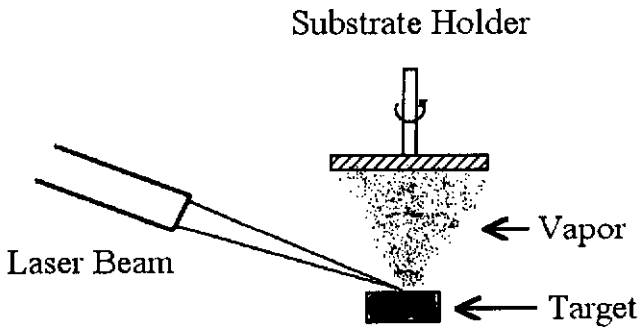

Fig. 1.9 A schematic diagram of pulsed laser deposition.

Magnetron sputtering – Ions are accelerated by a magnetic field to bombard a target surface. After absorbing the energy of the accelerated ions, the atoms of the target materials gain enough kinetic energy to "escape" from the target and move freely inside the vacuum chamber. Some of the target atoms impact and stick onto the substrate by random motion, a film is then formed [Klaus *et al.*, 1988]. The basic principle of magnetron sputtering is based on the momentum transfer from ions to the target material, therefore, the size of the ion 'bullet' is crucial and the chemical reactivity of the ion 'bullet' has to be considered. Since no chemical reaction is desired during the bombardment, inert argon gas has been commonly used for the ion 'bullet'. Magnetron sputtering is performed by applying a high voltage across a low-pressure gas to create plasma, which consists of electrons and gas ions in a high-energy state. The function of the magnetic field in magnetron sputtering is to intensify and confine electrons above the surface of the target and hence to cause a high gas ionization rate. During sputtering, energized plasma ions strike the target, causing atoms of the target to be ejected with enough energy to travel to the substrate and bond on it (Figure 1.10). By adjusting different deposition parameters, such as deposition power and time, film of different thicknesses can be obtained. Based on ion bombardment, strong adhesion between the film and substrate can be obtained. The disadvantages of magnetron sputtering are the long processing time for pumping down the sputtering environment, the limitation of target materials due to the vapor pressure of the target material [Klaus *et al.*, 1988], etc.

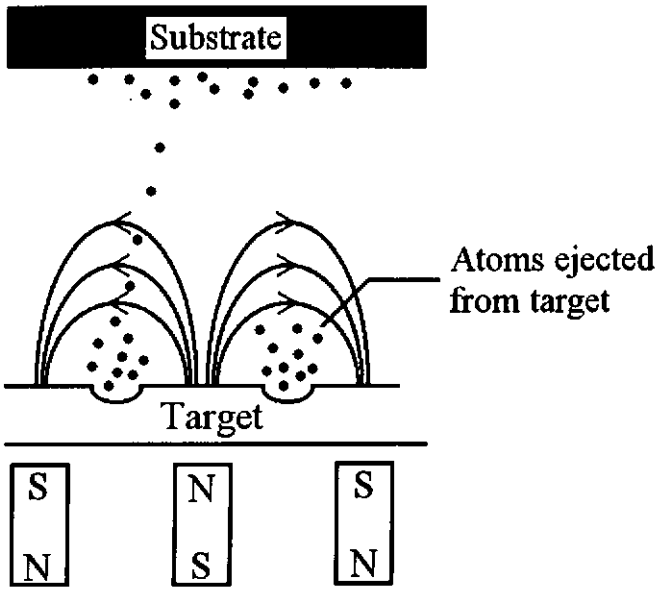

Fig. 1.10 A schematic diagram showing the mechanism of magnetron sputtering.

Metal organic chemical vapor deposition (MOCVD) – Organometallic compounds are used as source materials for the materials synthesis process. The source materials in vapor phase are introduced into a reaction chamber at approximately room temperature. When the gases reaching the heated substrate, it reacts to form the film on this substrate [Klaus *et al.*, 1988]. The deposition of film on substrate is based on three mechanisms: trapping, chemical reaction and sticking. Trapping of gases is the gas molecules trapped on the substrate by physical absorption. Chemical reaction is the reaction between the gases and the substrate. Gas molecule stacked on the surface of substrate with long enough time to bury and thus permanently incorporated into the depositing film. Therefore, the reaction chamber wall does not deliberately heated and do not directly influence the chemical reactions that occur in the chamber. By controlling the composition of the sources and the deposition temperature, a variety of films can be

obtained.

Sol-gel process – The word "sol-gel" is a combination of 'sol' and 'gel'. Sols and gels are two forms of matters that have been known to exist naturally for long time. A large number of materials and substances, such as ink, clays, blood, serum and milk, can exist in either form of sol and gel. In scientific wording, sol is a stable suspension of colloidal solid particles within a liquid [Hiemenz *et al.*, 1977], whereas gel is a porous 3-dimensionally interconnected solid network that extends in a stable fashion throughout a liquid medium and is only limited by the size of the container [Hiemenz *et al.*, 1977]. The process of gel formation from sol is called gelation. A sol can be transformed into a polymeric gel when it passes through a certain condition which is called a gel point [Seyferth *et al.*, 1984]. This needs a homogenous dispersion present in the initial sol rigidifies. Practically, it is at this point that the sol changes abruptly from a viscous liquid state to a solid phase called the gel.

The earliest sol was prepared in laboratory using gold by Faraday in 1853 [Hiemenz *et al.*, 1977]. Since then, sols and gels have attracted considerable scientific and research interest. Until 1980's, the sol-gel technology was well established that it could be used to deposit thin films [Puyane, 1983], and then it became more popular in the late 1980's [Dey, 1988; Tanaka, 1989]. A large variety of samples, such as thin film, fiber and powder, can be fabricated by sol-gel process. Spin coating and dip coating are the two commonly used methods for preparing thin film samples. For research purpose, the spin coating method is preferable to the dip coating method, because the thickness of the films prepared by the method is more uniform. In addition, it can produce a uniform film over

a large area. In the spin coating method, a film is simply prepared by dropping a few drops of sol on a substrate (Figure 1.11). The substrate then spins at a high speed and the solution is spread over the substrate surface to form a thin layer of film. After that, the film is heated at high temperature to remove the solvent and the other unwanted materials in the solution, such as organic materials used in preparing the precursor solution. A film of certain thickness can be obtained by repeating the spinning and heating processes a number of times. Finally, the thin film is annealed at a high temperature for crystallization.

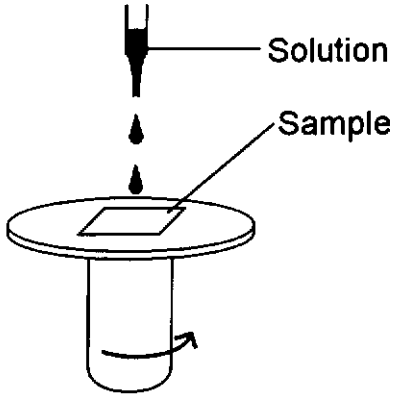

Fig. 1.11 Illustration diagram of spin coating technique.

Sol-gel process is a very useful and simple method for preparing materials, including materials of any oxide compositions and hybrid organic-inorganic materials. It can offer better stoichiometry control of the material composition and chemical homogeneity. Usually, the chemical process involved in preparing the precursor solution is completed at low temperature, so the kinetics of the various chemical reactions can be controlled easily. Moreover, it does not require any expensive and sophisticated equipment. Although the MOCVD process can also offer good stoichiometry control of the material composition

and chemical homogeneity, the required apparatus, such as the heat tube for vaporizing solutions, are very expansive. For the PLD and magnetron sputtering processes, a high, sometimes ultrahigh, vacuum environment is required, and hence an expansive vacuum system is needed. The time for achieving the high vacuum is also quite long.

1.3 Measurements of Piezoelectric Coefficients of Thin Films

In the past decades, a number of techniques have been established for the measurements of the longitudinal and transverse piezoelectric coefficients (d_{33} and d_{31}) of thin films. For the d_{33} measurement, both the direct piezoelectric effect and converse piezoelectric effect have been used. For example, the normal load method proposed by Lefki *et al.* [Lefki and Dormans, 1994] and Ren *et al.* [Ren *et al.*, 1997] and the pressure rig technique developed by Xu *et al.* [Xu *et al.*, 1999] are based on the direct piezoelectric effect. On the other hand, the measurement technique using a single or double beam laser interferometer is based on the converse piezoelectric effect [Li *et al.*, 1995; Pan *et al.*, 1989; Maiwa *et al.*, 1999; Kholkin *et al.*, 1996]. For the d_{31} measurement, a wafer flexure technique and a cantilever deflection technique have been developed by Shepard *et al.* [Shepard *et al.*, 1999] and Dubois *et al.* [Dubois, 1999], respectively. Both techniques are based on the direct piezoelectric effect.

1.3.1 d_{33} Measurement

In 1994, a simple experimental technique, the normal load method, was proposed by Lefki and Dormans for the d_{33} measurement of ferroelectric thin films [Lefki and Dormans, 1994]. The schematic diagram for the experimental setup is shown in Figure 1.12. The method is based on the direct piezoelectric effect. In the experiment, a uniaxial force is applied to the sample along the thickness direction and the induced electric charge is collected by a standard capacitor. The voltage across the standard capacitor is measured by a voltmeter, of which the reading is used to calculate the quantity of the induced charge. The effective d_{33} of the film is then given by the ratio of the induced electric charge to the applied uniaxial force.

The method is relatively simple. However, as pointed out by Ren *et al.* [Ren *et al.*, 1997] that a metallic tip should not be used to apply a force on the thin film. Different from ceramic bulk samples, the ceramic thin film is so fragile that it may be easily damaged during the application of a force via a stiff metallic tip. Instead, Ren *et al.* used a composite tip to apply a normal force on the thin film [Ren *et al.*, 1997]. Due to the elasticity of the composite tip, it can improve the contact between the surface of the tip and the film sample. The stress on the film surface is uniform and the possibility of damage caused by the tip is greatly reduced. Nevertheless, there is still a disadvantage for the method. Since the normal force is applied locally on the film sample, bending of the sample, especially for a sample with an initial curvature, will easily be induced, and hence lateral stresses are generated. As a result, the observed induced charges are increased by an amount contributed by the transverse piezoelectric effect.

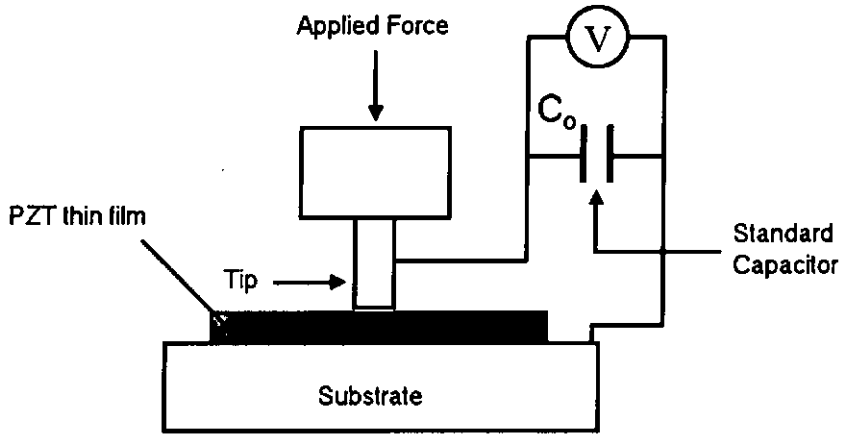

Fig. 1.12 Schematic diagram of the normal method for d_{33} measurement [Lefki and Dormans, 1994].

To avoid the bending of the sample due to the locally applied force, Xu *et al.* established a new method by applying the uniaxial force with pneumatic pressure [Xu *et al.*, 1999]. The schematic diagram of the experimental setup is shown in Figure 1.13. Since the same pneumatic pressure (the upper and lower chambers are connected) is applied on both sides of the sample, the force is balanced everywhere across the sample and hence the sample will not bend even if the sample has a curvature initially. Moreover, different from the normal load method in which the tip has to be carefully aligned for ensuring the orthogonality between the applied force and the sample surface, the force applied via the pressure is completely normal to the surface of the sample. However, additional fractional stress is induced at the interface of the film surface and the O-rings which are used to seal the system. The friction arises when there is a pressure change in the cavities. The pressure applies a force on the O-rings and pushes the O-rings outwards,

surface frictions and hence tensile in-plane stress are generated. Similar to the lateral stress generated by bending of the sample, the fractional stress will increase the induced charged. Since d_{31} and d_{33} have opposite signs in PZT, the piezoelectric charges induced by the normal and the in-plane components of the stresses add to each other. Nevertheless, the authors have developed procedure for eliminating the resulting effect. This is achieved by controlling the in-plane stress. First, they preload the cavities with a pressure P_2, which is higher than the pressure for measurement P_1, and then reduce the pressure to P_1. As a result, a compressive in-plane stress is imposed on the sample due to the O-ring recovery. By controlling P_2, the in-plane tensile stress can be eliminated by this compressive in-plane stress [Xu *et al.*, 1999].

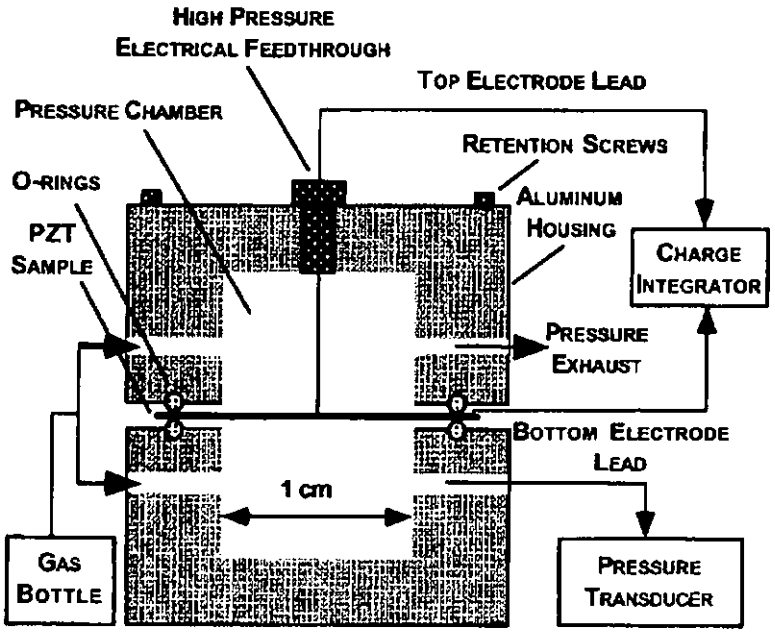

Fig. 1.13 A schematic diagram of the experimental setup for the pressure rig technique for the d_{33} measurement [Xu *et al.*, 1999].

Laser interferometery is a well-established technique for measuring small displacement. Since the basic principle of the technique is based on the interference between a probing laser beam and a reference laser beam, the resulting resolution can be in the order of 10^{-12} m. Homodyne interferometer and heterodyne interferometer are the typical types of the laser interferometers [Karasik, 1994, Chapter 2]. Figure 1.14 shows the schematic diagram of an experimental setup using a Mach-Zehnder type heterodyne laser interferometer for the d_{33} measurement of ferroelectric thin films. The measurement is based on the converse piezoelectric effect. Upon the application of a voltage V to the sample (of thickness t), the induced surface displacement of the sample A is measured by the laser interferometer, and the longitudinal piezoelectric coefficient d_{33} is hence given by

$$d_{33} = \frac{\partial S_3}{\partial E_3} = \frac{A/t}{V/t} = \frac{A}{V} \tag{1.5}$$

Due to the fine resolution and simple operation, single beam laser interferometry has widely been applied for the d_{33} measurement of ferroelectric thin films. However, there is a serious drawback of the technique, which is caused by the bending of the sample (Figure 1.15). When a field is applied along the thickness direction ($\hat{3}$) of the sample, there is not only change of the thickness of the sample induced by the piezoelectric effect, but also change of the lateral dimensions of the film generated by the Poisson effect. If the sample is not tightly fixed to a holder, these lateral stresses will bend the sample as shown in Figure 1.15. Since the single beam laser interferometry technique measures only the displacement of the front surface of the sample which is the sum of the thickness change and the bending (ΔL_b), the resulting value of d_{33} is usually much larger than the true value. To remedy this drawback, a double beam laser interferometry technique has

recently been developed, in which both the displacements of the front and back surfaces are measured.

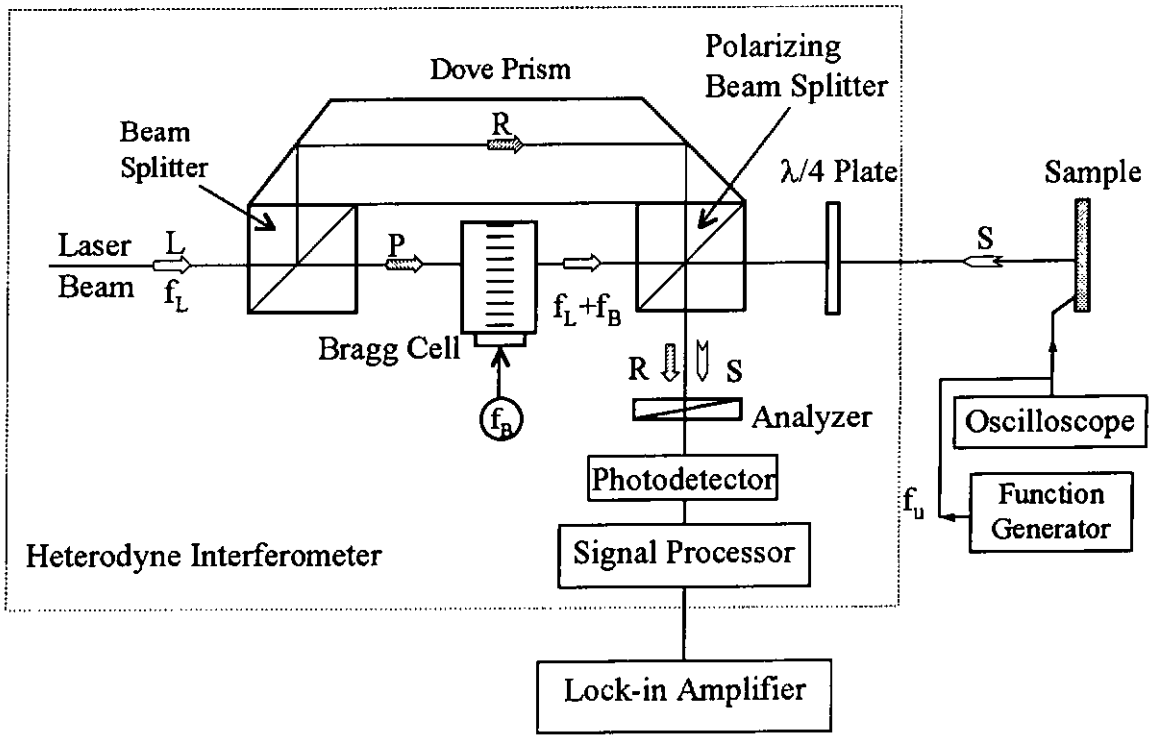

Fig. 1.14 Schematic diagram of the experimental setup for the measurement of d_{33} using a Mach-Zehnder type heterodyne laser interferometer.

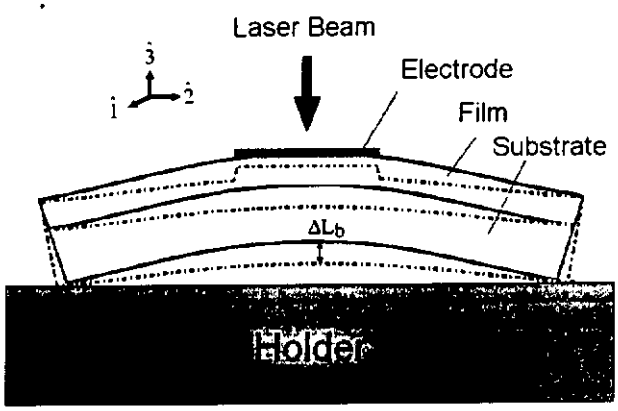

Fig. 1.15 Bending effect of the substrate on the displacements measured with the single-beam interferometer in a piezoelectric thin film [Kholkin *et al.*, 1996].

As mentioned in the previous section, both the displacements of the front and back surfaces of the sample are measured in the double beam laser interferometry technique, so that the change of the sample thickness can be correctly determined by deducting the front surface displacement by the back surface displacement (i.e. the bending of the sample). The schematic diagram of an experimental setup for the d_{33} measurement of ferroelectric thin films using a double beam laser interferometer is shown in Figure 1.16. Different from the single beam laser interferometer, two probing laser beams are incident on the front and back surfaces of the sample at the same time in order to measure their displacements (Figure 1.17).

In principle, the double beam laser interferometery technique can accurately determine the d_{33} value of ferroelectric thin films. However, sophisticated optical system, cautious optical alignment, and meticulous operation are strictly required, otherwise there are significant errors existed in the measurement. In order to have accurate results, the two probing beams incident on the front and back surfaces of the sample must be of equal intensity and the same polarization at the interference point, i.e. photo-detector. Therefore, a number of $\lambda/4$ plates are used in the experimental setup. The optical path difference between the probing beam and the reference beam should be shorter than the coherence length of the laser beam, which is the condition for interference. Moreover, the sensitivity of the measurement is also affected by the aperture of the photo-detector; the aperture should be smaller than the diameter of the central fringe.

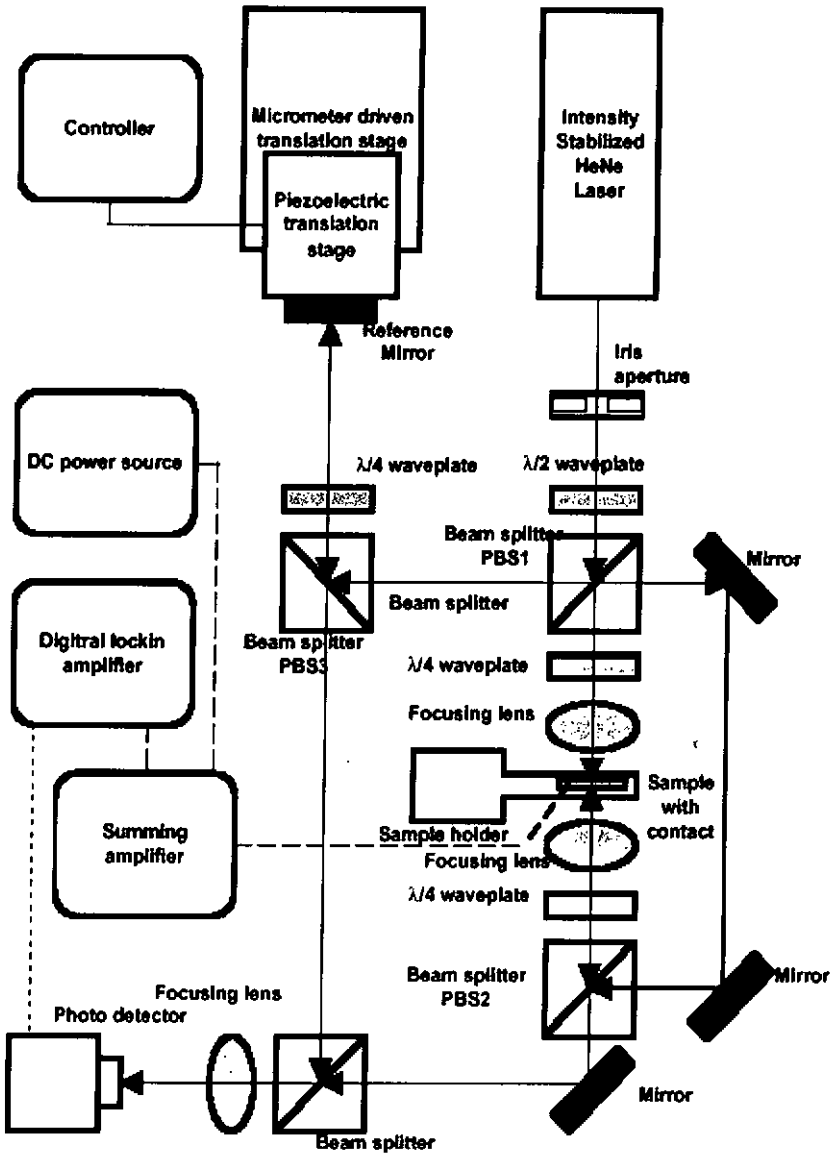

Fig. 1.16 Schematic diagram of the experimental setup for the measurement of d_{33} using a double beam laser interferometer including the electronic system [Maiwa *et al.*, 1999].

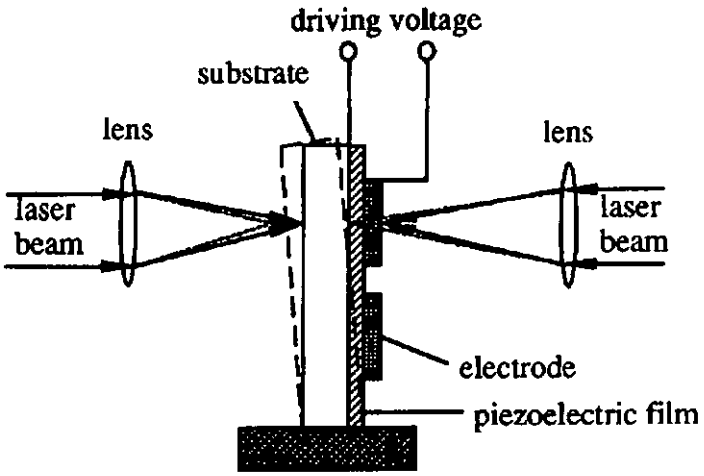

Fig. 1.17 Schematic diagram of the sample holder for the double beam laser interferometery technique showing two probing beams incident on the front and back surfaces of the sample at the same time [Kholkin *et al.*, 1996].

In summary, although there are a number of methods and techniques for measuring the d_{33} value of ferroelectric thin films, not every method can give an accurate d_{33} value of the sample. For the normal load method, charge induced by the transverse piezoelectric effect can cause a significant error in the observed d_{33} value. For the pressure rig technique, a complex system is required for the measurement. Although the double beam laser interferometry technique can give an accurate d_{33} value of the sample, it requires caution optical alignment since the sensitivity of the system is greatly dependent on the optical alignment. On the other hand, the signal beam laser interferometery technique is the most simple and effective method for the d_{33} measurement, since it does not requires any sophisticated optical system, cautious optical alignment, and meticulous operation as compared to the other methods. However, the experimental setup, especially the sample holder, must be specially designed for eliminating the errors resulted from the bending of

the sample.

1.3.2 d_{31} Measurement

The wafer flexure technique is one of the methods developed for the measurement of the transverse piezoelectric coefficient d_{31} of ferroelectric thin films, which is based on the direct piezoelectric effect [Shepard *et al.*, 1999]. The schematic diagram of the experimental setup is shown in Figure 1.18. Different from the other techniques, in which the sample is required to be prepared in the form of a cantilever, a whole silicon wafer with a ferroelectric thin film deposited on it is used for the wafer flexure technique. Compressed gas is injected in the chamber, the wafer is hence flexed and the thin film is strained. From the pressure reading of the pressure transducer and the Poisson's ratio and Young's Modulus of the silicon wafer, the strain and hence the stress of the thin film are calculated. Because of the direct piezoelectric effect, charge is induced on the thin film surface. An electric charge integrator is used to measure the induced charge, and the induced electric displacement is calculated by dividing the observed amount of charge by the electrode area. The transverse piezoelectric coefficient d_{31} of the ferroelectric thin film is then given by the ratio of the induced electric displacement to the stress. Shepard *et al.* showed that the observed d_{31} value of a sol-gel derived PZT (Zr/Ti = 52/48) film did not change with the compressed gas pressure ranging from 10 to 50 MPa and with the position across the wafer.

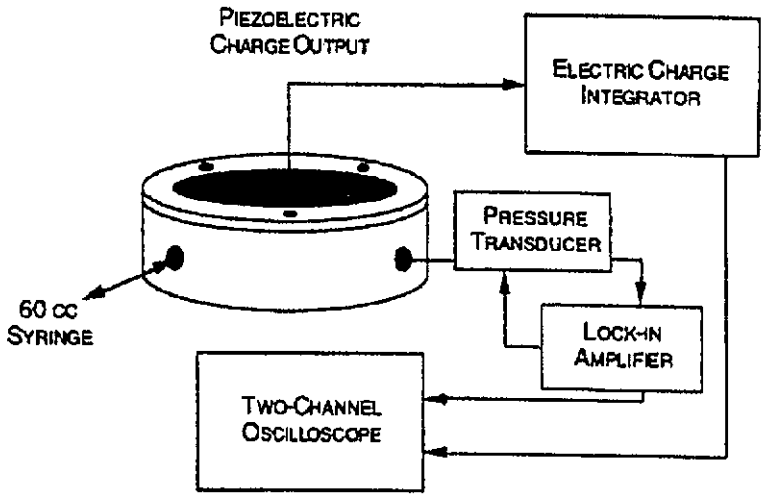

Fig. 1.18 Schematic diagram of the experimental setup for the d_{31} measurement of ferroelectric thin films using the wafer flexure technique [Shepard *et al.*, 1999].

Another method for the measurement of the transverse piezoelectric coefficient of ferroelectric thin films has been established by Dubois *et al.* [Dubois *et al.*, 1999]. Since it is very difficult to measure the elastic properties of PZT films and there is not too much information of it, Dubois *et al.* measured another transverse piezoelectric coefficient e_{31} of PZT films instead of d_{31}. In their work, e_{31} was defined as

$$e_{31} = \frac{d_{31}}{s_{11}^E + s_{12}^E} = \frac{D_3}{s_{11}^E + s_{12}^E} \tag{1.6}$$

According to Dubois *et al.*, the e_{31} coefficient is more practically useful since it relates the induced charges (electric displacement) directly to the deformation (strain). The schematic diagram of the experimental setup using a cantilever deflection technique [Dubois *et al.*, 1999] is shown in Figure 1.19. A rectangular substrate with a ferroelectric thin film deposited on it is clamped at one end in a sample holder and the other end is left

free. A piezoelectric actuator is used to bend the substrate, generating a deflection and hence a strain in the thin film along the length direction. With the set-value of the deflection, the Poisson's ratio of the substrate and the Young's Modulus of the thin film, the stress in the thin film is calculated. The charges induced under a top electrode are collected using a charge amplifier, and the induced electric displacement is calculated by dividing the observed amount of charge by the electrode area. The transverse piezoelectric coefficient e_{31} is then given by the ratio of the induced electric displacement to the stress. Dubois *et al.* also showed that the observed e_{31} values of the thin films at different positions across the substrate were the same. The cantilever deflection technique is very similar to the wafer flexure technique, except that a uniaxial stress is generated along the length direction of the sample in the cantilever deflection technique while a two-dimensional stress is generated in the plane of the sample in the wafer flexure technique.

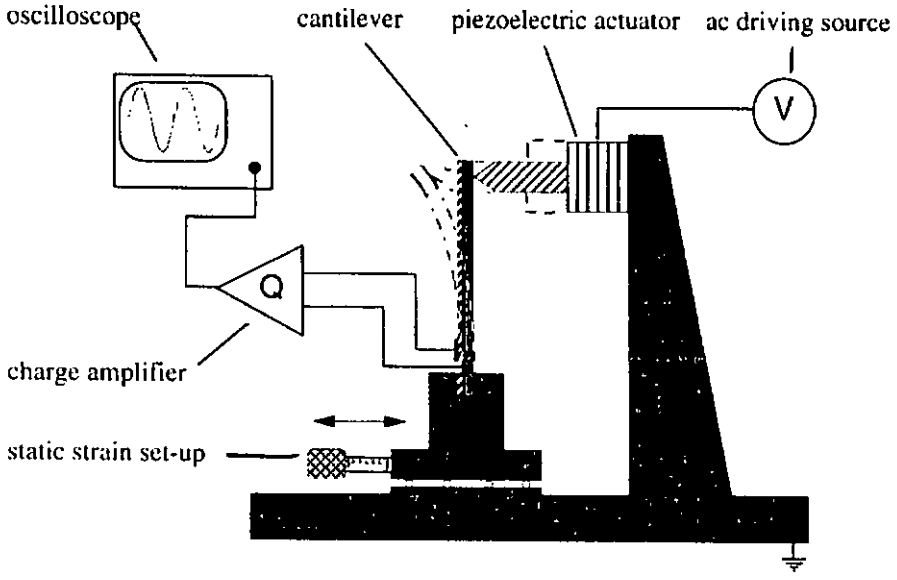

Fig. 1.19 Schematic diagram of the experimental setup for the e_{31} measurement using the cantilever deflection technique [Dubois *et al.*, 1999].

1.4 Scope of the Work

The main objectives of the present work are to establish effective techniques for measuring the longitudinal piezoelectric coefficient d_{33} and transverse piezoelectric coefficient e_{31} of lead zirconate titanate (PZT) ceramic films, to study the effects of amount of excess lead, annealing temperature, poling field and poling time on the piezoelectric properties of PZT films, and also to investigate the depolarization phenomenon of films and explain the phenomenon with the Preisach model.

The procedures for preparing the PZT precursor solution by the sol-gel technique and for fabricating the PZT films using the multiple-spin-coating technique were described in Chapter 2. In the same chapter, the crystallite structure, microstructure, and the polarization hysteresis loop of the sol-gel derived films were examined.

The measurements of the longitudinal piezoelectric coefficient d_{33} and transverse piezoelectric coefficient e_{31} have been successfully established by using the single laser beam interferometry and cantilever deflection technique, respectively. The details of the measurements were described in Chapter 3. The bending of the substrate has been effectively and significantly suppressed by gluing the substrate on a large and rigid platform with mounting wax in the d_{33} measurement. Various experiments have been done in order to examine the bending of the substrate, and the resulting d_{33} value was comparable to the literature value of PZT film with the same composition. The effects of amount of excess lead, annealing temperature, poling field and poling time on the observed d_{33} and $e_{31}$of values of PZT films were then investigated and the results were

reported in Chapter 4. At last, I have demonstrated that a polarized PZT film could be completely depolarized by application of ac fields of diminishing amplitude. The depolarization phenomenon was explained with the Preisach model in Chapter 4.

Chapter Two
Sample Preparation and Characterization of PZT Thin Film

As mentioned in Chapter 1, there are a number of techniques developed for the fabrication of ferroelectric thin films. Among them, the sol-gel technique is the most effective and useful technique. It does not require any expensive vacuum system and sophisticated equipment. It allows the production of any oxide compositions and new hybrid organic-inorganic compositions. Most of the chemical processes involved in the preparation of the precursor solution are completed at low temperatures, therefore the kinetics of various chemical reactions can be easily controlled. Thus, it can offer better stoichiometry control of the film composition and chemical homogeneity. Together with the spin coating technique, a uniform film over a large area can be produced.

In this work, the sol-gel technique was used to prepare a PZT precursor solution. The PZT composition near the morphotropic phase boundary (i.e. Zr/Ti = 53/47) was chosen because of their better piezoelectric properties. Multiple-spin-coating technique was used to prepare PZT thin films on silicon substrates from the precursor solution. Before the study of the piezoelectric properties, the basic ferroelectric properties of the PZT films were first examined. The crystalline structure of the PZT films was studied using an x-ray diffractometer with nickel-filtered CuKα radiation (X'pert System, Philips Electronic Instruments), the microstructure was examined using a scanning electron microscope (Lecia 440), and the polarization hysteresis loop was determined using a

ferroelectric tester (Sawyer-Tower bridge).

2.1 Preparation of Precursor Solutions

In the preparation of a precursor solution, a number of factors have to be considered. Solvent is the elementary element in the preparation of the precursor solution. Besides being able to dissolve the "main" chemicals, which are the required chemicals of the film, the solvent should also meet with certain requirements. Firstly, the boiling temperature of the solvent should be well above room temperature and below the boiling temperatures of the "main" chemicals used, such that the "main" chemicals will not evaporate easily when removing the solvent from the precursor solution at the last step. Secondly, the solvent should be chemically stable in such a way that no unwanted material will be formed. Thirdly, non-toxic solvent is preferable, so that no extra precaution is needed to be considered during the burn-out and annealing processes. On the other hand, certain requirements have to be fulfilled in selecting the "main" chemicals. The chemicals should easily be hydrolyzed and form homogenous colloidal solution. No additional chemical reaction should occur in such a way that no precipitate is formed during the dissolving and mixing processes. The resulting precursor solution should be free from any unwanted substance.

In this work, lead (II) acetate trihydrate $Pb(CH_3COO)_2 \cdot 3H_2O$, zirconium (IV) n-propoxide $Zr(OCH_2CH_2CH_3)_4$ and titanium (IV) n-butoxide $Ti(O(CH_2)_3CH_3)_4$ were chosen for the main chemicals and 2-methoxyethanol $CH_3OCH_2CH_2OH$ was used as the

solvent. The boiling temperatures of lead (II) acetate trihydrate, zirconium (IV) n-propoxide and titanium (IV) n-butoxide are 280°C, 208°C and 310°C, respectively, which are well above the boiling temperature of the solvent (124°C). Both zirconium (IV) n-propoxide and titanium (IV) n-butoxide can react with water to form precipitates of ZrO or TiO. Therefore, the precursor solution has to be prepared in a dry environment.

PZT precursor solutions with Zr/Ti ~ 53/47 and different amounts of excess lead were prepared. The procedure of the preparation of the precursor solution is depicted in the flow chart shown in Figure 2.1. At first, certain amount of lead (II) acetate trihydrate was kept in an oven at 135°C for 8 hours for dehydration. The dried lead (II) acetate was then dissolved into 2-methoxyethanol (MOE) under continuous heating and stirring. After all the lead acetate was dissolved, the resulting solution was cooled down to room temperature. Suitable amounts of zirconium (IV) n-propoxide and titanium (IV) n-butoxide were added into the solution. Then the solution was heated at a temperature slightly above the boiling temperature of MOE and was stirred continuously for chemical reaction and evaporation of excess MOE. After the chemical reaction was completed and suitable concentration of the precursor solution was obtained, the precursor solution was cooled down to room temperature and filtered with cotton to remove any impurities and foreign substances in the precursor solution. The concentration of the precursor solution was set to 0.5 M. The resulting precursor solution was then kept in an argon environment in order to prevent the reaction with water. To obtain better quality of the film, the precursor solution was kept at least 1 day for stabilization before use.

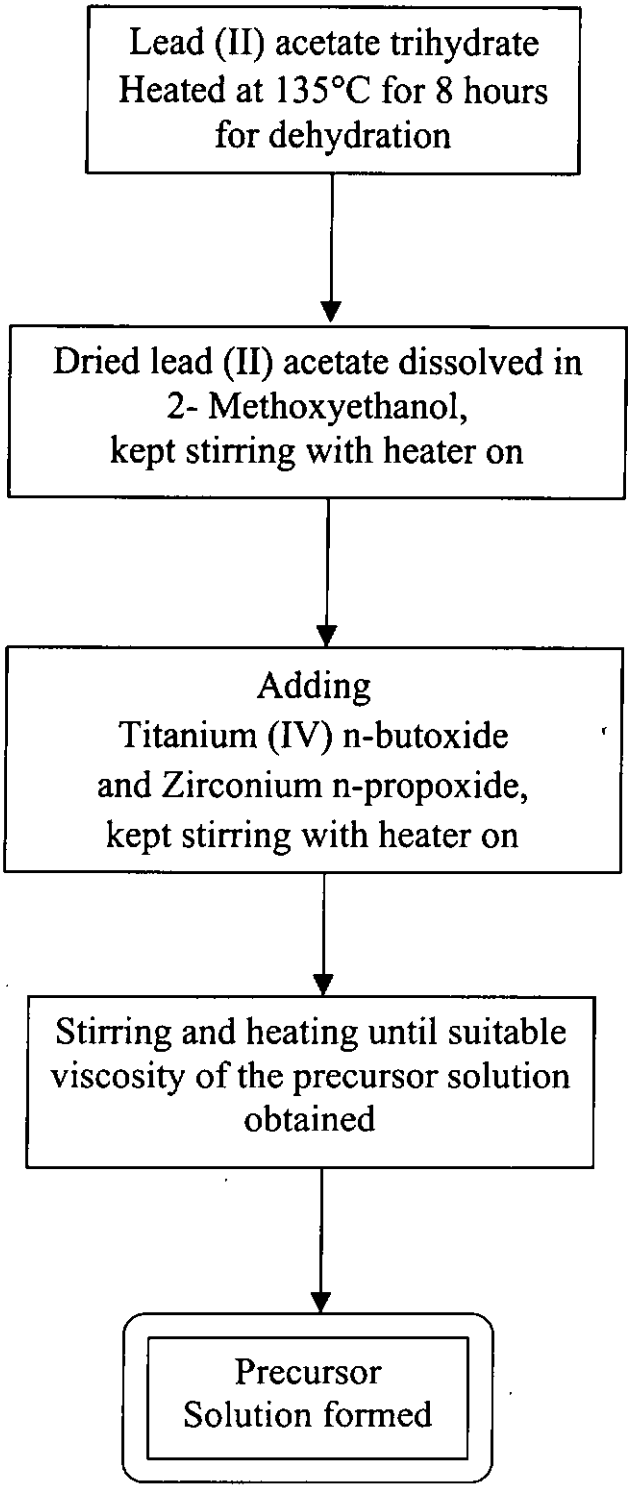

Fig. 2.1 Flow chat of the preparation of PZT precursor solution.

2.2 Fabrication of PZT Thin Films

Multiple-spin-coating technique was used to prepare PZT thin films from the precursor solution. The precursor solution was dropped onto a clean $Pt/Ti/SiO_2/Si$ substrate using a dropper. The substrate then spun at two different rotation speeds for different periods using a spinner (KW-4A, Chemat Technology). First, the substrate spun at a low speed (800 rpm) for 6 seconds to spread the solution over the whole surface of the substrate. Then the substrate spun at a high speed (3000 rpm) for 50 seconds to obtain a thin layer of film with uniform thickness. The thickness of each layer of film is about 100 nm. After that, the film sample was first dried on a hot plate at about 300°C. The film is covered in order to protect it from the dirt in air falling onto it. The dried film was then pyrolyzed in a rapid thermal processor (RTP 500) by heating at 150°C for 3 min, then at 450°C for 10 min and finally at 600°C for 3 min. At 150°C, the solvent was completely removed. The film was then kept at 450°C to decompose and remove the organic materials. Finally, the film partially crystallized at 600°C. By repeating the process a number of times, a PZT film of certain thickness was obtained. The PZT film was then annealed at different high temperatures for 1 hour in furnace for further crystallization (RHF 1600, Carbolite). PZT films of thickness 1 μm and 2 μm were fabricated. After that, a series of gold/chromium (Au/Cr) top electrodes was deposited on the film by dc magnetron sputtering for the subsequent poling and measurements. Chromium was first deposited on the film at 60 W for 2 min; gold was then deposited at 70 W for 3 min. The thickness of the gold/chromium (Au/Cr) top electrodes was measured to be 100 nm, using a surface profiler (KLA-Tencor P-10).

2.3 Crystallite Structure of PZT Thin Films

The crystallite structure of the PZT films was studied using an x-ray diffractometer with nickel-filtered CuKα radiation (X'pert System, Philips Electronic Instruments). X-ray diffraction (XRD) is a common method for the analysis of crystallite structures, such as crystallite phase identification, lattice parameter determination, grain size determination and texture analysis. The technique is mainly based on the constructive interference between the x-rays diffracted from the regular structure of a material. In order to have constructive interference, two criteria must be satisfied. The first one is that the material under examination should have a crystal structure, i.e. unit cell, in such a way that the arrangement of atoms forms a set of planes with interplanar spacing d with respect to the incident x-ray (Figure 2.2). The second criterion is that the relation between the interplanar spacing d and the wavelength λ of the x-ray should obey the Bragg's law:

$$\lambda = 2d \sin\theta \tag{2.1}$$

where θ is the angle of incidence, as illustrated in Figure 2.2.

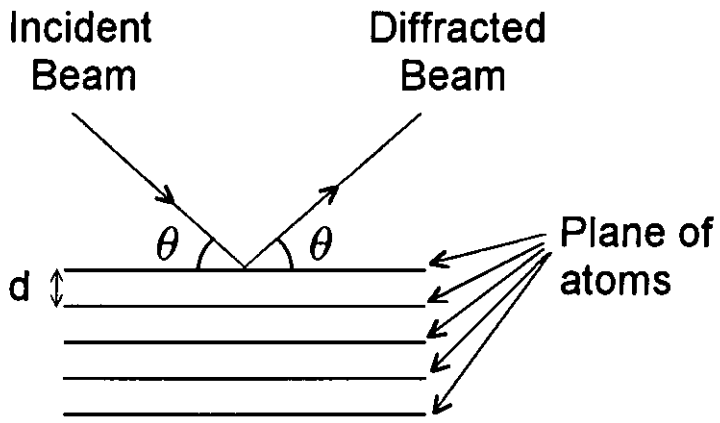

Fig. 2.2 A set of atomic planes in a crystal, at an angle θ from the incident beam [Chung *et al.*, 1992].

The allowed planes for constructive interference are those for which the structure factor is not zero, and which is going to explain. For example, the structure factor of face-centered cubic (FCC) crystal structure is not zero when the Millar indices h, k and l of the planes are either all even or all odd, so that the allowed planes for constructive interference have Miller indices 111, 200 220 and so forth. In contrast, for a body-centered cubic (BCC) structure, the structure factor is not zero when the addition of h, k and l ($h + k + l$) equal to an even integer, so that the allowed planes for constructive interference have Miller indices 110, 200, 211, 220, and so forth. Thus, the systematic absence of diffraction from certain planes provides a signature for identifying the atom arrangement in the unit cell.

The X-ray diffraction patterns of the PZT films annealed at different temperatures are shown in Figures 2.3 – 2.5. The thickness of the films is 2 μm. It is seen that all the samples exhibit a well-crystallized phase of PZT [Barrow *et al.*, 1997; Zhou *et al.*, 1997].

The ratios of the intensities of the (100) peak to the (111) peak are quite different in these three samples, and which is due to the difference in annealing temperature. It can be seen in Figure 2.5 that the (100) and (200) peaks are relatively strong while the (110) peak is absent from the XRD. This is because the annealing temperature is high enough for the PZT film to form crystals in a lower energy state which is (100) predominant texture. As compared Figures 2.4 and 2.5, it can be found that the ratio of the intensity of the (111) peak to the (110) peak is almost constant. By considering the three film samples, the PZT films annealed at 600°C and 650°C are polycrystalline without predominant texture.

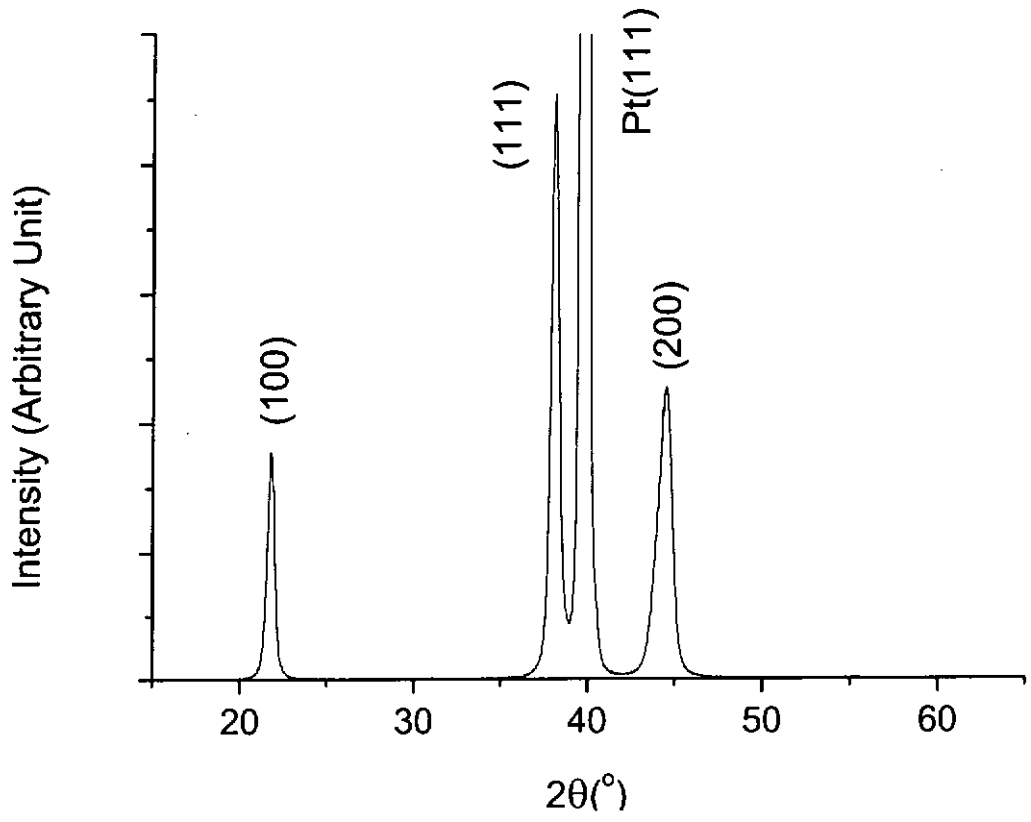

Fig. 2.3 XRD pattern of PZT(53/47) sample with 10% excess lead. The thickness of the film is 2 μm and the film is annealed at 600°C for 1 hour.

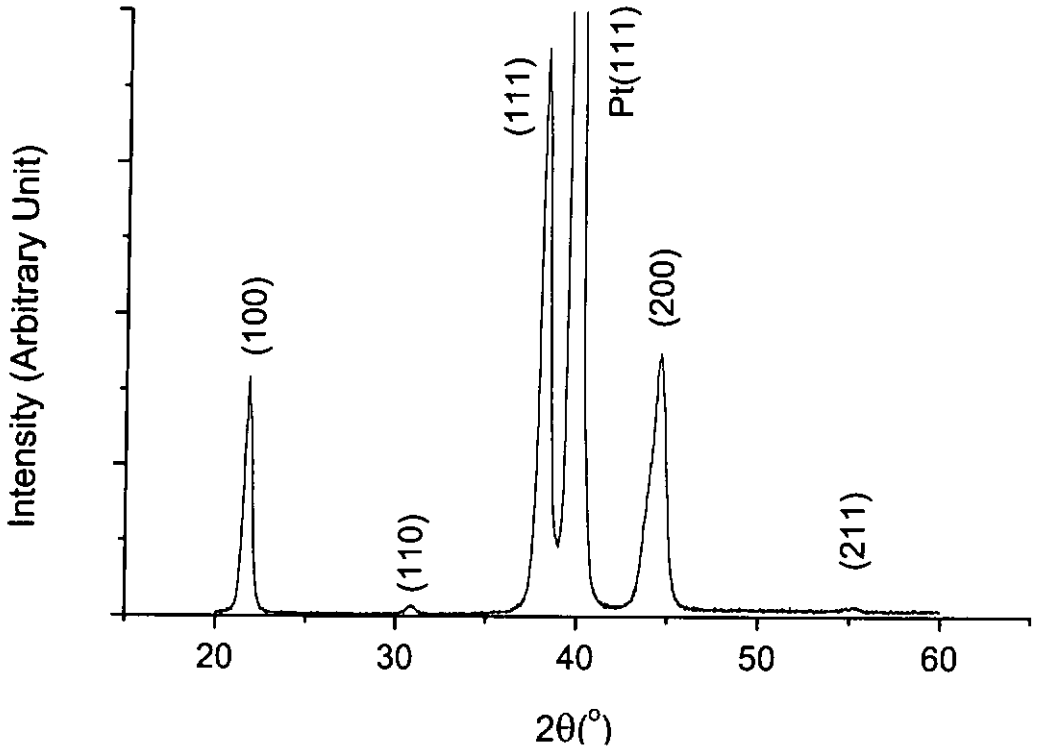

Fig. 2.4 XRD pattern of PZT(53/47) sample with 10% excess lead. The thickness of the film is 2 μm and the film is annealed at 650°C for 1 hour.

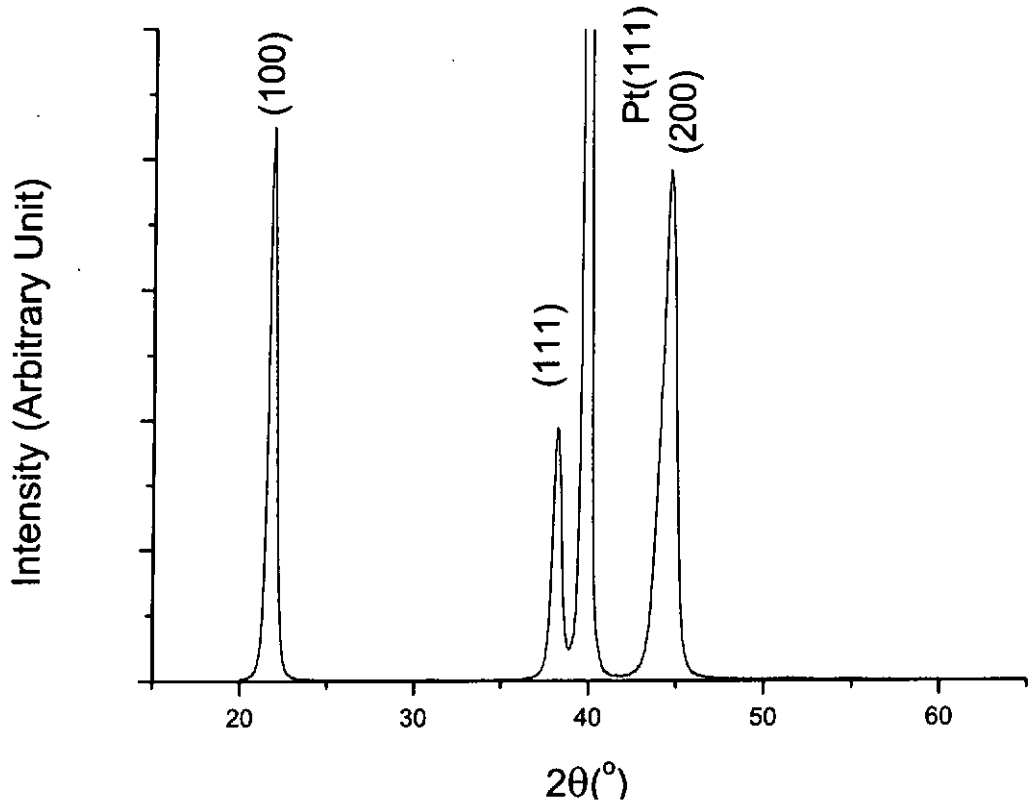

Fig. 2.5 XRD pattern of PZT(53/47) sample with 10% excess lead. The thickness of the film is 2 μm and the film is annealed at 700°C for 1 hour.

2.4 Microstructure of PZT Thin Films

The fracture surface of the PZT films was examined using a scanning electron microscope (SEM, Leica 440). Figures 2.6 and 2.7 show the micrographs of the fracture surface (with different magnifications) of a PZT thin film with 10% excess lead and annealed at 650°C for 1 hour. The thickness of the film is about 2 μm. It is also seen that the film is quite dense and has uniform thickness. Similar microstructures have also been

observed for the other PZT films with various amounts of excess lead and annealed at various temperatures. The films of different thicknesses also have similar microstructures.

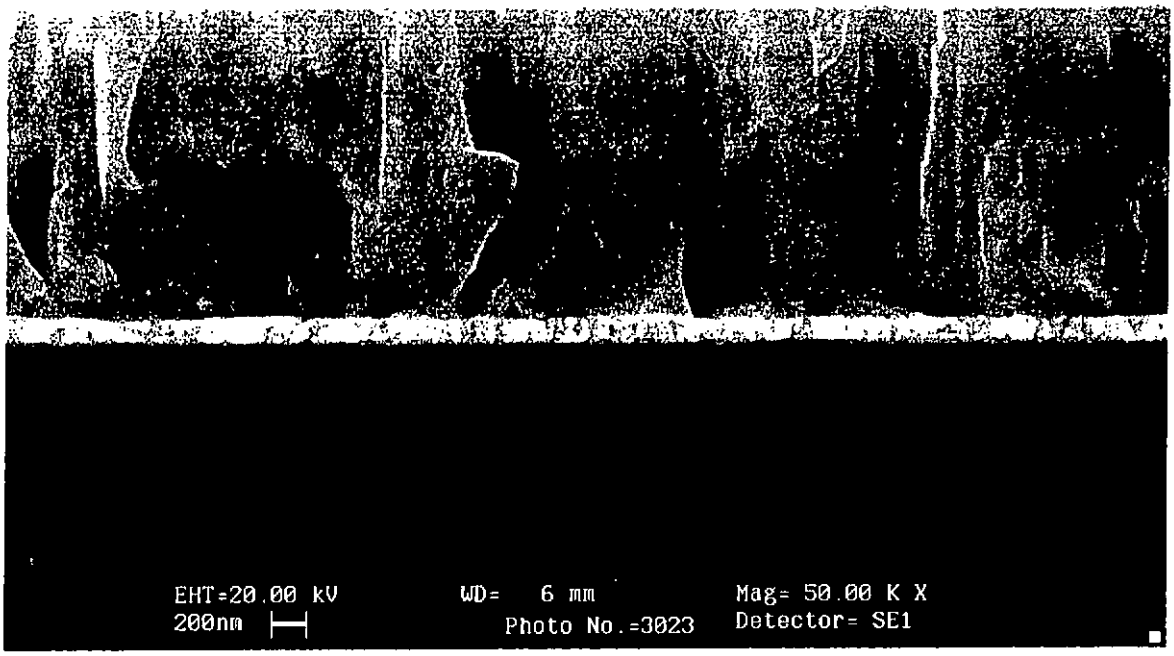

Fig. 2.6 SEM micrograph of the fracture surface of the PZT thin film with 10% excess lead and annealed at 650°C for 1 hour. The thickness of the film is 2 μm.

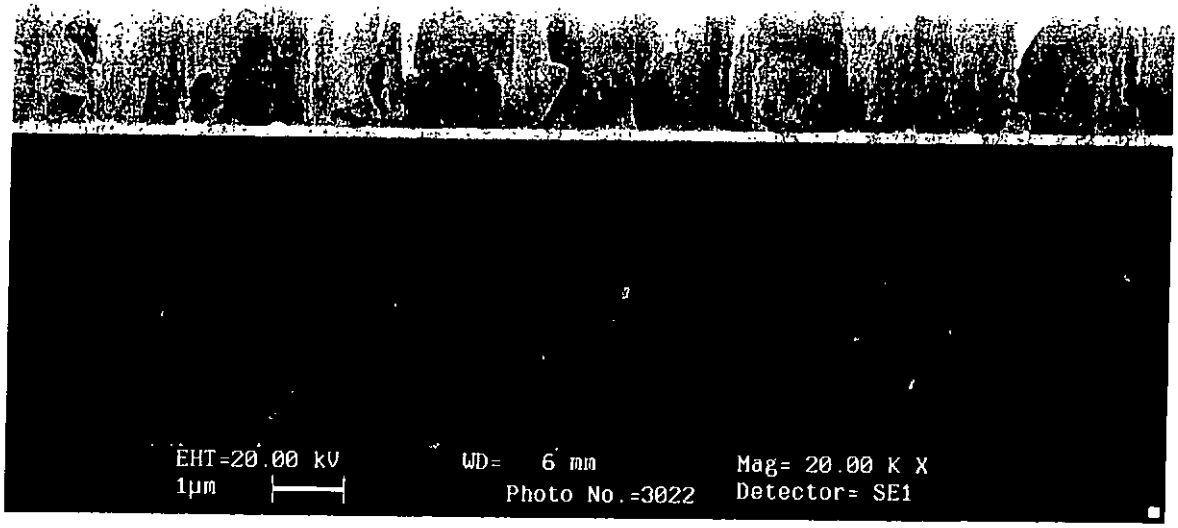

Fig. 2.7 SEM micrograph of the fracture surface of the PZT thin film with 10% excess lead and annealed at 650°C for 1 hour. The thickness of the film is 2 μm.

2.5 Polarization Hysteresis Loop of PZT Thin Films

The existence of polarization hysteresis is an evidence of the ferroelectricity in PZT thin films. For a ferroelectric material, the spontaneous polarization P_s can be reversed by an electric field. This reversibility is a consequence of the fact that the polar structure of a ferroelectric crystal is a slightly distorted non-polar structure. In general, uniform alignment of electric dipoles (spontaneous polarization) only occurs in certain regions of a crystal, while in other regions of the crystal electric dipoles may be in the reverse

direction (such as twinning). Such a region with uniform polarization is called a ferroelectric domain. The interface between two domains is called domain wall. The spontaneous polarization of a domain may be reversed by the application of a strong electric field. This dynamic process of reversing the domain is called domain switching, and the process depends on temperature and the applied electric field [Batthias *et al.*, 1948]. The relation between the net macroscopic polarization of a ferroelectric material and the applied electric field is manifested as a polarization hysteresis loop.

A Sawyer-Tower bridge is one of the typical experimental setups for measuring the polarization hysteresis loop of a ferroelectric material. Figure 2.8 shows the schematic circuit for the Sawyer-Tower bridge [Sawyer and Tower, 1930]. A function generator (HP 8116A, Hewlett-Packard) is used to supply an alternating voltage V_{ac} which is then amplified by 100 times using a power amplifier (BOP1000, KEPCO) before applying to the sample. The actual voltage applied to the sample is measured using an oscilloscope (HP 54645A, Hewlett-Packard), from which the electric field E applied to the sample is calculated. A reference capacitor with capacitance C_o is connected in series with the sample. C_o is usually much larger (about 1000 times) than the capacitance of the sample, so that it can store the polarization charges generated during the polarization switching but without affecting the process. Accordingly, the change of the polarization P of the sample can be calculated from the voltage V across the reference capacitor, which is measured using the oscilloscope, by

$$P = \frac{C_o V}{A} \tag{2.2}$$

where A is the electrode area. The plot of P versus E gives a hysteresis loop of a ferroelectric material.

In the present work, an ac field at frequency 100 Hz was applied to the film sample as shown in Figure 2.9. The top electrode of the sample was connected to the ground while the bottom electrode was connected to the applied field. The ac field was increased from 1.5 MV/m, in a step of 3.0 MV/m, until a saturated hysteresis loop was obtained. The resulting polarization orientation of the sample was determined by the last half cycle of the ac field, i.e. pointing to the bottom electrode. Figure 2.10 shows the hysteresis loop of a PZT film with 10% excess lead and annealed at 650°C for 1 hour. The thickness of the film is 2 μm. From the hysteresis loop, the remanent polarization P_r of the film was determined to be 19.9 $\mu C/cm^2$ and the coercive voltage was 4.0 V. The other PZT films with various amounts of excess lead and annealed at various temperatures exhibit similar polarization hysteresis loops, and have similar values of the remanent polarization and coercive fields. These indicate that the PZT films have good ferroelectric properties. In the next chapter, their piezoelectric properties will be discussed.

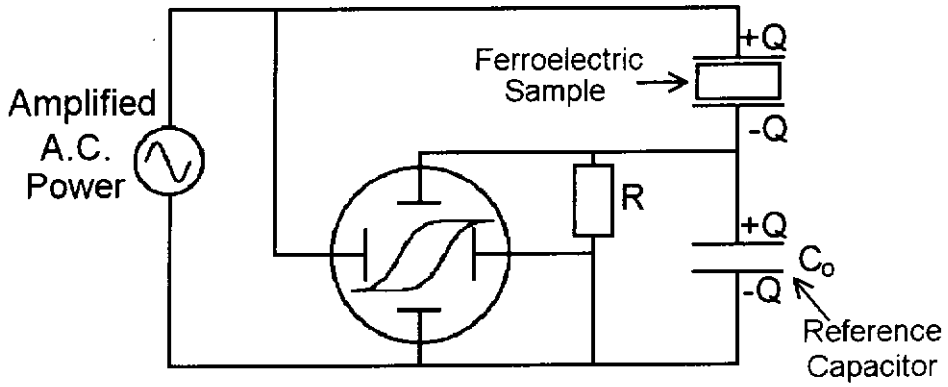

Fig. 2.8 Schematic circuit of Sawyer-Tower bridge for the observation of P-E characteristics in ferroelectrics (after Sawyer and Tower [Sawyer and Tower, 1930]).

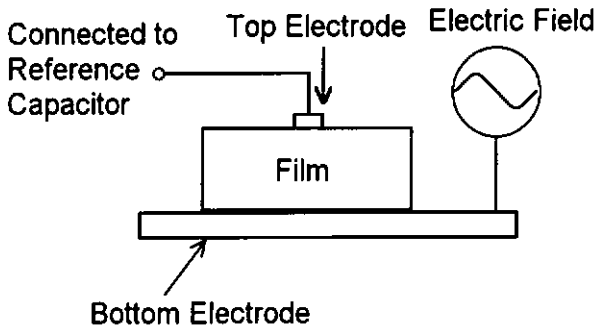

Fig. 2.9 Schematic diagram of the configuration of sample for hysteresis measurement. The electric field was applied to the bottom electrode of the film sample, while the top electrode was connected to the reference capacitor inside the Sawyer-Tower bridge.

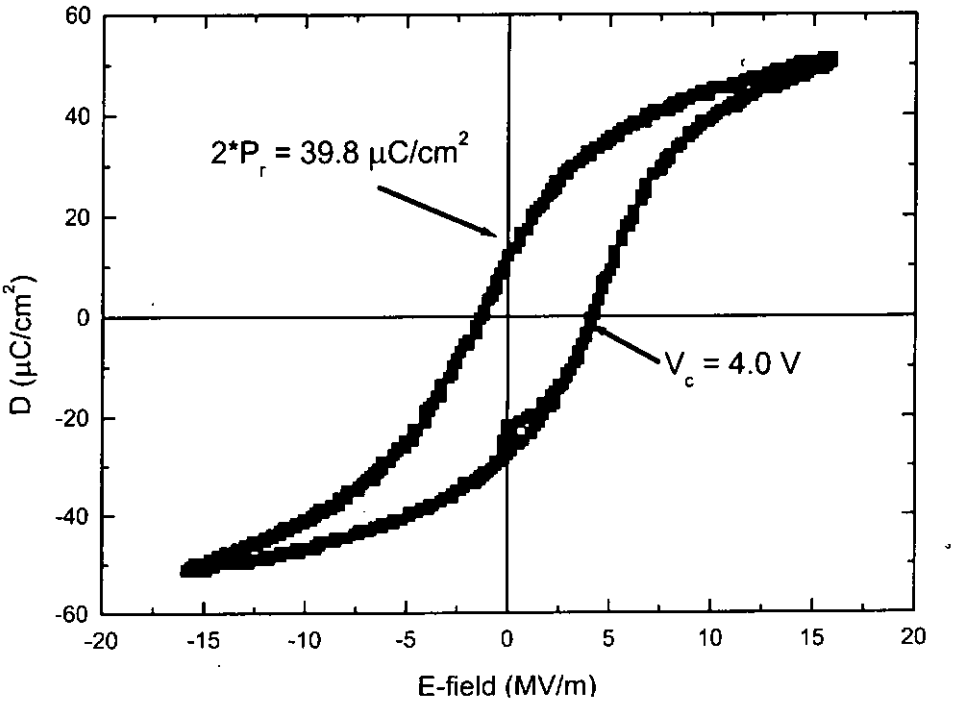

Fig. 2.10 Polarization hysteresis loop measurement of a PZT thin film with 10% of excess lead. The thickness of the film is 2 μm and the film is annealed at 650°C for 1 hour.

Chapter Three
Measurements of Longitudinal and Transverse Piezoelectric Coefficients

3.1 Measurement of Longitudinal Piezoelectric Coefficient

3.1.1 Piezoelectric Constitutive Equations

As mentioned in Chapter 1, the piezoelectric coefficient is an important parameter in designing micro-electromechanical devices. Therefore, understanding the fundamental piezoelectricity is necessary. The definitions for the piezoelectric effects have been introduced in Chapter 1. The basic piezoelectric action can be described by a set of piezoelectric constitutive equations, in tensor notation, as [Xu, 1991, p.26]:

$$D_i = d_{ijk} T_{jk} + \varepsilon_{ij} E_j \tag{3.1}$$

$$S_{ij} = s^E_{ijkl} T_{kl} + d_{ijk} E_k \tag{3.2}$$

where D_i is the electric displacement, E_i is the electric field, T_{ij} is the stress, S_{ij} is the elastic strain, d_{ijk} is the piezoelectric coefficient, ε_{ij} is the permittivity, s^E_{ijkl} is the elastic compliance at constant electric field, and $i, j, k, l = 1, 2, 3$.

The piezoelectric constitutive equations can also be written in matrix notation:

$$D_i = d_{ip}T_p + \varepsilon_{ij}E_j \tag{3.1}$$

$$S_p = s^E_{pq}T_q + d_{pi}E_i \tag{3.2}$$

where $i, j = 1, 2, 3$ and $p, q = 1, 2, 3, 4, 5, 6$, and the following scheme is used to replace the subscripts:

Tensor Notation (ij)	11	22	33	23, 32	13, 31	12, 21
Matrix Notation (pq)	1	2	3	4	5	6

The subscript $i = 1, 2, 3$ denotes the x_1, x_2 and x_3 directions; while the subscript $p = 1, 2, 3$ denotes the longitudinal components and $p = 4, 5, 6$ denotes the shear components. The definitions for the piezoelectric effects (Equations 1.1 – 1.3) are written in matrix notation. By using the matrix notation, the high ranked tensors can be written as a matrix for the ease of calculation. For example, the third ranked tensor d_{ijk} can be written as d_{ip} which is a 3×6 matrix, while the fourth ranked tensor s^E_{ijkl} can be written as s^E_{pq} which is a 6×6 matrix.

3.1.2 Effective Longitudinal Piezoelectric Coefficient of Thin Films

In Chapter 1, the piezoelectric coefficients for the direct and converse piezoelectric effects have been defined as Equations 1.1 and 1.2. Measurement of the longitudinal piezoelectric coefficient can be carried out based on either the direct or the converse piezoelectric effects. For the measurement based on the converse effect (Equation 1.2), an electric field is applied to the sample and the induced strain is measured. However, if

the sample is in thin film form, correction has to be added.

In early 1990's, Royer *et al.* found that the observed d_{33} value of a thin film sample is different from that of a bulk sample [Royer and Kmetik, 1992]. They suggested that it was caused by the difference in boundary conditions between the thin film and bulk samples. For a bulk sample, when an electric field is applied, it can deform freely in directions both parallel (due to the converse piezoelectric effect) and normal (due to the Poisson effect) to the electric field. However, for a thin film sample, the boundary condition is different. The thin film is deposited on a substrate, and hence it is clamped by the substrate in such a way that it cannot deform freely in the lateral direction. The effect of the lateral stresses imposed on the film by the substrate will cause the observed value of the piezoelectric coefficient different from the true value. This effect is called the substrate clamping effect. Royer *et al.* [Royer and Kmetik, 1992] suggested that the error caused by the substrate clamping effect could be determined. They considered the following piezoelectric constitutive equation, in matrix notation:

$$S_p = s^E_{pq} T_q + d_{pi} E_i \tag{3.2}$$

where $i = 1, 2, 3$ and p and $q = 1, 2, 3, 4, 5, 6$. If the thin film sample is completely clamped by the substrate, no strain can be induced along x_1 and x_2 directions at the interface between the film and the substrate. Therefore, the strain components S_1, S_2, S_6 are equal to zero. If the measurement is carried out at a frequency well below the resonance frequency of the sample, these assumptions are valid in the whole thickness of the sample. Since the film sample is only laterally clamped by the substrate, there is no stress at the free surfaces of the sample (i.e. $T_3 = T_4 = T_5 = 0$). For the application of an electric field along the thickness direction of the film sample, $E_1 = E_2 = 0$; and Equation

3.2 becomes:

$$S_p = s_{p1}^E T_1 + s_{p2}^E T_2 + s_{p6}^E T_6 + d_{3p} E_3 \tag{3.3}$$

For a polarized polycrystalline ferroelectric thin film, it has the symmetry the same as the point group 6_{mm}. The matrices of the material properties for various symmetries have been reported previously [Sirotin, 1982; Lines, 1979; Nye, 1985; Xu, 1991]. The matrices of the compliance and piezoelectric coefficient for the 6_{mm} (Wurtzite) symmetry is given as:

$$s^E = \begin{pmatrix} s_{11}^E & s_{12}^E & s_{13}^E & 0 & 0 & 0 \\ s_{12}^E & s_{11}^E & s_{13}^E & 0 & 0 & 0 \\ s_{13}^E & s_{13}^E & s_{33}^E & 0 & 0 & 0 \\ 0 & 0 & 0 & s_{44}^E & 0 & 0 \\ 0 & 0 & 0 & 0 & s_{44}^E & 0 \\ 0 & 0 & 0 & 0 & 0 & 2\left(s_{11}^E - s_{12}^E\right) \end{pmatrix} \tag{3.4}$$

$$d = \begin{pmatrix} 0 & 0 & d_{31} \\ 0 & 0 & d_{31} \\ 0 & 0 & d_{33} \\ 0 & d_{15} & 0 \\ d_{15} & 0 & 0 \\ 0 & 0 & 0 \end{pmatrix} \tag{3.5}$$

Accordingly, Equation 3.3 can be expressed as:

$$S_1 = s_{11}^E T_1 + s_{12}^E T_2 + d_{31} E_3 = 0 \tag{3.6a}$$

$$S_2 = s_{12}^E T_1 + s_{11}^E T_2 + d_{31} E_3 = 0 \tag{3.6b}$$

$$S_3 = s_{13}^E \left(T_1 + T_2\right) + d_{33} E_3 \tag{3.6c}$$

$$S_6 = 2(s_{11}^E - s_{12}^E) T_6 = 0 \tag{3.6d}$$

By adding Equations 3.6a and 3.6b, it gives:

$$S_1+S_2 = \left(s_{11}^E + s_{12}^E\right)T_1 + \left(s_{11}^E + s_{12}^E\right)T_2 + 2d_{31}E_3$$

$$= \left(s_{11}^E + s_{12}^E\right)\left(T_1 + T_2\right) + 2d_{31}E_3 = 0 \qquad (3.7)$$

hence

$$\left(T_1 + T_2\right) = -\frac{2d_{31}E_3}{s_{11}^E + s_{12}^E} \qquad (3.8)$$

Substituting Equation 3.8 into Equation 3.6c, it has

$$S_3 = s_{13}^E\left(-\frac{2d_{31}E_3}{s_{11}^E + s_{12}^E}\right) + d_{33}E_3$$

$$= \left(d_{33} - \frac{2s_{13}^E d_{31}}{s_{11}^E + s_{12}^E}\right)E_3 \qquad (3.9)$$

Therefore, the observed piezoelectric coefficient $d_{33}^{'}$ (or effective piezoelectric coefficient) for a thin film completely clamped on a substrate is given as:

$$d_{33}^{'} = \frac{S_3}{E_3} = d_{33} - \frac{2s_{13}^E}{s_{11}^E + s_{12}^E}d_{31} \qquad (3.10)$$

For a PZT thin film, s_{11}^E is positive, s_{12}^E and s_{13}^E are negative and d_{31} is also negative [Auld, 1990, p. 373-375]. Therefore, the observed $d_{33}^{'}$ value for a thin film is smaller than the observed d_{33} for a bulk sample.

3.1.3 Measurement Setup - Single Beam Laser Interferometer

A number of experimental setups have been developed for the d_{33} measurement and have been described in Chapter 1. In the present study, the effective longitudinal

piezoelectric coefficient $d_{33}^{'}$ was measured based on the converse piezoelectric effect by using a Mach-Zehnder type heterodyne (single beam) laser interferometer (SH-120, B.M. Industries, France). The schematic diagram of the experimental setup is shown in Figure 3.1.

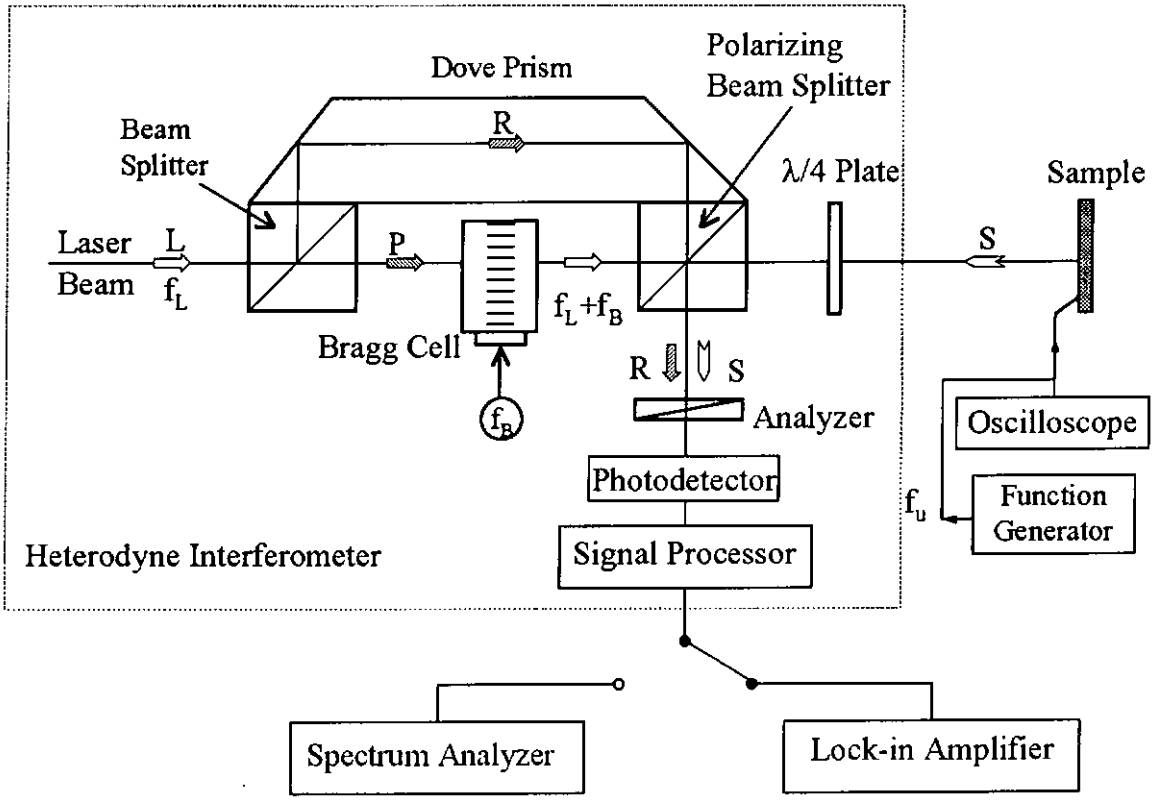

Fig. 3.1 Schematic diagram of the experimental setup for the d_{33} measurement.

A function generator (HP 8116A, Hewlett-Packard) was used to apply an ac field across the film sample, and a digital storage oscilloscope (HP 54645A, Hewlett-Packard) was used to measure the exact voltage applied to the sample. The surface displacement of the film sample was measured using the single beam laser interferometer. The He-Ne laser in the interferometer produces a linearly polarized laser beam L at frequency f_L and wavelength λ_L = 632.8 nm. The complex amplitude of the laser beam can be written as:

$$L = l\exp(i2\pi f_L t) \tag{3.11}$$

where l is the amplitude of the laser beam L and t is time. The beam L is split into a reference beam R and a probe beam P by a beam splitter. The reference beam R is directed through a Dove prism, while the probe beam P transmits through a Bragg cell located between two beam splitters. The complex amplitude of the reference beam R can be written as:

$$R = r\exp(i2\pi f_L t) \tag{3.12}$$

where r is the amplitude of the reference beam R. The frequency of the probe beam P is shifted by f_B (70 MHz) in the Bragg cell. P is then directed to the sample. Upon reflection on the sample, the probe beam (now labeled as S) is phase modulated by the surface displacement of the sample:

$$S = s\exp[i(2\pi f_L + 2\pi f_B)t + \phi(t)] \tag{3.13}$$

where s is the amplitude of the phase modulated beam S and

$$\phi(t) = 2k_L A\sin(2\pi f_A t) \tag{3.14}$$

where $k_L = \frac{2\pi}{\lambda_L}$, f_A and A are the vibrating frequency and amplitude of the surface displacement of the sample, respectively.

Both the beams R and S are directed into a photodetector. The interference of the beams R and S on the photodetector delivers a current I at frequency f_B, phase modulated by the surface displacement of the sample:

$$I \propto \cos[2\pi f_B t + 2k_L A\sin(2\pi f_A t)] \tag{3.15}$$

Half of the current I is then directed out for the measurement, while the other half is directed to a signal processor in which the high frequency (f_B) component of the current is

filtered and a signal d proportional to the surface displacement is yielded.

$$d \propto \sin(\phi(t)) \tag{3.16}$$

In the present work, a spectrum analyzer (HP 3589A, Hewlett-Packard) was used to measure the frequency components of the current I, and a lock-in amplifier (SR830 DSP, Stanford Research Systems) was used to measure the amplitude of the filtered signal d. For the current I, it can be expanded into a Bessel development:

$$I \propto \mathrm{Re}\left\{\exp(i2\pi f_B t)\left[J_o\left(\frac{4\pi A}{\lambda_L}\right) + 2iJ_1\left(\frac{4\pi A}{\lambda_L}\right)\sin(2\pi f_A t) + 2iJ_2\left(\frac{4\pi A}{\lambda_L}\right)\sin(4\pi f_A t) + \ldots\right]\right\} \tag{3.17}$$

If A is small compared to λ_L, the ratio of the amplitudes of the current components at f_B and $f_B \pm f_A$ can be approximated as:

$$\frac{J_o\left(\frac{4\pi A}{\lambda_L}\right)}{J_1\left(\frac{4\pi A}{\lambda_L}\right)} \cong \frac{\lambda_L}{2\pi A} \tag{3.18}$$

where J_o and J_1 are the Bessel functions of the zeroth and the first order, respectively. Therefore, by the measurement of the amplitudes of the current components (in dBm) at f_B (A_0) and $f_B \pm f_A$ (A_1) (Figure 3.2), the displacement amplitude can be calculated as follows:

$$20\log\left[\frac{\left|J_o\left(\frac{4\pi A}{\lambda_L}\right)\right|}{\left|J_1\left(\frac{4\pi A}{\lambda_L}\right)\right|}\right] = A_o - A_1 = 20\log\left(\frac{\lambda_L}{2\pi A}\right), \tag{3.19}$$

and hence

$$A = \frac{\lambda_L}{2\pi 10^{\left(\frac{A_o - A_1}{20}\right)}} \tag{3.20}$$

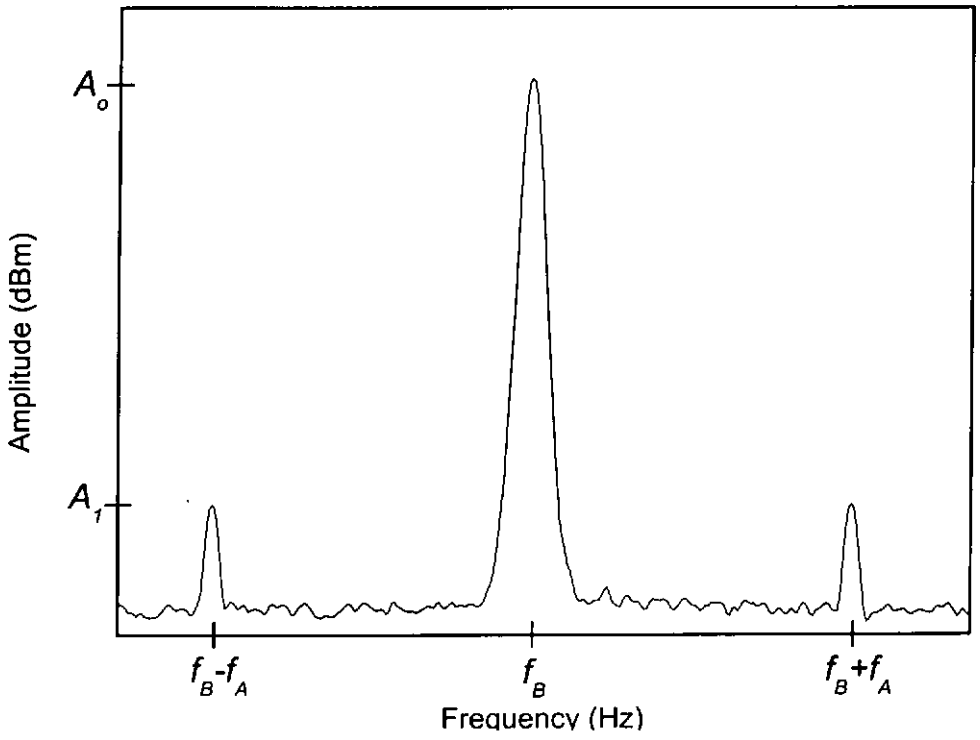

Fig. 3.2 Frequency spectrum recorded by a spectrum analyzer.

Similarly, if the surface displacement A is small compared to λ_L, the filtered signal d can be expressed as:

$$d \propto \frac{4\pi}{\lambda_L} A \tag{3.21}$$

In the present work, a PZT ceramic sample (PKI 552, Piezo Kinetics, Inc) was used to calibrate the observed amplitude of the signal d to the surface displacement A, and the corresponding calibration curve is shown in Figure 3.3. The thickness of the sample was 2 mm. An ac field with a frequency of 15 kHz and an amplitude ranging from 25×10^{-6} MV/m to 250×10^{-6} MV/m was applied to the sample. The applied ac field was smaller than the coercive field of the sample (0.8 MV/m, provided by Piezo Kinetics, Inc.). The surface displacement of the sample A was determined from the current components at f_B and $f_B\pm f_A$ using the spectrum analyzer, while the voltage of the signal d was measured using the lock-in amplifier.

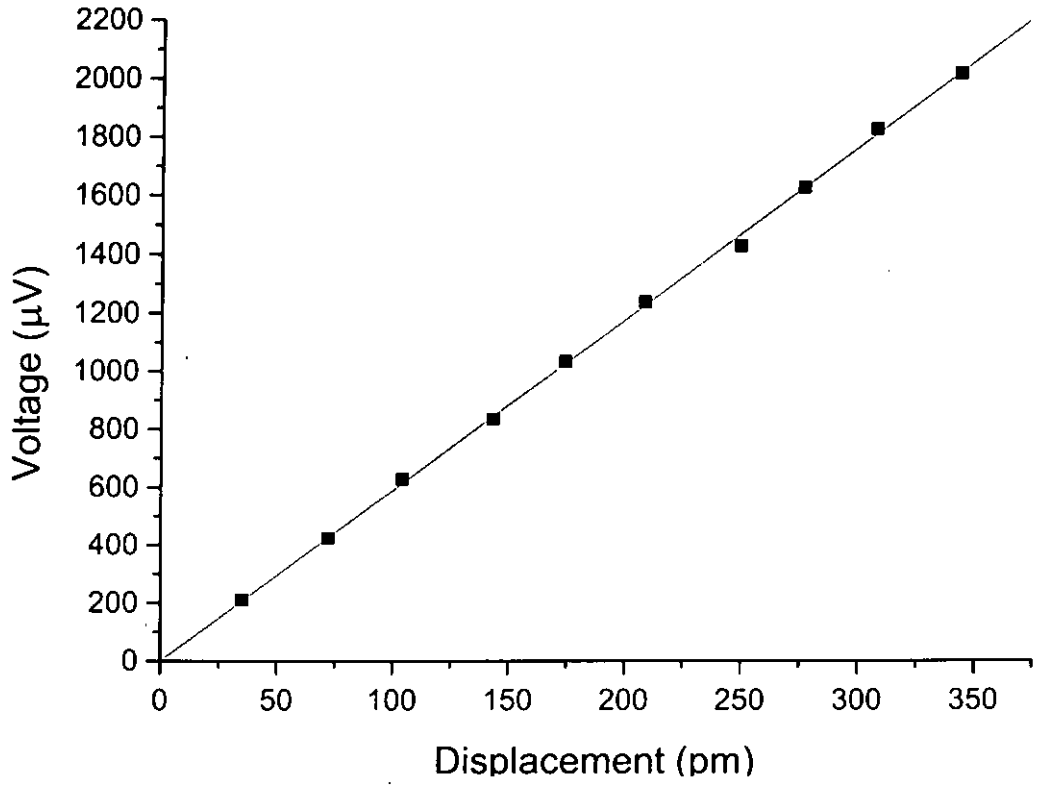

Fig. 3.3 Calibration curve of the voltage measured using the lock-in amplifier versus the surface displacement measured using the spectrum analyzer.

It has been noted that, for the measurement of small surface displacement using the spectrum analyzer, the signals corresponding to the current components at $f_B \pm f_A$ are very small and often comparable to the background noise; hence the measurement becomes difficult and inaccurate. Therefore, in the present work, the surface displacement of the thin film, in the order of 10^{-10}m, was calculated from the observed voltage of the filtered signal d with the use of the calibration curve (Figure 3.3). Accordingly, the effective piezoelectric coefficient $d_{33}^{'}$ (Equation 3.10) was calculated as:

$$d_{33}^{'} = \frac{S_3}{E_3} = \frac{A/t}{V/t} = \frac{A}{V} \tag{3.22}$$

where V is the voltage applied to the sample and t is the thickness of the sample.

3.1.4 Method for Elimination of Substrate Bending

Besides the clamping effect, there is another important effect, bending effect, caused by the tight adhesion of the film on the substrate. When an electric field is applied along the thickness direction ($\hat{3}$) of a film sample, there is not only change of the film thickness due to the piezoelectric effect, but also change of the lateral dimensions of the film induced by the Poisson effect. If the film sample is tightly adhered on a substrate, the lateral deformation is restricted (causing the clamping effect) and hence there are lateral stresses imposed on the substrate by the film. If the substrate is not tightly fixed to a holder, these lateral stresses will bend the film/substrate as shown in Figure 3.4. Since the single beam laser interferometry technique measures only the displacement of the front

surface of the film sample which is the sum of the thickness change (S_3) and the bending (ΔL_b), the resulting value of $d_{33}^{'}$ becomes larger. In the present work, instead of using a double beam laser interferometry technique to eliminate the error caused by the substrate bending, the substrate is tightly fixed to a holder to ensure no bending of the substrate occurred.

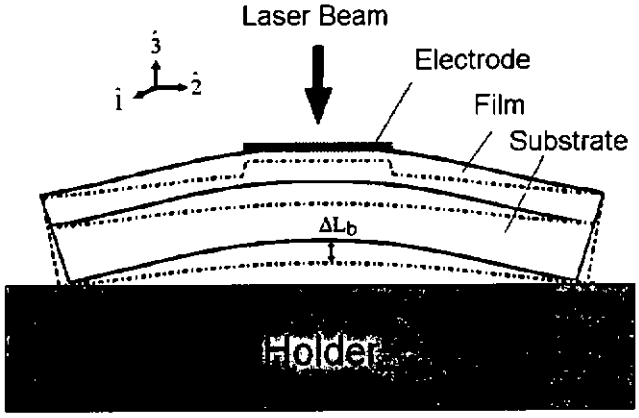

Fig. 3.4 Bending of the substrate in the d_{33} measurement.

Figure 3.5 shows schematically how the sample (film/substrate) is fixed tightly on a holder in the present work. The sample was glued on a printed circuit board (PCB) which is much larger and thicker than the sample. One of the functions of the PCB is to provide a stiff platform in order to suppress the bending. The other function is to provide enough spaces for wiring. Since the diameter of the electrode is 1 mm, it is quite difficult to apply both electrical contact (with some test fixture) and optical contact (the diameter of the laser beam is about 0.4 mm) on the top electrode at the same time. The top electrode is hence electrically connected to a large electrode pad on the PCB through a thin wire (diameter = 40 μm) using a wire-bonder (AB510, ASM). The electric field is then applied on the electrode pads. In order to determine an effective method to glue the

sample to the PCB, four adhesive materials: double sides tape, quick dry silver paint (G3691, AGAR Scientific Ltd.), mounting wax (Mounting wax, Gatan) and epoxy resin (Araldite, produced by Ciba-Geiby), were used; and the distribution of the surface displacement across the sample had been measured to examine if the bending was completely suppressed.

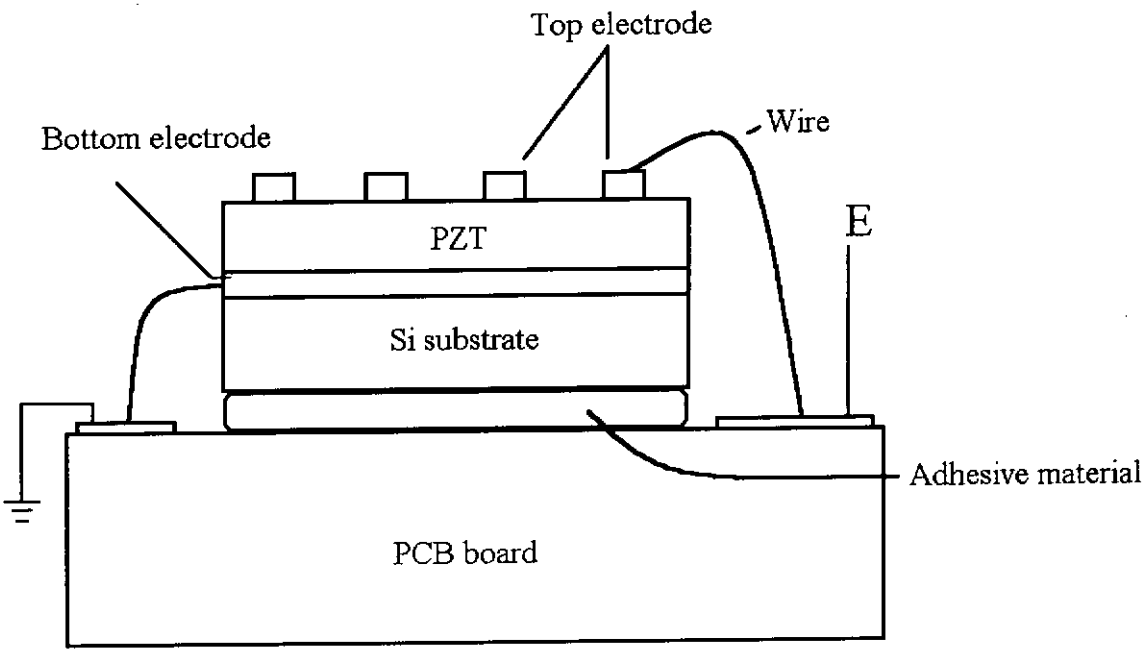

Fig. 3.5 Sample fixture for the d_{33} measurement.

3.2 Measurement of Effective Transverse Piezoelectric Coefficient

Besides the longitudinal piezoelectric coefficient d_{33}, the transverse piezoelectric coefficient e_{31} is another important parameter for designing micro-electromechanical systems (MEMS). In the present work, e_{31} of thin films is measured based on the direct piezoelectric effect, and the schematic diagram of the experimental setup is shown in

Figure 3.6. In the measurement, a rectangular sample (film/substrate) is clamped at one end while the other end is left free. A piezoelectric actuator is used to apply a dynamic force to bend the sample. A longitudinal strain is then generated along the length of the sample ($\hat{1}$); and charges are induced on the film surface as a result of the direct piezoelectric effect. Since the film is clamped on the substrate only, it can deform freely along the thickness direction ($\hat{3}$). In addition, the film also deforms along the width direction ($\hat{2}$) following the Poisson contraction of the substrate (detailed discussion is given below). Therefore, the observed transverse piezoelectric coefficient (or effective transverse piezoelectric coefficient) $e_{31,f}$ is different from the usual transverse piezoelectric coefficient e_{31}. In the definition of e_{31} ($=\partial D_3/\partial S_1$), only a dimensional change in the $\hat{3}$ direction is allowed.

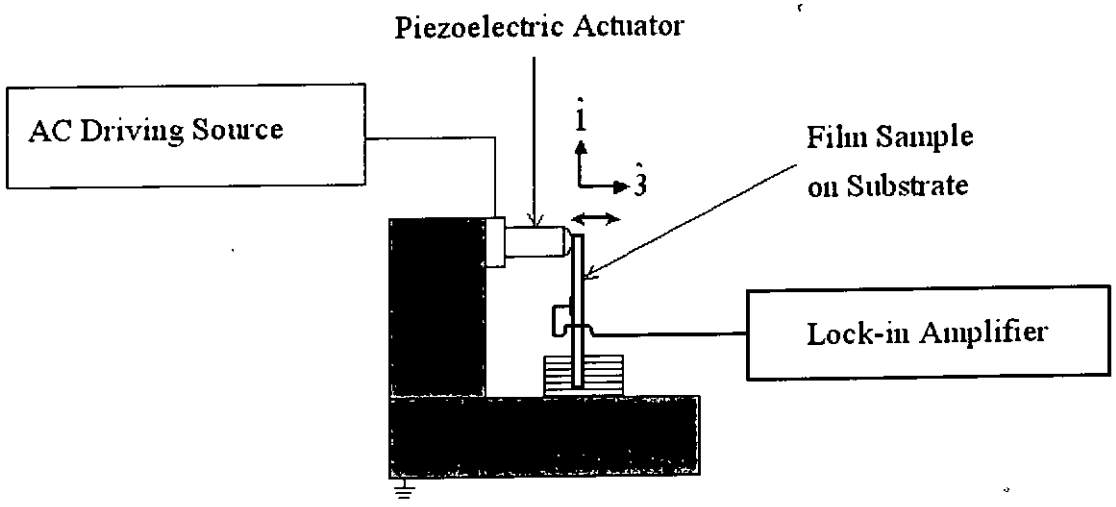

Fig. 3.6 Experimental set-up for the $e_{31,f}$ measurement.

As mentioned, the rectangular sample is bent in order to generate a longitudinal strain or stress along the length of the sample ($\hat{1}$) (Figure 3.7). The constitutive equations for the system are then:

$$D_i = d_{ip}T_p + \varepsilon_{ij}E_j \tag{3.23}$$

$$S_p = s^E_{pq}T_q + d_{pi}E_i \tag{3.24}$$

where $i, j = 1, 2, 3$ and $p, q = 1, 2, 3, 4, 5, 6$. Since the film is clamped on the substrate and can deform freely along the $\hat{3}$ direction, $T_3 = T_4 = T_5 = 0$. No external electric field is applied in the measurement, $E_1 = E_2 = E_3 = 0$. Therefore, for a polarized polycrystalline ferroelectric thin film with the 6_{mm} symmetry (Equations 3.4 and 3.5), the constitutive equation becomes:

$$D_3 = d_{31}T_1 + d_{31}T_2 \tag{3.25}$$

$$S_1 = s^E_{11}T_1 + s^E_{12}T_2 \tag{3.26a}$$

$$S_2 = s^E_{12}T_1 + s^E_{11}T_2 \tag{3.26b}$$

$$S_3 = s^E_{13}T_1 + s^E_{13}T_2 \tag{3.26c}$$

By adding Equations 3.26a and 3.26b, it gives:

$$T_1 + T_2 = \frac{S_1 + S_2}{s^E_{11} + s^E_{12}} \tag{3.27}$$

then substituting Equation 3.27 into 3.25,

$$D_3 = \frac{S_1 + S_2}{s^E_{11} + s^E_{12}} d_{31} \tag{3.28}$$

Hence the effective transverse piezoelectric coefficient $e_{31,f}$ can be determined as:

$$e_{31,f} = \frac{D_3}{(S_1 + S_2)} = \frac{d_{31}}{s^E_{11} + s^E_{12}} \tag{3.29}$$

If the thickness of the film is much smaller than that of the substrate, it can be assumed that the strains S_1 and S_2 are the same throughout the thickness of the film, and their values are identical to the strains of the substrate. Therefore, S_2 can be linked to S_1

by the Poisson's ratio v_c of the substrate material, i.e.

$$S_2 = -v_c S_1 \tag{3.30}$$

Then, Equation 3.29 becomes

$$e_{31,f} = \frac{D_3}{(1 - v_c)S_1} \tag{3.31}$$

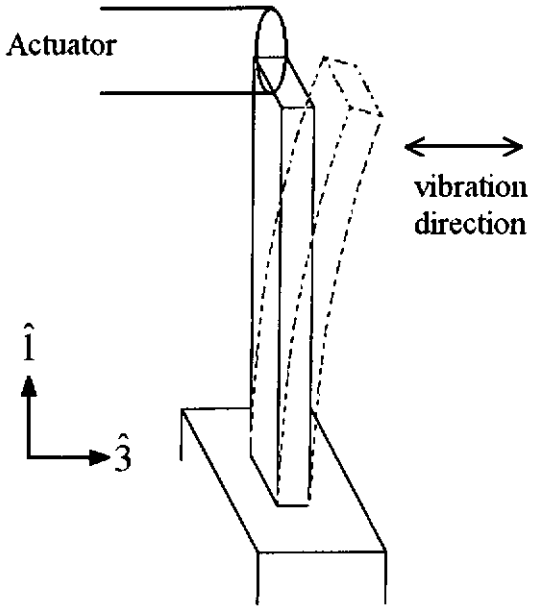

Fig. 3.7 The rectangular sample is bent by the application of a force at the free end using a multilayer piezoelectric actuator.

For a rectangular sample with the end clamped (or named cantilever, Figure 3.8), the deflection in the $\hat{3}$ direction z as a function of x (the position along the $\hat{1}$ direction) is described by [Timoshenko *et al.*, 1970]:

$$z = \frac{F}{6YI}\left(3\ell x^2 - x^3\right), \tag{3.32}$$

$$I = \frac{bh^3}{12} \tag{3.33}$$

where F is the force applied to bend the cantilever by the actuator, ℓ, b and h are the length, width and thickness of the cantilever, respectively, and Y is the Young's modulus of the substrate. At the free end of the cantilever, i.e. $\ell = x$, the deflection z_ℓ is maximum and equals to:

$$z_\ell = \frac{Fl^3}{3YI} \tag{3.34}$$

The radius of curvature R of the cantilever can be approximated as:

$$\frac{1}{R} = \frac{d^2z}{dx^2} \tag{3.35}$$

By taking the second derivative of Equation 3.32, Equation 3.35 becomes

$$\frac{1}{R} = \frac{F}{YI}(\ell - x) \tag{3.36}$$

By substituting Equation 3.34 into Equation 3.36, a general expression for the curvature is given as:

$$\frac{1}{R} = \frac{3z_\ell(\ell - x)}{l^3} \tag{3.37}$$

The strain S_1 at the surface of the cantilever is, therefore:

$$S_1 = \frac{h}{2R} = \frac{3hz_\ell(\ell - x)}{2\ell^3} \tag{3.38}$$

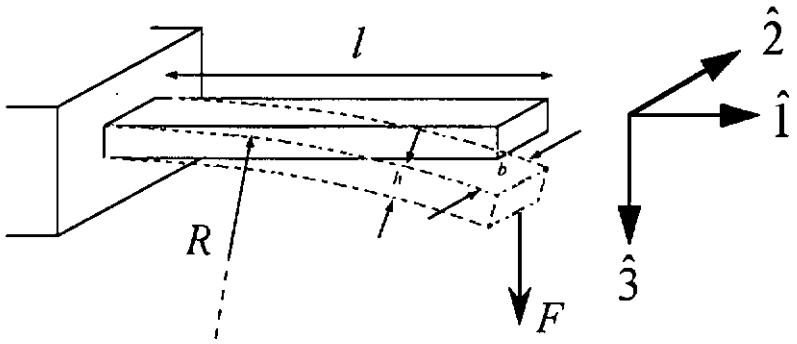

Fig. 3.8 Schematic diagram showing the bending of the cantilever. F is the force applied by the actuator, R is the radius of curvature of the cantilever, l is the length of the cantilever, b is the width of the cantilever and h is the thickness of the cantilever.

Due to the direct piezoelectric effect, charges Q are induced on the surface of the electrode of area A.

$$\begin{aligned} dQ &= D_3 \cdot dA \\ &= e_{31,f}(1-\upsilon_c)S_1 \cdot dA \\ &= \frac{3hz_\ell e_{31,f}(1-\upsilon_c)}{2\ell^3}(\ell - x)\cdot dA \end{aligned} \tag{3.39}$$

For a circular top electrode with its extremities located at x_0 and x_1 (Figure 3.9),

$$dA = 2\sqrt{r^2 - \kappa^2}\cdot dx \tag{3.40}$$

where $r = (x_1\text{-}x_0)/2$ is the radius of the top electrode, and

$$\kappa = x - \frac{x_0 + x_1}{2} \tag{3.41}$$

Therefore, the induced charges on the circular top electrode is given by:

$$dQ = \frac{3hz_\ell e_{31,f}(1-\upsilon_c)}{\ell^3}(\ell - x)\sqrt{r^2 - \kappa^2}\cdot dx \tag{3.42}$$

$$Q = \frac{3hz_\ell e_{31,f}(1-\upsilon_c)}{\ell^3}\int_{x_0}^{x_1}(\ell - x)\sqrt{r^2-\kappa^2}\cdot dx$$

$$= \frac{3hz_\ell e_{31,f}(1-\upsilon_c)}{\ell^3}\frac{\pi r^2}{2}\left[\ell - \frac{x_0+x_1}{2}\right] \tag{3.43}$$

Since a dynamic force at frequency f ($=\omega/2\pi$) is applied to bend the sample, the deflection at the free end z_ℓ and hence the induced charge Q are time varying at the same frequency, i.e.

$$Q(t) = \frac{3\pi r^2 hz_\ell e_{31,f}(1-\upsilon_c)}{2\ell^3}\left[\ell - \frac{x_0+x_1}{2}\right]\cdot e^{i\omega t} \tag{3.44}$$

Therefore, a current signal I (magnitude) is resulted:

$$I = \frac{dQ}{dt} = \frac{3\pi r^2 \omega hz_\ell e_{31,f}(1-\upsilon_c)}{2\ell^3}\left[\ell - \frac{x_0+x_1}{2}\right] \tag{3.45}$$

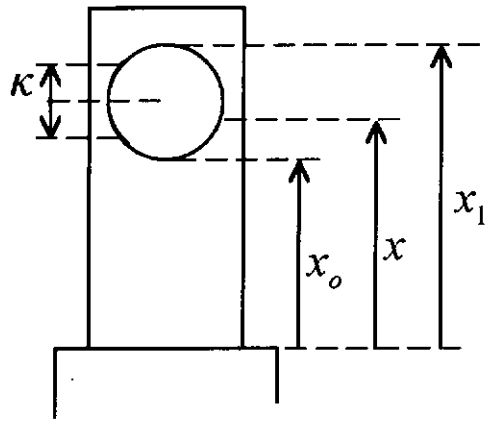

Fig. 3.9 Schematic diagram showing the position of a top circular electrode.

In the present work, a multilayer piezoelectric actuator (ASB003A, Tokin Inc.) was used to apply a dynamic force to bend the sample. The actuator was driven at a frequency f of 10 Hz using ac drive source which consists of a function generator (HP8116A,

Hewlett-Packard) and a power amplifier (BOP1000, KEPCO). The deflection at the end of the sample z_ℓ was measured using a photonic sensor (MTI-2000, Mechanical Technology Inc.). The current I induced on the circular top electrode was measured using a lock-in amplifier (SR830 DSP, Stanford Research Systems). Hence, the effective transverse piezoelectric coefficient $e_{31,f}$ was calculated from Equation 3.45.

Similar to the d_{33} measurement, the sample (film/substrate) is glued on a PCB (Figure 3.10). Since the top electrode is very small (diameter = 1 mm), the top electrode is electrically connected to a large electrode pad on the PCB through a thin wire (diameter = 40 μm) using a wire-bonder (AB510, ASM) for the ease of the measurement of the induced current. The thin wire is so long that it will not affect the bending of the cantilever.

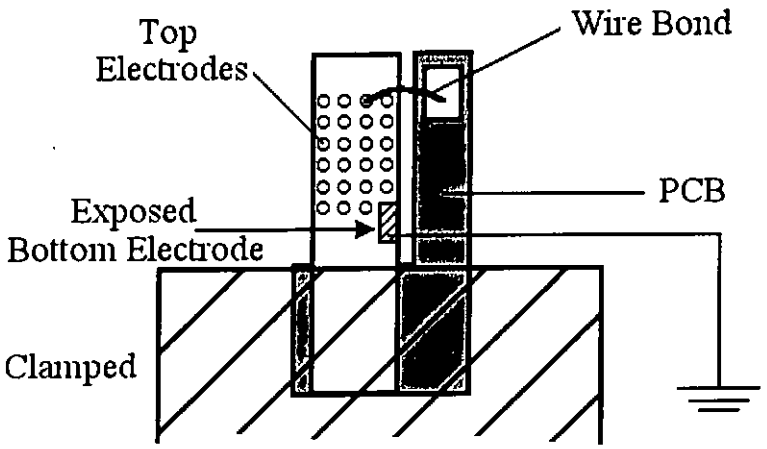

Fig. 3.10 The sample fixture for $e_{31,f}$ measurement. The top electrode is wire bonded to the electrode pad on the PCB for ease of collection of charge from the sample.

Chapter Four

Results and Discussion

4.1 Evaluation of the d_{33} and e_{31} Measurements

As-prepared piezoelectric materials do not exhibit any piezoelectric effect owing to the random orientation of the ferroelectric domains in the ceramics. Therefore, an external electric field is needed to align the domains to the field direction so as to induce the piezoelectricity of the sample (Figure 4.1). This process is called poling. In the present work, the samples are polarized at room temperature by increasing the magnitude of an external dc field in steps.

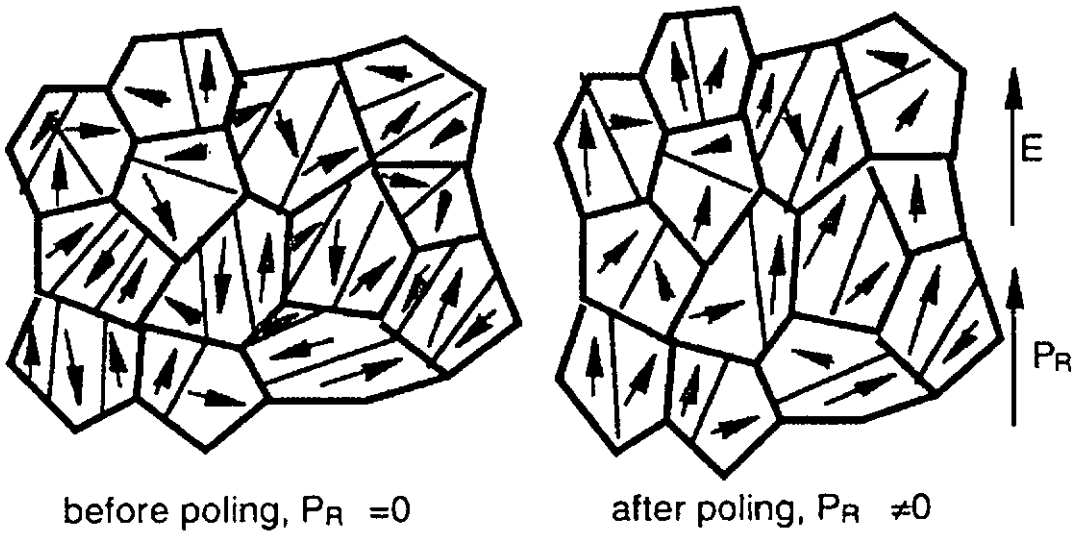

Fig. 4.1 A polycrystalline ferroelectric with random orientation of grains before poling; the remanent polarization P_R is equal to zero. After poling, the grains are aligned such that the P_R becomes non-zero.

The experimental setup for poling the PZT film samples is shown in Figure 4.2. The top electrode of the film is connected to the positive terminal of a dc supply (Griffin) while the bottom electrode is grounded. Poling of sample is conducted at room temperature. The poling field is increased in steps, with an increment of 1 MV/m; and the sample is polarized under each poling field for 3 min. A PZT film sample of thickness of 2 μm and with 10% excess lead is used for the evaluation of the d_{33} and e_{31} measurements. The maximum poling field is 10 MV/m. The effect of the poling field on the piezoelectric properties will be discussed in the next section.

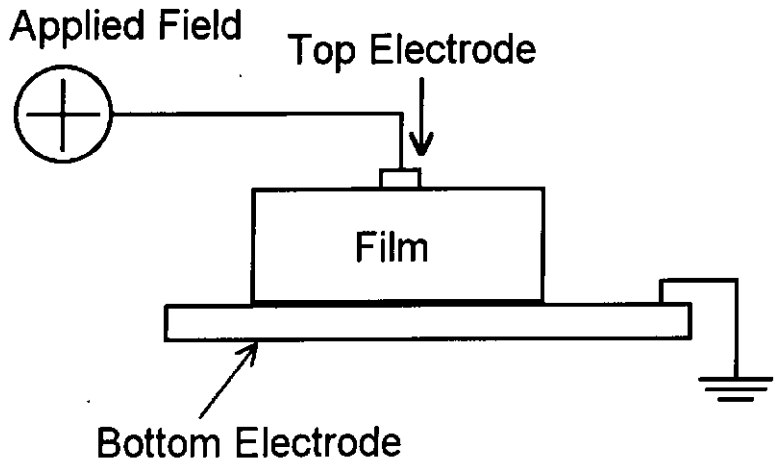

Fig. 4.2 A schematic diagram of the experimental setup for sample poling.

4.1.1 Effect of Adhesive Materials on the d_{33} Measurement

As mentioned in Chapter 3, in order to suppress bending of the substrate, the sample (film/substrate) is glued on a printed circuit board (PCB) which is much larger and thicker than the sample (Figure 3.5). If the substrate bends, the observed displacement will be the

sum of the thickness change of the film attributed to the piezoelectric effect and the displacement of the substrate due to bending. Hence the resulting $d_{33}^{'}$ value becomes inaccurate. In the present work, four adhesive materials: double-sided adhesive tape, quick dry silver paint (G3691, AGAR Scientific Ltd.), mounting wax (Mounting wax, Gatan) and epoxy resin (Araldite, produced by Ciba-Geiby), are used in order to determine an effective method to glue the sample.

Figure 4.3 shows the surface displacement of the film glued on the PCB using different adhesive materials as a function of the applied voltage. The film is annealed at 700°C for 1 hour. As shown in Figure 4.3, the relation between the displacement and the applied voltage is quite linear and passes through zero for all the samples, indicating that the applied voltage is not so large to exceed the linear region of the piezoelectric effect. It can be seen that the observed surface displacement of the polarized film is different when different adhesive materials is used. Since the double-sided adhesive tape is quite soft, it is believe that it cannot bond the sample tightly on the PCB such that the bending of the substrate cannot be effectively suppressed. As a result, the observed surface displacement is quite large. On the other hand, the silver paint after dried is quite stiff, the bending of the substrate can then be more effectively suppressed. It is shown by the decrease in the observed surface displacement, more than half of that for the film glued using adhesive tape. Mounting wax and mixed epoxy are the stiffest materials among the four adhesive materials; it is then believed that the bending of the substrate can be completely suppressed when these two materials are used. Therefore, as shown in Figure 4.3, the observed surface displacement for the film glued on the PCB using these materials are the smallest in the measurement voltage range. In the present work,

mounting wax was then used to glue the sample on the PCB. The other advantage of using mounting wax is that it becomes soft at 130°C, such that the sample can be easily detached from the PCB without damaging the PZT film. On the other hand, if epoxy is used, the sample can only be detached from the PCB at about 300°C. At such a high temperature, the PZT film may be depolarized and damaged.

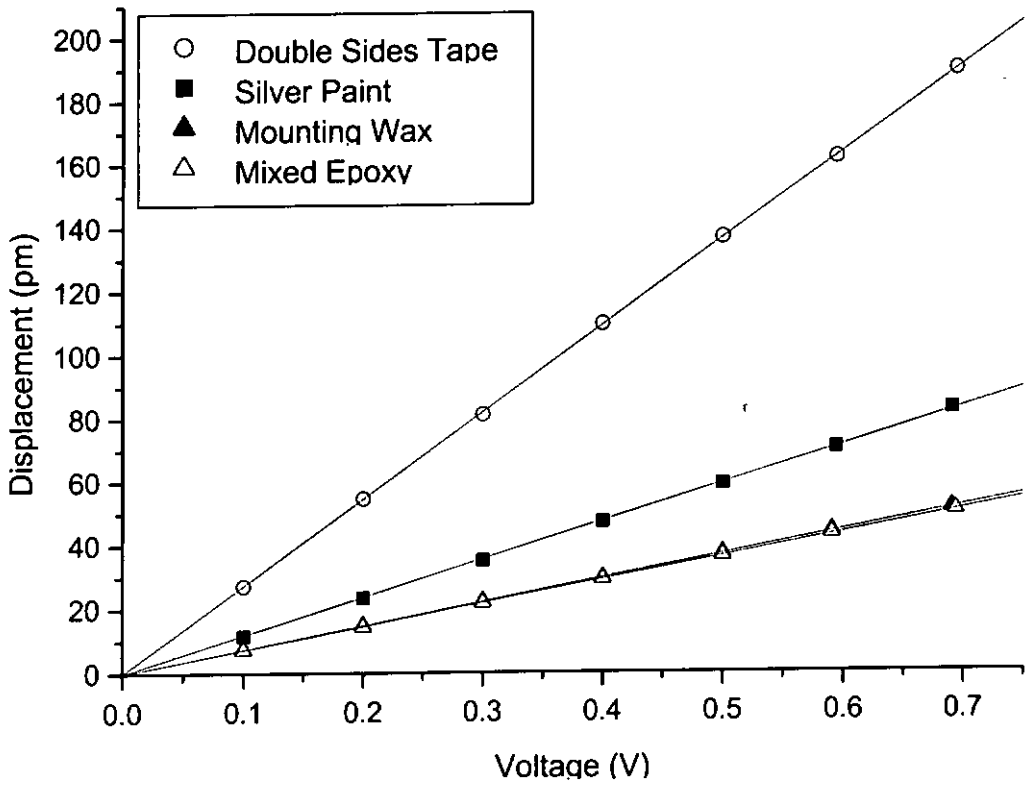

Fig. 4.3 Variation of the surface displacement with applied voltage for the PZT film glued on the PCB using different adhesive materials: double sides tape, quick dry silver paint, mounting wax and mixed epoxy.

4.1.2 Substrate Bending Effect on the d_{33} Measurement

Although the results in the last section suggest that the bending of the substrate should be effectively and completely suppressed by gluing the sample on the PCB with mounting wax, more evidence should be given to support the claim. If the substrate bends, it will deform in a convex shape as shown in Figure 3.4. As a result, the electrodes (reflecting the laser beam for the measurement) adjacent to the driving electrode (the electrode at which the external voltage is applied) will give a non-zero surface displacement. Therefore, by measuring the surface displacement at those electrodes, the substrate bending can be checked. Figure 4.4 shows the distribution of surface displacement across a PZT film glued on a PCB with mounting wax. The film is annealed at 650°C for 1 hour. A small electric field of magnitude 0.2 MV/m and frequency 15 kHz is applied at the driving electrode (as indicated by the dot lines in the figure). The center-to-center separation between the electrodes is 2 mm. As a result of the converse piezoelectric effect, the surface displacement at the driving electrode is quite large, about 30 pm. Beyond the driving electrode, the surface displacement decreases drastically, indicating that the substrate is successfully suppressed. It should be noted that the observed surface displacement at the adjacent electrodes is comparable to the experimental error of the single beam laser interferometer (more details will be given in the following section).

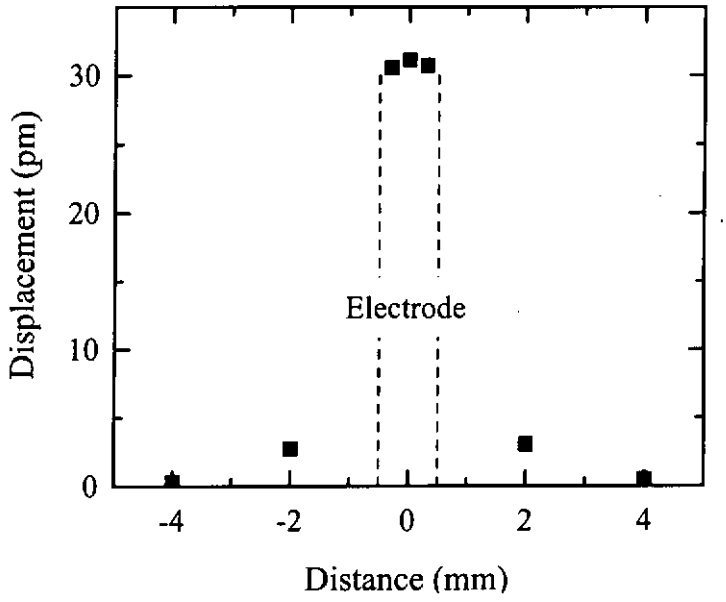

Fig. 4.4 Distribution of the surface displacement across the PZT film sample. The driving electrode (indicated by the dot lines) is located at centre.

4.1.3 Mechanical Resonance of the Film

Besides the substrate bending, the mechanical resonance of the film can also induce significant error in the d_{33} measurement. Therefore, the frequency of the driving voltage should be far below the mechanical resonant frequencies of the film. In order to check if any resonance of the film is excited in the measurement, the surface displacement of the PZT film at different driving frequencies is measured. Figure 4.5 shows the variation of the observed surface displacement of a PZT film sample in the frequency range of 10 kHz to 100 kHz. The film is annealed at 650°C for 1 hour. The amplitude of the applied ac

field is 0.2 MV/m. It should be noted that the surface displacement is measured by using the spectrum analyzer instead of the lock-in amplifier, since the calibration curve is frequency dependent (Figure 3.3; Section 3.1.3). It can be seen from Figure 4.5 that the surface displacement is almost constant in the frequency range of 10 to 100 kHz, indicating that the mechanical resonance of the film has not been excited.

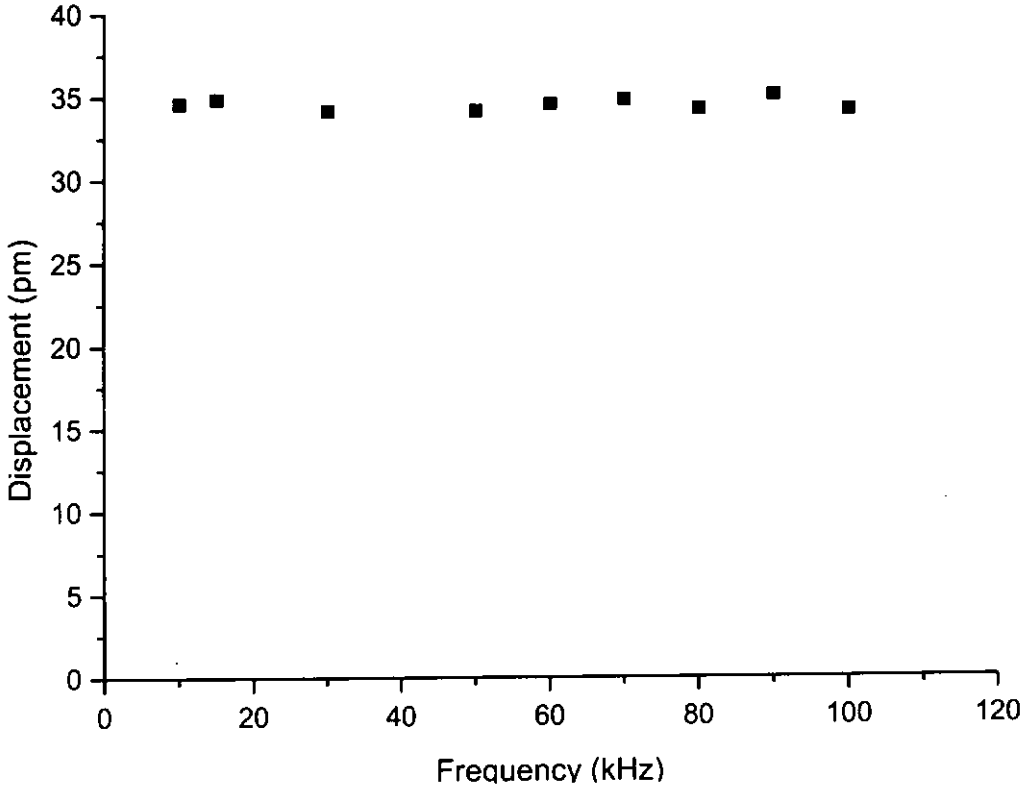

Fig. 4.5 The surface displacement of the PZT film at different driving frequencies. The film is of thickness of 2 μm, with 10% excess lead and annealed at 650°C for 1 hour.

Based on the above results, the d_{33} measurement should be free from any significant error. As a countercheck, the d_{33} of a PZT thin film is measured and compared with the literature values. The film is of thickness 2 μm, with 10% excess lead and annealed at 650°C for 1 hour. The frequency of the applied voltage is 15 kHz and the amplitude ranges from 0.1 V to 0.7 V (or 0.05 MV/m to 0.35 MV/m). Figure 4.6 shows the surface displacement as a function of applied voltage. It is seen that the piezoelectric response remains linearly in the range of applied voltage 0 – 0.7 V. As discussed in Section 3.13, the $d_{33}^{'}$ value is determined from the slope of the straight line (Equation 3.22). Accordingly, the observed $d_{33}^{'}$ value of the film is about 90 pm/V, which is comparable to the literature values of the PZT film with the same composition, 70 – 100 pm/V [Dubois *et al.*, 1999; Xu *et al.* 2001].

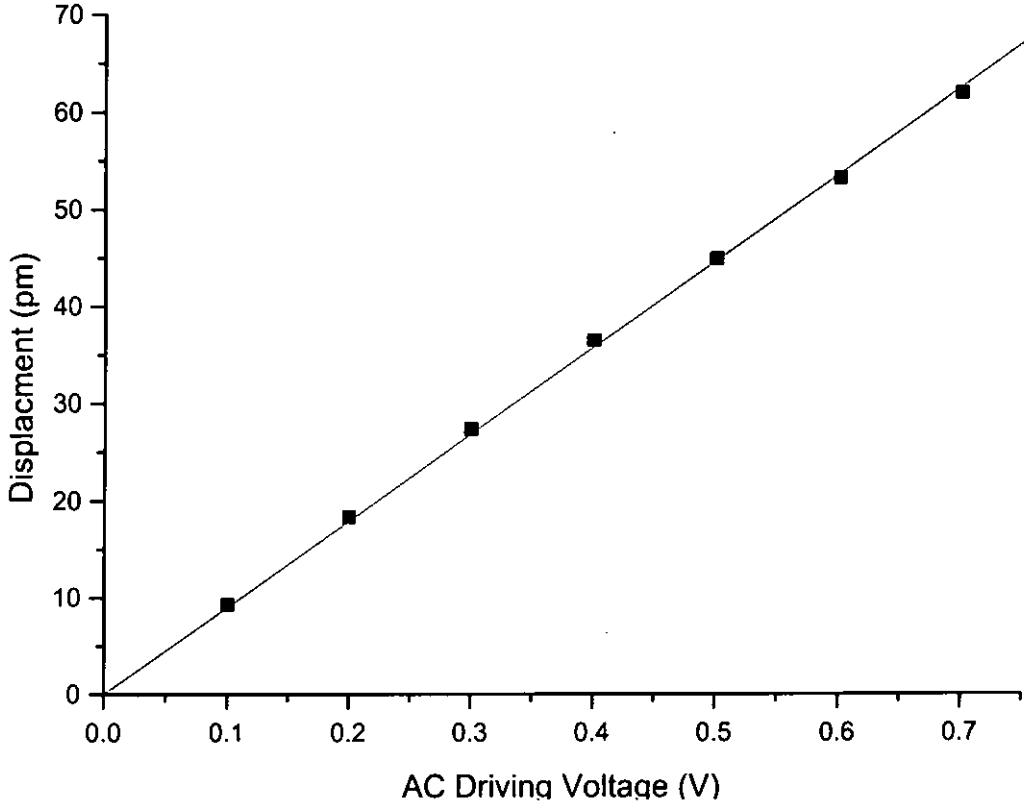

Fig. 4.6 Variation of the surface displacement with applied voltage for a PZT film. The PZT film is of thickness 2 μm, with 10% excess lead and annealed at 650°C for 1 hour.

4.1.4 Evaluation of the e_{31} Measurement

As a rough check of the e_{31} measurement, the $e_{31,f}$ value of a PZT film is measured and compared with the literature value. The PZT film is annealed at 650°C for 1 hour. Figure 4.7 (in linear scale) shows the induced current (I) as a function of the deflection at the free end (z_t) for the film with the electrode located at x = 7.9 mm (refer to Figure 3.9).

It can be seen that a linear relation between I and z_t is observed, and the straight line passes through the origin. This suggests that the measurement is in principle correct (refer to Equation 3.45) and free from any significant systematic errors. Using the Poisson ratio of silicon substrate $\nu_c = 0.172$ [Brantley, 1973] and Equation 3.45, the $e_{31,f}$ value is calculated to be 8.8 C/m^2. Since a number of observed values is used for the calculation (Equation 3.45), the resulting experimental error for the observed $e_{31,f}$ value is not small, about ±10% (details will be given in the following section). Taking into consideration of the experimental error, our result is quite close to the literature value of the PZT film with the same composition, 7 – 8 C/m^2 [Dubois *et al.*, 1999].

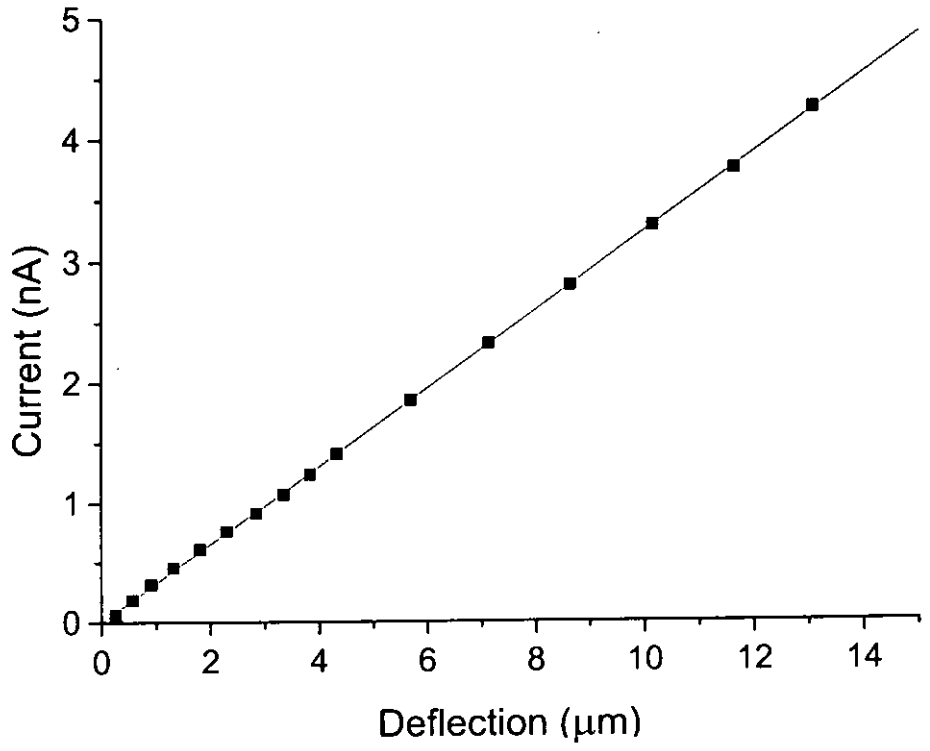

Fig. 4.7 Induced current as a function of the deflection at the free end of the cantilever for the PZT film. The PZT film is of thickness 2 μm, with 10% excess lead and annealed at 650°C for 1 hour.

In theory, the induced current changes with position x because of the different strain levels (Section 3.2); but the $e_{31,f}$ value does not. Therefore, as a further check of the measurement, the $e_{31,f}$ value at different x of a PZT film are measured and the results are listed in Table 4.1. The homogeneity of the film is verified by the d_{33} measurement. The PZT film is of thickness 2 μm and annealed at 650°C for 1 hour. As shown in Table 4.1, the observed $e_{31,f}$ values at different positions are almost the same (taking into consideration of the experimental error). This also suggests that the e_{31} measurement should be free from any significant systematic errors.

Table 4.1 The observed $e_{31,f}$ values at different positions of a PZT film. Position x is measured from the clamping edge of the cantilever (refer to Figure 3.9). The PZT film is of thickness 2 μm, with 10% excess lead and annealed at 650°C for 1 hour.

x (mm)	$e_{31,f}$ (C/m^2)
3.9	9.0
7.9	8.8
13.9	8.2

4.1.5 Experimental Errors in the d_{33} and e_{31} Measurement

Error always occurs in measurements, and can be defined as the difference between the measured and the true value (as per standard) [Nakra and Chaudhry (1985), p. 33]. The different types of errors can be broadly classified as systematic errors, instrument errors, loading errors, environmental errors and random errors. Systematic errors are those that tend to have the same magnitude and sign for a given set of conditions. It may

be noted that systematic errors can be corrected or eliminated by properly calibrating the instrument. Instrument errors are inherent in the instrument systems. These may be caused due to poor design/construction of the instrument. Besides, loading errors are usually not due to the instrument; it is caused by the act of the measurement on the physical system being tested. A common example is the introduction of an additional resistance in a circuit which may alter the circuit current by a significant amount. Other than these errors, there are some errors not caused by the instrument, which are environmental errors. Environmental errors are caused due to variation of conditions external to the measuring device, including the conditions in the area surrounding the instrument. The last one is random errors. These errors are caused due to random variation in the parameters or in the system of measurement. Such errors vary in magnitude and may be either positive or negative based on chance. This type of error can be detected by a lack of consistency in the measured values when the same input is imposed repeatedly on the instrument. Other than those errors, deviation from an accurate value can occur due to instrument and which is uncertainty. Due to the limitation of the apparatus, the smallest measurable unit of the apparatus is considered as the external estimate of uncertainty. For example, when a true input value of 100 V is given to a well-calibrated voltmeter, which has a resolution of 0.1 V, the expected voltmeter reading would obviously be 100 V. Now if the input voltage is increased or decreased in the range of 0.1 V, the voltmeter would still indicate 100 V as the instrument is unable to distinguish the change up to or below the resolution of the instrument. Therefore, it would be reasonable to say that the measured value of 100 V has the external estimate of uncertainty equal to ±0.1 V.

In the present work, the instruments involved in the measurements are properly calibrated and the experimental setup is carefully designed to eliminate any loading errors. All the measurements are conducted in almost the same environmental condition, so the environmental error is reduced to minimum. Therefore, the accuracy of the measurement could be estimated by considering only the external estimate of uncertainty.

If $U = f(x_1, x_2, x_3, \ldots, x_n)$, where U is a physical quantity, $x_1, x_2, x_3, \ldots, x_n$ are independent measurements, then the standard errors for U is [Nakra, B. C. and Chaudhry, K. K. (1985), p. 37]

$$s_U^2 = \left(\frac{\partial U}{\partial x_1}\right)^2 s_{x_1}^2 + \left(\frac{\partial U}{\partial x_2}\right)^2 s_{x_2}^2 + \ldots + \left(\frac{\partial U}{\partial x_n}\right)^2 s_{x_n}^2 \qquad (4.1)$$

where s_{x_1}, s_{x_2}, ...and s_{x_n} are the standard errors of the corresponding independent variables.

For the d_{33} measurement, the d_{33}' value is calculated from Equation 3.22 (Section 3.13), or:

$$d_{33} = \frac{A}{V} = \frac{V_{lock-in}/q}{V} \qquad (4.2)$$

where $V_{lock-in}$ is the voltage of the filtered signal d measured using the lock-in amplifier, q is the slope of the calibration curve (Figure 3.3), and V is the applied voltage. According to Equation 4.1, the standard error of the observed d_{33}' value, $s_{d_{33}}$, is given by:

$$s_{d_{33}}^2 = \left(\frac{\partial d_{33}}{\partial V_{lock-in}}\right)^2 s_{V_{lock-in}}^2 + \left(\frac{\partial d_{33}}{\partial V}\right)^2 s_V^2 + \left(\frac{\partial d_{33}}{\partial q}\right)^2 s_q^2 \qquad (4.3)$$

where $\frac{\partial d_{33}}{\partial V_{lock-in}} = \frac{1}{qV}$,

$\frac{\partial d_{33}}{\partial V} = -\frac{V_{lock-in}}{qV^2}$,

$\frac{\partial d_{33}}{\partial q} = -\frac{V_{lock-in}}{q^2V}$,

$s_{V_{lock-in}}$, s_V and s_q are the standard errors of $V_{lock-in}$, V and d, respectively.

As an example, for a PZT film of thickness 2 μm, with 10% excess lead and annealed at 650°C,

$V = 0.4$ V, $s_V = 0.01$ V;

$V_{lock-in} = 216\,\mu$V, $s_{V_{lock-in}} = 2\,\mu$V;

$q = 5.9$, $s_q = 0.5$;

the calculated d_{33}' value is 90 pm/V and the standard error is about 3.9 pm/V or 4.4 %. After considering also the random error, the experimental error for the observed d_{33}' value is about ± 7%.

For the e_{31} measurement, the $e_{31,f}$ value is calculated from Equation 3.45 (Section 3.2), or:

$$e_{31} = \frac{\ell^3 I_o}{3\pi^2 r^2 fhz_\ell (1-\upsilon_c)}\left(\ell - \frac{x_0 + x_1}{2}\right)^{-1} \qquad (4.4)$$

According to Equation 4.1, the standard error of the observed $e_{31,f}$ value, $s_{e_{31}}$, is given by:

$$s_{e_{31}}^2 = \left(\frac{\partial e_{31}}{\partial I_o}\right)^2 s_{I_o}^2 + \left(\frac{\partial e_{31}}{\partial \ell}\right)^2 s_\ell^2 + \left(\frac{\partial e_{31}}{\partial h}\right)^2 s_h^2 + \left(\frac{\partial e_{31}}{\partial z_\ell}\right)^2 s_{z_\ell}^2 + \left(\frac{\partial e_{31}}{\partial \nu_c}\right)^2 s_{\nu_c}^2$$

$$+ \left(\frac{\partial e_{31}}{\partial r}\right)^2 s_r^2 + \left(\frac{\partial e_{31}}{\partial x_o}\right)^2 s_{x_o}^2 + \left(\frac{\partial e_{31}}{\partial x_1}\right)^2 s_{x_1}^2 \qquad (4.5)$$

where $\dfrac{\partial e_{31}}{\partial I_o} = \dfrac{e_{31}}{I_o}$,

$$\frac{\partial e_{31}}{\partial \ell} = 3\frac{e_{31}}{\ell} - \frac{e_{31}}{\ell - \dfrac{x_o + x_1}{2}},$$

$$\frac{\partial e_{31}}{\partial h} = -\frac{e_{31}}{h},$$

$$\frac{\partial e_{31}}{\partial z_\ell} = -\frac{e_{31}}{z_\ell},$$

$$\frac{\partial e_{31}}{\partial \nu_c} = \frac{e_{31}}{1-\nu_c},$$

$$\frac{\partial e_{31}}{\partial r} = -2\frac{e_{31}}{r},$$

$$\frac{\partial e_{31}}{\partial x_o} = \frac{e_{31}}{2\left(\ell - \dfrac{x_o + x_1}{2}\right)},$$

$$\frac{\partial e_{31}}{\partial x_1} = \frac{\partial e_{31}}{\partial x_o},$$

s_{I_o}, s_ℓ, s_h, s_{z_ℓ}, s_{ν_c}, s_r, s_{x_o} and s_{x_1} are the standard errors of the current signal I, the length of the cantilever ℓ, the thickness of the substrate h, the deflection at the end of the cantilever z_ℓ, the Poisson's ratio ν_c, the radius of electrode r and location of two extremes of the electrode x_o and x_1, respectively.

As an example, for a PZT film of thickness 2 μm, with 10% excess lead and annealed at 650°C,

I_o = 3030 pA, s_{I_o} = 30 pA ;

ℓ = 16.5 mm, s_ℓ = 0.5 mm;

h = 0.40 mm, s_h = 0.01 mm;

z_ℓ = 13 μm, s_{z_ℓ} = 1.3 μm;

ν_c = 0.172, s_{ν_c} = 0.01;

r = 0.50 mm, s_r = 0.01 mm;

x_0 = 8.0 mm, s_{x_0} = 0.5 mm;

x_1 = 9.0mm, s_{x_1} = 0.5 mm;

the calculated e_{31} value is 8.8 C/m^2 and the standard error is about 0.65 C/m^2 or 7.3%. After considering also the random error, the experimental error for the observed e_{31} value is about ±10%.

4.2 Effects of Poling Field and Time

The influences of poling field on the observed $d_{33}^{'}$ and $e_{31,f}$ values of the PZT film are studied, and the results are shown in Figures 4.8 and 4.9. The PZT film is of thickness 2 μm, with 10% excess lead and annealed at 650°C for 1 hour. It will be shown in the following section that the optimum amount of excess lead and optimum annealing temperature for preparing PZT films with the best piezoelectric properties are 10% and

650°C, respectively. The poling field is increased in steps, with an increment of 1 MV/m. The sample is polarized under each poling field for 3 min. Electric breakdown occurs in the film when the poling field is higher than 11 MV/m (22 V). It can be seen that both the observed $d_{33}^{'}$ and $e_{31,f}$ values increase with increasing poling field, and become saturated as the poling field increases to 9 MV/m (Figures 4.8 and 4.9). This result suggests that the field required to align or re-orient a domain ("local" coercive field) is different for different domains. At a low poling field, there is only a small portion of domains aligned to the external field direction, and hence the observed $d_{33}^{'}$ and $e_{31,f}$ values are small. As the poling field increases, more domains are aligned and consequently the observed $d_{33}^{'}$ and $e_{31,f}$ values increase. However, at a poling field higher than the maximum "local" coercive field, all the domains are aligned and hence the observed $d_{33}^{'}$ and $e_{31,f}$ values become saturated.

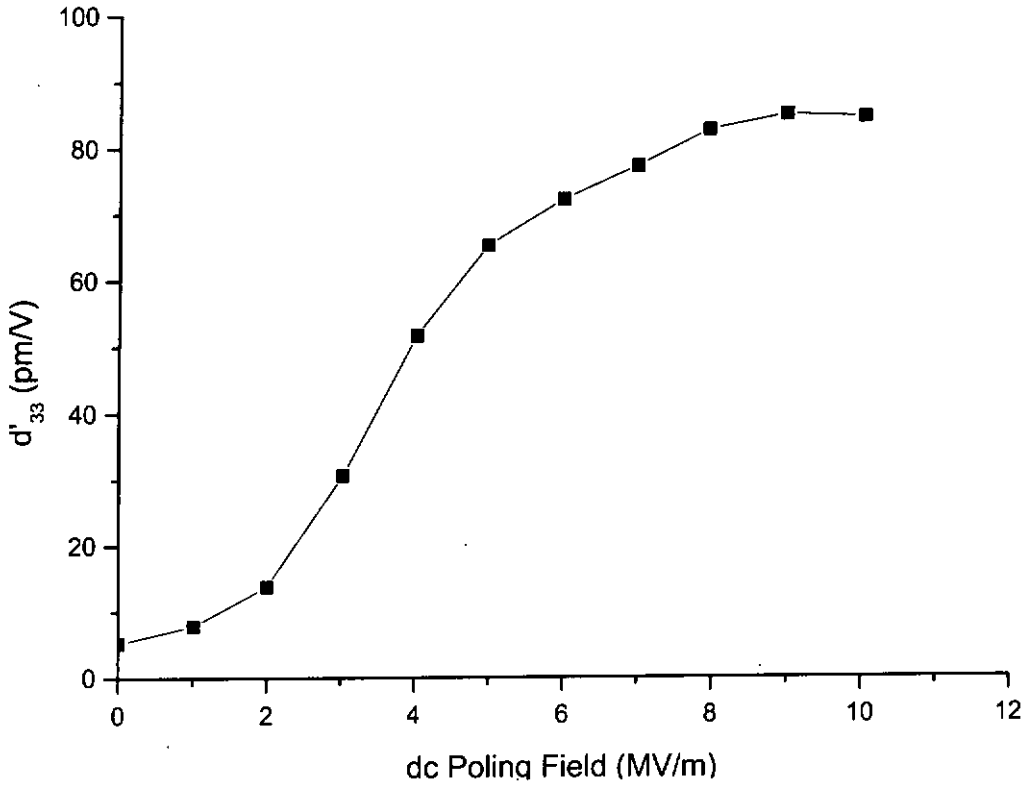

Fig. 4.8 The piezoelectric coefficient $d_{33}^{'}$ of a PZT film polarized under different poling fields. The PZT film is of thickness 2 μm, with 10% excess lead and annealed at 650°C for 1 hour.

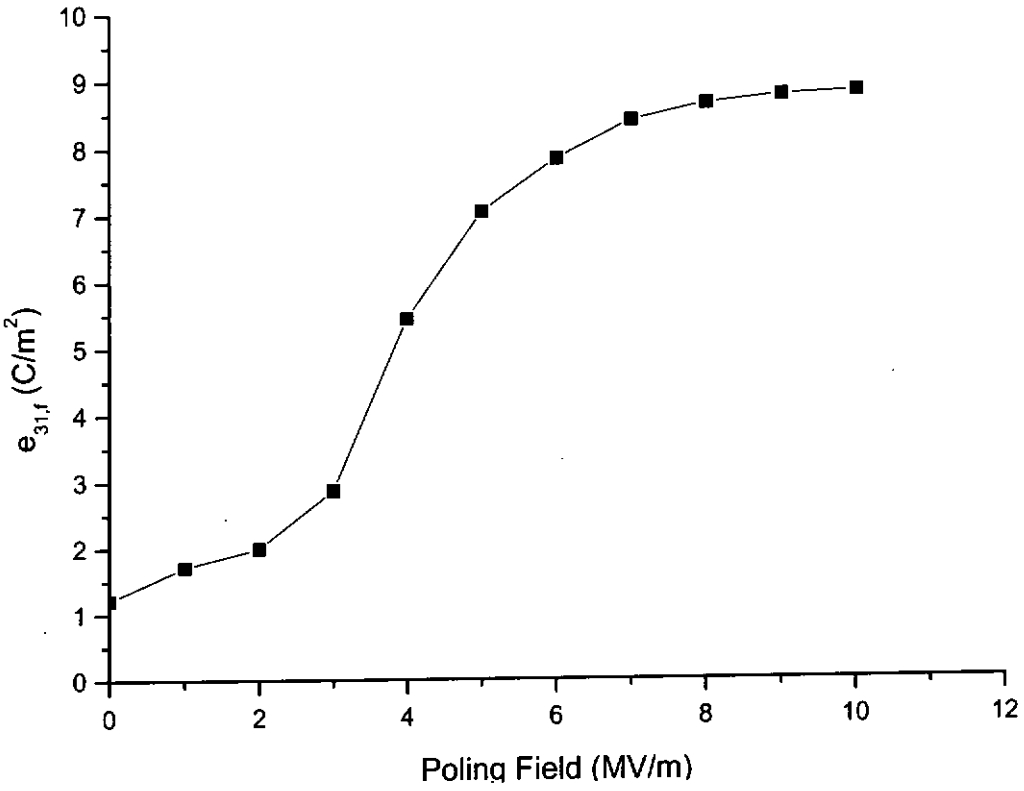

Fig. 4.9 The piezoelectric coefficient $e_{31,f}$ of a PZT film polarized under different poling fields. The PZT film is of thickness 2 μm, with 10% excess lead and annealed at 650°C for 1 hour.

Similar results are also observed for a PZT film of thickness 1 μm. Figures 4.10 and 4.11 show the observed $d_{33}^{'}$ and $e_{31,f}$ values of the PZT film as functions of poling field. However, it is noted that the observed $d_{33}^{'}$ and $e_{31,f}$ values increase slower with increasing poling field and become saturated at a higher poling field as compared to the 2 μm film. This is probably due to the dead layer at the interface between the film and the electrode [Cillessen, 1997]. The dielectric constant of the dead layer is smaller than that of the PZT film, so that there is only a small fraction of the external electric field distributed to the

PZT film. The effect of the dead layer becomes weaker as the thickness of the film increases. Therefore, a larger external electric field is required to fully polarize a thinner film. Nevertheless, when the films of thickness 1 and 2 μm are fully polarized, the resulting piezoelectricity are the same, giving almost the same (maximum) observed $d_{33}^{'}$ and $e_{31,f}$ values. Cheng *et al.* have studied the thickness dependence of piezoelectric properties for PZT thin films [Cheng *et al.*, 2001]. They showed that d_{33} of a film of thickness smaller than 1 μm is smaller than that of a film of thickness larger than 1 μm, while there is no significant change of d_{33} coefficient for thicker films. Yang *et al.* suggested that the larger the grain size, the better the ferroelectric properties can be obtained [Yang *et al.*, 2001]. The grain size is dependent not only on the processing condition (e.g. annealing temperature), but also on the thickness of film. As a result, the thicker the film, the larger the grain size, and hence the better the ferroelectric properties can be obtained. However, the grain size cannot increase infinitely [Amanuma *et al.*, 1993]. Therefore, for films of thickness larger than a certain value (e.g. 1 μm), the piezoelectric coefficient remains unchanged.

It is also seen from Figures 4.8 - 4.11 that electric breakdown occurs at a higher field in the 1 μm film. This agrees with the work of Gerson and Marshall. They showed that the breakdown field of the bulk ceramics is inversely proportion to the thickness of the sample [Gerson and Marshall, 1959]. In fact, the breakdown field also depends on a number of factors, such as composition, dopant, homogeneity, porosity and crevices of the sample.

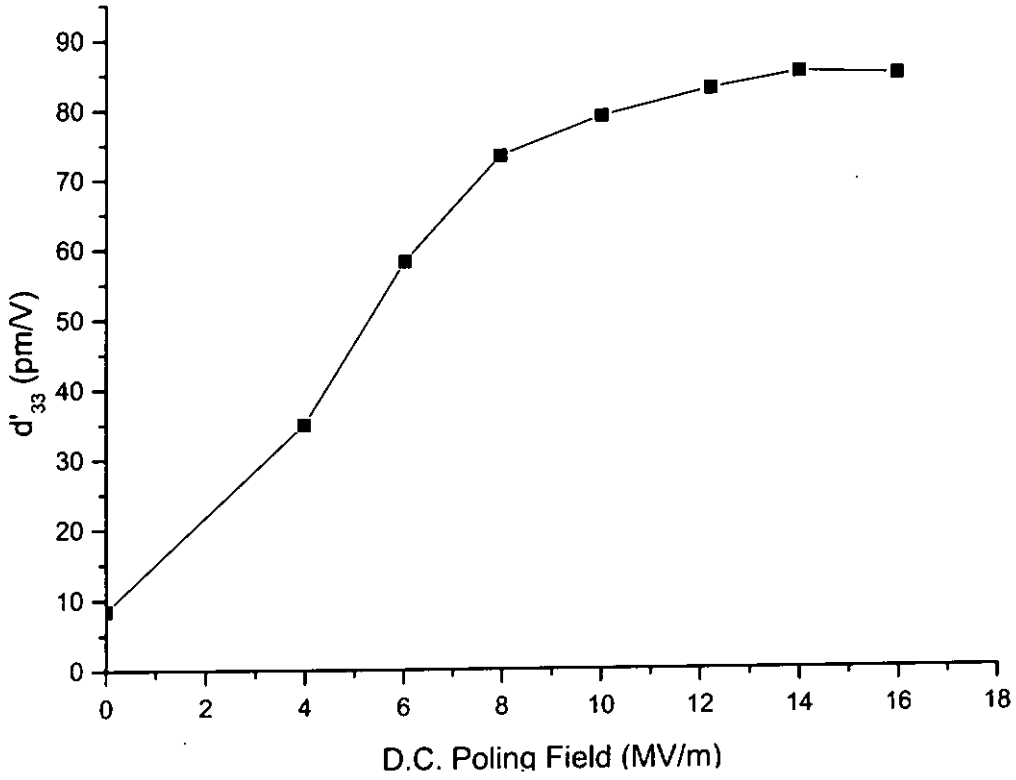

Fig. 4.10 The piezoelectric coefficient $d_{33}^{'}$ of a PZT film polarized under different poling fields. The PZT film is of thickness 1 μm, with 10% excess lead and annealed at 650°C for 1 hour.

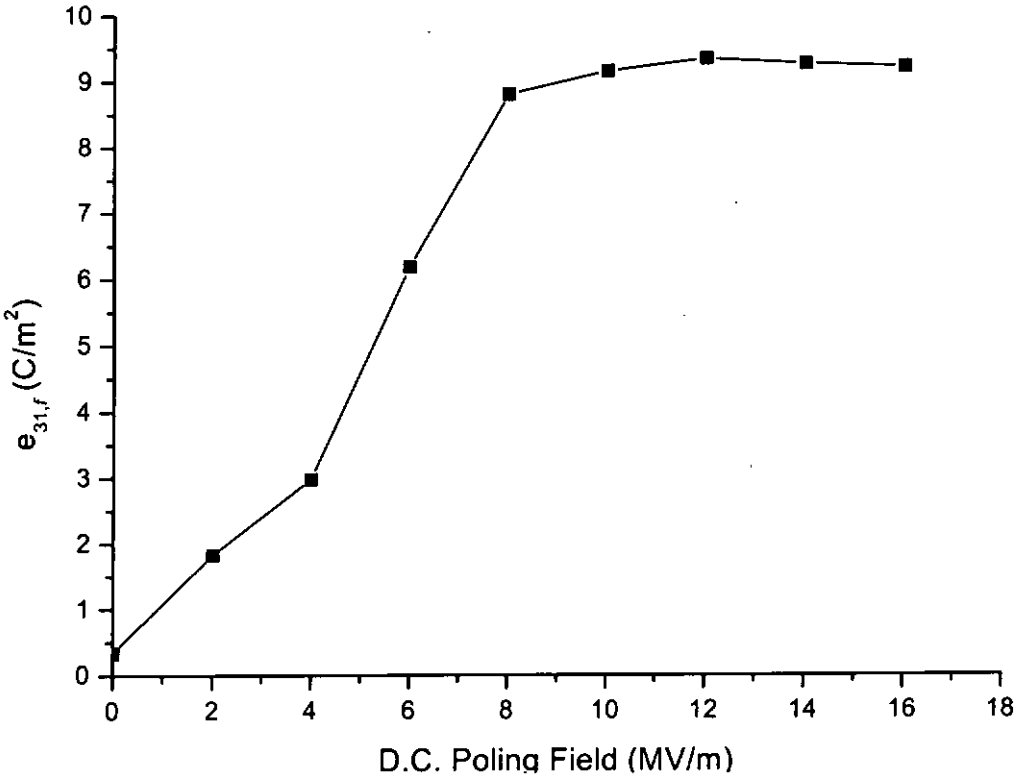

Fig. 4.11 The piezoelectric coefficient $e_{31,f}$ of a PZT film polarized under different poling fields. The PZT film is of thickness 1 μm, with 10% excess lead and annealed at 650°C for 1 hour.

Figures 4.12 and 4.13 show the variation of the observed $d_{33}^{'}$ value of a PZT film with poling time. The PZT film is of thickness 1 μm and polarized under a dc field of 6 MV/m and 16 MV/m, respectively. It can be seen that the observed $d_{33}^{'}$ values become saturated in a very short time, regardless of the poling field. This agrees with the work of Larsen *et al.* They showed that the domain switching in thin films is very fast, and can complete in hundreds of pico-second [Larsen *et al.*, 1992]. The maximum observed $d_{33}^{'}$

value of the film polarized under a field of 6 MV/m and 16 MV/m are about 50 pm/V and 80 pm/V, respectively, and which are very close to the values obtained by polarizing the film with a field increased to the same field in steps (Figure 4.10). This suggests that the poling field is the major parameter for controlling the piezoelectric property of the PZT film. The results also imply that each domain has different value of the "local" coercive field. Only the domains with the "local" coercive field smaller than the poling field can be aligned. The long poling time has no effect on the domains with the "local" coercive fields larger than the poling field.

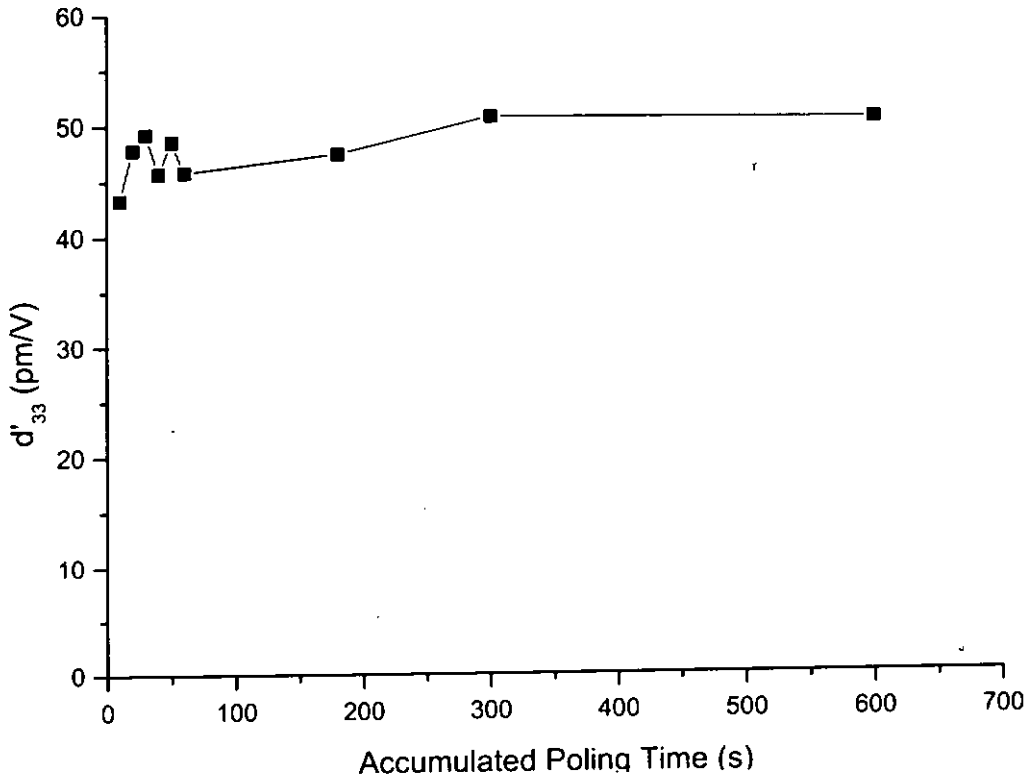

Fig. 4.12 Variation of the observed $d_{33}^{'}$ value of a PZT film with poling time. The PZT film is of thickness of 1 μm, with 10% of excess lead and annealed at 650°C for 1 hour. The dc poling filed is 6 MV/m.

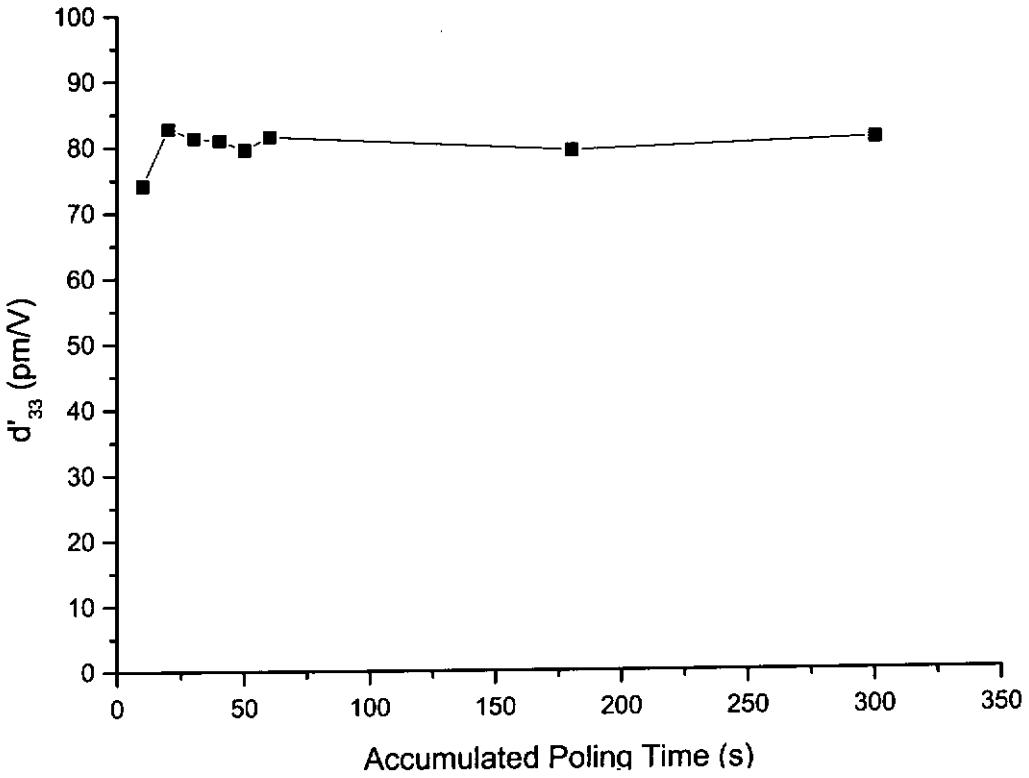

Fig. 4.13 Variation of the observed $d_{33}^{'}$ value of a PZT film with poling time. The PZT film is of thickness of 1 μm, with 10% of excess lead and annealed at 650°C for 1 hour. The dc poling filed is 16 MV/m.

4.3 Effects of Excess Lead and Annealing Temperature

The ferroelectric properties of PZT films are determined not only by the Zr/Ti compositions, but also by the number and type of defects such as lead and oxygen vacancies in the film [Aggarwal *et al.*, 1999]. Above 500°C, lead ions or PbO molecules that are not incorporated in the perovskite lattice have high diffusivity and volatility. The

vapor pressure of PbO is approximately 100 times larger than that of PZT at 600°C [Härtl *et al.*, 1969]. For compensating the loss of lead at high temperatures, an excess of lead is usually added during initial stages of the preparation of PZT.

If the stoichiometry of a PZT sample is lost, either A-site (Pb) or B-site (Zr, Ti) vacancies will form. If the lead compensation is not enough, lead vacancies $\left(V_{Pb^{2+}}\right)^{''}$ will form, resulting from the loss of Pb in the form of PbO via the Schottky reaction [Kruger, *et al.*, 1971, p.307; Aggarwal *et al.*, 1998]:

$$\left(Pb^{2+}_{Pb^{2+}}\right)^{x} + \left(O^{2-}_{O^{2-}}\right)^{x} = \left(V_{Pb^{2+}}\right)^{''} + \left(V_{O^{2-}}\right)^{\bullet\bullet} + PbO$$

A Lead vacancy will also form as a result of the oxidation of Pb^{2+} to Pb^{3+} [Aggarwal *et al.*, 1998]:

$$3\left(Pb^{2+}_{Pb^{2+}}\right)^{x} + \frac{1}{2}O_2 = \left(V_{Pb^{2+}}\right)^{''} + 2\left(Pb^{3+}_{Pb^{2+}}\right)^{\bullet} + PbO$$

On the other hand, if the lead compensation is overload, B-site (Zr, Ti) vacancies will form. In this case, Pb will sit in interstitial sites, form a second phase of PbO, or forms a perovskite structure with octahedral site vacancies. Based on computer simulations and current knowledge on defect chemistry of perovskite, interstitial defects does not likely form [Aggarwal *et al.*, 1999]. Second phase of PbO will not form at a low concentration of excess Pb (< 0.12) [Ikeda *et al.*, 1962]. Therefore, the perovskite cells with B-site vacancies $\left(V_{Ti^{4+}}\right)^{''''}$ will usually form:

$$\left(V_{Pb^{2+}}\right)'' + 3\left(V_{O^{2-}}\right)^{\bullet} + \left(V_{Ti^{4+}}\right)'''' + PbO + O_2 = \left(Pb^{2+}_{Pb^{2+}}\right)^{x} + 3\left(O^{2-}_{O^{2-}}\right)^{x} + \left(V_{Ti^{4+}}\right)'''' + 4h^{\bullet}$$

In all cases, the holes $(X)^{\bullet}$ will lower the resistivity of the films and deteriorate the ferroelectric properties when they interact with the domain walls. Therefore, it is necessary to control the stoichiometry of the PZT samples by adding a proper amount of excess lead.

Besides, the ferroelectric properties of PZT films are strongly dependent on the crystallinity. In practice, annealing PZT films at high temperature is needed for complete crystallization. It has been shown that PZT films can be annealed at temperature ranging from 600°C to 700°C, depending on the type of the precursor solution and annealing time [Fujimori *et al.*, 1999; Aggarwal *et al.*, 1999; Suzuki *et al.*, 1996]. PZT thin films can crystallize at much lower temperatures than the typical sintering temperatures for bulk ceramics. This is because the diffusion distance for providing a homogenous, stoichiometric mixture at the molecular level in thin films is much smaller [Muralt, 2000, p. 904]. Based on the above understanding, the effects of excess lead and annealing temperature on the piezoelectric properties are studied in order to determine the optimum conditions. In the present work, the amount of excess lead (added to the precursor solution) is ranged from 2% to 20%, and the annealing temperature is ranged from 600°C to 700°C. The annealing time is fixed at 1 hour.

Figure 4.14 shows the variations of the observed $d_{33}^{'}$ value with the percentage of excess lead and annealing temperature. The PZT films are fully polarized, and the maximum (or saturated) observed $d_{33}^{'}$ values are shown in the figure (Section 4.2). As shown in Figure 4.14, the optimum amount of excess lead is about 10% and the optimum annealing temperature is about 650°C. For the film with 10% excess lead, although 600°C is high enough for PZT to crystallize, the resulting grain is small, so the observed $d_{33}^{'}$ value is smaller than those of the films annealed at higher temperatures. For the films with 2% excess lead, the observed $d_{33}^{'}$ value is quite low. This may be due to the insufficient lead compensation. At high annealing temperature 700°C, the lead loss is more serious and hence the observed $d_{33}^{'}$ value decreases significantly. However, for the films with 20% excess lead, the observed $d_{33}^{'}$ value is also low. This, on the other hand, may be due to the surplus lead compensation.

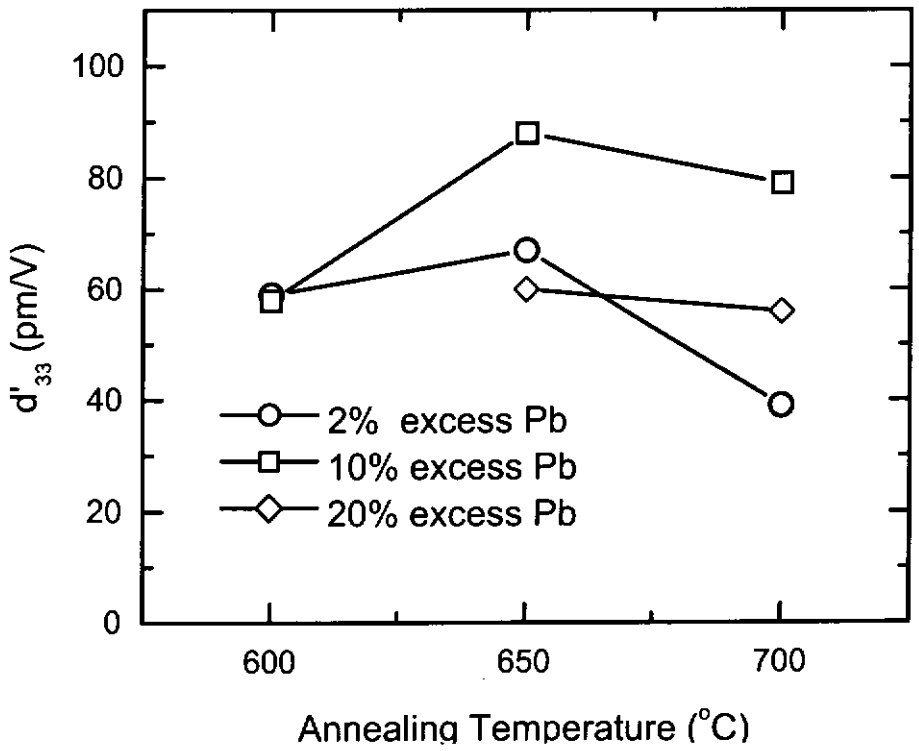

Fig. 4.14 Variations of the observed $d_{33}^{'}$ value with the percentage of excess lead and annealing temperature for PZT films. All the film samples are prepared under the same conditions, except annealing temperature, and have the same thickness (2 μm).

4.4 Depolarizing PZT Films

In applications other than nonvolatile memory, only a very small electric field is allowed to apply to a well-polarized ferroelectric sample, otherwise the sample will be depolarized. However, there is not too much information on how and to what extent the sample is depolarized. On the other hand, if one wants to completely depolarize a polarized sample, the typical method is to heat the sample up to the paraelectric phase (Section 1.2.2). However, this will certainly introduce additional thermal history to the sample, and the resulting effect is not very clear yet. Obviously, the additional heating may alter the specific defect structure and hence prevent repeated measurements of the same sample from the virgin (as-deposited) state. Therefore, it is of great interest to understand the depolarization process and hence to establish a new method to depolarize a ferroelectric sample without heating it.

Recently, Higgins *et al.* [Higgins *et al.*, 2002] have used a "shrinking hysteresis loop" method to depolarize a ferroelectric thin film and explained the phenomenon with a simple model of non-interacting micro-domains. In their model, the intrinsic hysteresis loop of each dipolar unit (a micro-domain) is a step function going from the down state to the up state at the "local" coercive field E_{lc}. Each dipolar unit has a different E_{lc} value. In their work, a ferroelectric film is first polarized under an ac field of amplitude E_1. The film is then depolarized under a series of ac fields of which the amplitude is decreased progressively from E_1 to 0 (Figure 4.15a). The observed hysteresis loop shrinks gradually at each step and "spiral" down to the origin with zero net polarization. They explained that when an ac field of amplitude E_2 ($E_2 < E_1$) is applied to the film, only the

dipolar units with $E_{lc} < E_2$ will switch to the up state, leaving a fraction of dipolar units with E_{lc} in the interval of (E_1-E_2) frozen in the down state. Similarly, a fraction of dipolar units will be frozen in the up state after the negative cycle of the ac field. Therefore, a nearly equal number of oppositely polarized domains that are frozen for the rest of the procedure are produced. This process continues at each step and the net polarization continues to decrease due to the cancellation of a progressively larger number of oppositely polarized frozen domains, ending up with a very small net polarization [Higgins *et al.*, 2002].

Microscopic spatial distributions of up and down domains are shown in the work of Higgins *et al.* for demonstrating the small net polarization. However, the macroscopic piezoelectric property, such as piezoelectric coefficients, has not been evaluated. In principle, the conventional Sawyer-Tower technique, which is used to measure the switching polarization, is incapable of providing the absolute values of the net polarization. In addition, since a series of ac fields of which the amplitude is decreased progressively to zero is used to depolarize a polarized film, it cannot provide additional information on the distributions of the "local" coercive fields in the dipolar units. For example, it cannot show whether the "local" switch-up and switch-down fields of a dipolar unit are the same. If the "local" switch-up and switch-down fields of each dipolar unit are the same and a cycle of ac field of amplitude E_2 (Figure 4.15b) is applied, the fraction of dipolar units with $E_{lc} < E_2$, which switches to the up state in the first half cycle of the ac field, will switch back to the down state in the last half cycle. This is different from the explanation of Higgins and suggests that there should be no changes in the polarization distribution and hence the film will not be depolarized.

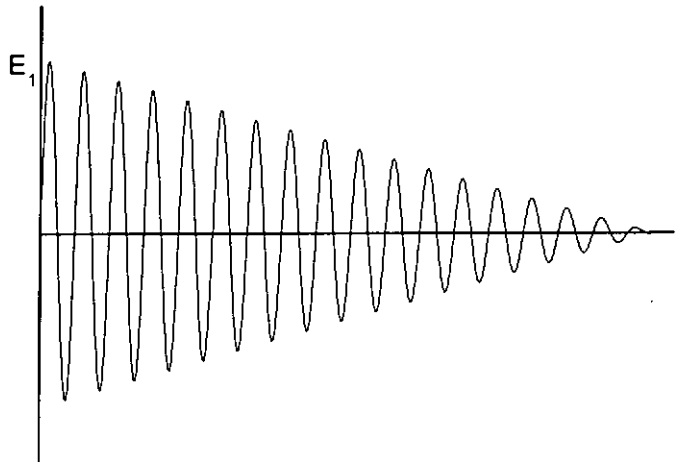

(a)

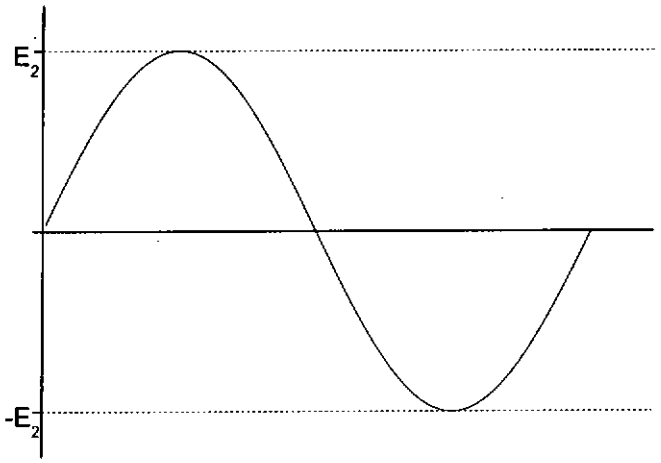

(b)

Fig. 4.15 (a) AC fields with amplitude decreased progressively from E_1 to 0. (b) A cycle of AC field of amplitude E_2.

In the present work, instead of using a large number of steps of ac field with progressively decreasing amplitude, a polarized PZT film is depolarized by the application of a few number of ac field steps of diminishing amplitude. At each step, the net polarization of the film is evaluated by the measurement of the piezoelectric

coefficients $d_{33}^{'}$ and $e_{31,f}$ using a single beam laser interferometer and the newly established cantilever technique, respectively. The depolarization phenomenon is explained with the concept of the Preisach model [Tsang *et al.*, 2001, 2002]. The model is similar to the model of Higgins, except that the interaction between the dipolar units has been taken into account. In the previous sections, it has been shown that the optimum amount of excess lead and annealing temperature for preparing PZT films with the best piezoelectric properties are 10% and 650°C, respectively; and that the piezoelectric properties of the films of thickness 1 and 2 μm are almost the same. Therefore, PZT films of thickness 1 μm, with 10% excess lead and annealed at 650°C for 1 hour are used for the depolarization study.

4.4.1 The Preisach Model

The Preisach model was first proposed by Preisach in 1935 [Preisach, 1935], which is a method of calculating the hysteresis behavior in ferromagnetic materials. Turik [1963], Hughes and Wen [1997], and Bartic *et al.* [2001] applied this model to research hysteresis behavior of ferroelectric materials. Similar to the model of Higgins, each dipolar unit (micro-domain) in the Preisach model is assumed to switch up as the external field increases to a value larger than a switch-up field, U, and switch down as the external field decreases to a value smaller than a switch-down field, V. The resulting squared hysteresis loop is called a hysteron (Figure 4.16).

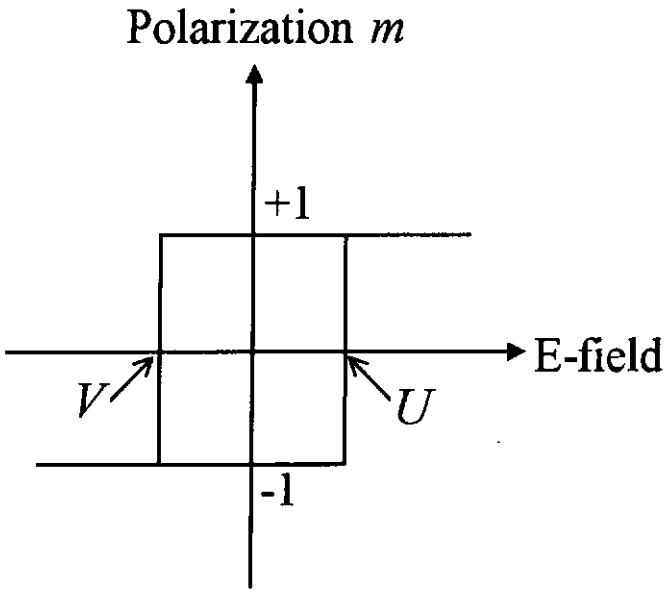

Fig. 4.16 A hysteron – a squared hysteresis loop with two normalized spontaneous polarization states.

An isolated hysteron has a symmetrical loop about the zero field axis, i.e. $U = -V$. As a result of the interaction between the dipolar units, the magnitudes of the switch-up and switch-down fields (i.e. $|U|$ and $|V|$) become different from each other. Thus, depending on the strength of the interaction field and its distribution, U and V can have any values provided that $U > V$ [Tsang *et al.*, 2001, 2002]. The distribution of U and V in the Preisach dipolar units is an intrinsic characteristic of a material and is described by the Preisach function $P(U,V)$, which is defined over the Preisach plane (i.e. the U-V plane with $U \geq V$) as shown in Figure 4.17. It should be noted that each point in the Preisach plane represents a group of dipolar units with the switching fields U and V. A dark point denotes the down state while a white point denotes the up state. Accordingly, all the dipolar units in the Preisach plane shown in Figure 4.17, which are switched by application of a sufficiently large field, are in the up state. Using the Preisach function,

the resulting (saturation) polarization P_s is then given by [Preisach, 1935],

$$P_s = \iint_{U \geq V} P(U,V)dUdV = \int_{-\infty}^{\infty} \int_{-\infty}^{U} P(U,V)dVdU \qquad (4.6)$$

In general, if an arbitrary field E is applied to the material, the polarization is given by

$$P(E) = \iint_{S^+} P(U,V)dUdV - \iint_{S^-} P(U,V)dUdV \qquad (4.7)$$

where S^+ is the region in which the dipolar units are in the up state (white region) and S^- is the region in which the dipolar units are in the down state (dark region).

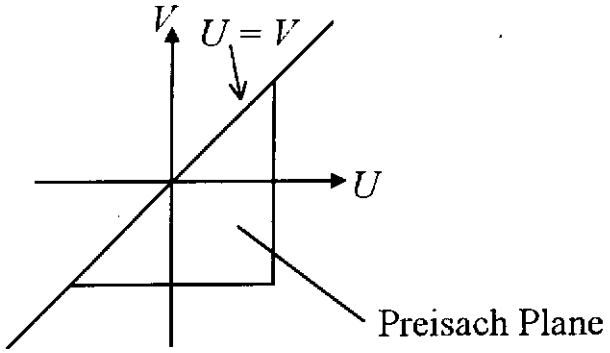

Fig. 4.17 The Preisach plane.

By assuming the Preisach function as a Gaussian-Gaussian distribution, hysteresis loops for various ferroelectric materials have been simulated and agree well with the experimental results [Tsang *et al.*, 2001, 2002]. As discussed in Section 4.2, our results reveal that each domain in a ferroelectric PZT film has different value of the "local" coercive field (the field required to switch or re-orient the domain) (Figures 4.8 - 4.13), and there should exist a distribution of the "local" coercive field in the domains. This agrees with the argument in the Preisach mode, and hence indicating that it is of great

interest to understand the depolarization mechanism in terms of the model.

4.4.2 AC Poling

Since the depolarization is achieved by application of ac field, it is of necessity to study first the piezoelectric properties of PZT films polarized by ac fields. To "ac-polarize" a PZT film, a number of ac field cycles at 1 Hz is applied to the film. The amplitude of the field is increased from 1.5 MV/m to 23 MV/m in 8 steps. A Sawyer-Tower circuit (Figure 2.7) is used to apply the field and to measure the remanent polarization P_r (Figure 2.9) at the same time. At each step, the piezoelectric coefficients $d_{33}^{'}$ and $e_{31,f}$ of the film are measured.

Figure 4.18 shows the variations of the observed P_r and $d_{33}^{'}$ values of the PZT film with ac field in the poling process, while Figure 4.19 shows the variations of the observed P_r and $e_{31,f}$ values (solid symbols). Since the PZT film was partially polarized after the dc-sputter deposition of the top electrode [Kwok, 2002], the as-deposited film has an initial $d_{33}^{'}$ and $e_{31,f}$ values of 12 pm/V and 1.4 C/m^2, respectively. The evidence can be found in the P-E Loop (Figure 2.10). The positive shift indicates that there is an internal field pointing towards the bottom electrode of the film and this field induce the initial $d_{33}^{'}$ and $e_{31,f}$ values. It can be seen that P_r, $d_{33}^{'}$ and $e_{31,f}$ increase almost linearly with increasing ac field from 0 to 13 MV/m, and remain almost unchanged at higher fields. Similar to the case for polarizing a PZT using a dc field (Figure 4.8), the results show that the dipolar

units (micro-domains) switch at different fields and the distribution of the dipolar units having the "local" coercive field in the range of 0 to 13 MV/m is quite uniform. However, it is noted that both the maximum (saturated) values of $d_{33}^{'}$ and $e_{31,f}$ are smaller than those for a "dc-polarized" film (45 pm/V vs 90 pm/V and 7.0 C/m^2 vs 8.8 C/m^2). This may be due to the short duration of the applied field as compared with the switching time of the domains. As discussed in Section 4.2, it takes about 20 seconds for the observed $d_{33}^{'}$ and $e_{31,f}$ values to become saturated. In the ac-poling process, the frequency of the ac field is 1 Hz, and 6 cycles of the ac voltage is applied to the film at each field. That means the "ac-poling time" is much less than 20 seconds. The polarization hysteresis loop and P_r of the film do not change significantly if more cycles of the ac voltage are applied. The short "ac-poling time" may also be the reason for that the PZT film can withstand higher electric field without electric breakdown (Figures 4.8 and 4.9).

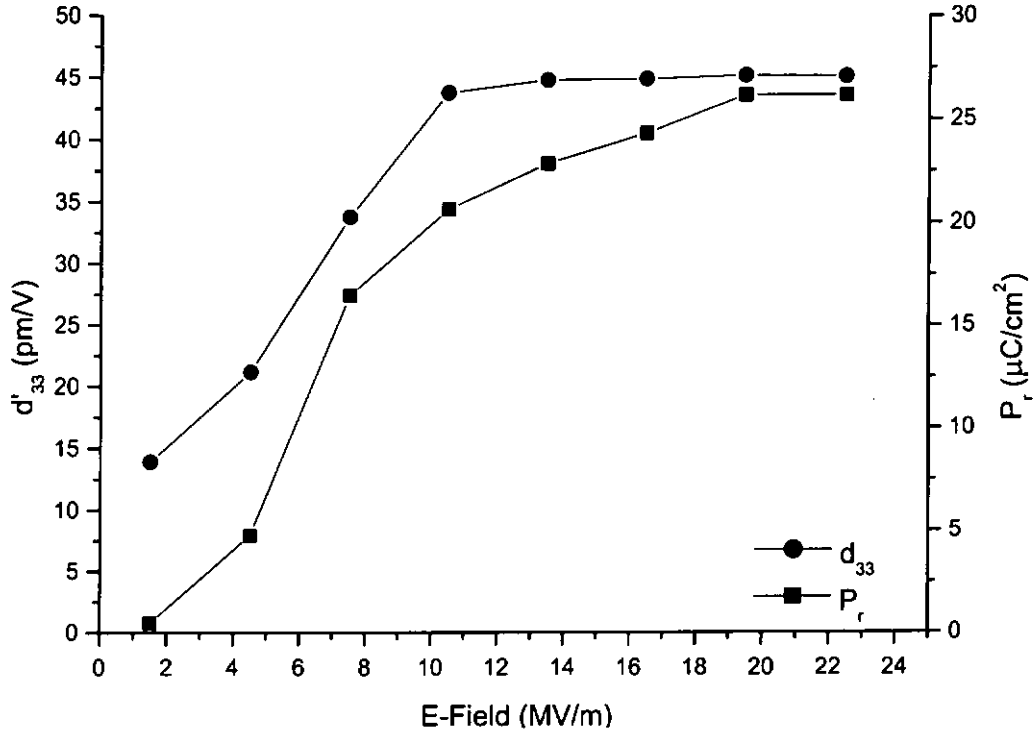

Fig. 4.18 Variations of the observed remanent polarization P_r and longitudinal piezoelectric coefficient $d_{33}^{'}$ of a PZT film with ac field in the poling process.

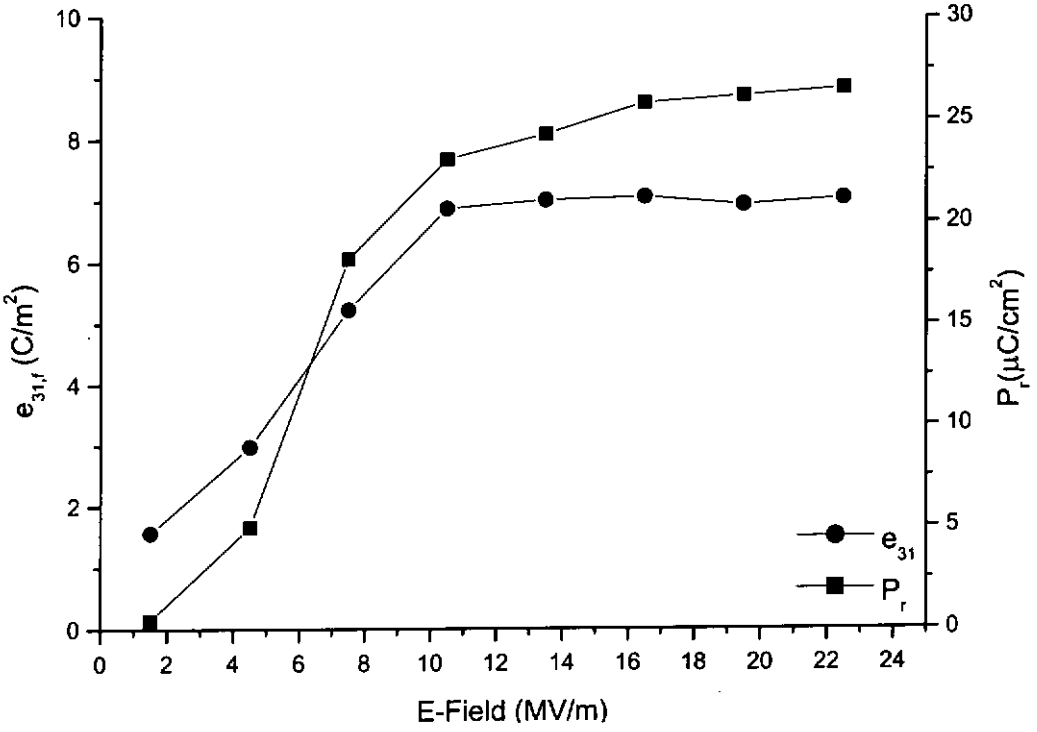

Fig. 4.19 Variations of the observed remanent polarization P_r and transverse piezoelectric coefficient $e_{31,f}$ of a PZT film with ac field in the poling process.

4.4.3 AC Depoling

The depoling procedure is basically the reversed procedure of ac poling. To "ac-depolarize" a PZT film, a number of ac field cycles at 1 Hz is applied to the polarized film. The amplitude of the field is decreased from 19.5 MV/m to 0.2 MV/m in 8 steps. Similarly, the piezoelectric coefficients $d_{33}^{'}$ and $e_{31,f}$ of the film are measured at each step.

Figure 4.20 shows the variations of the observed P_r and $d_{33}^{'}$ values of the PZT film with ac field in the depoling process, while Figure 4.21 shows the variations of the observed P_r and $e_{31,f}$ values (open symbols). It can be seen that not only P_r but also $d_{33}^{'}$ and $e_{31,f}$ decrease with decreasing ac field, and $d_{33}^{'}$ and $e_{31,f}$ have almost the same value as the as-deposited film as the field decreases to 0.2 MV/m. This clearly demonstrates that the net polarization of the film is reduced after each step, and the film is quite completely depolarized after the whole process.

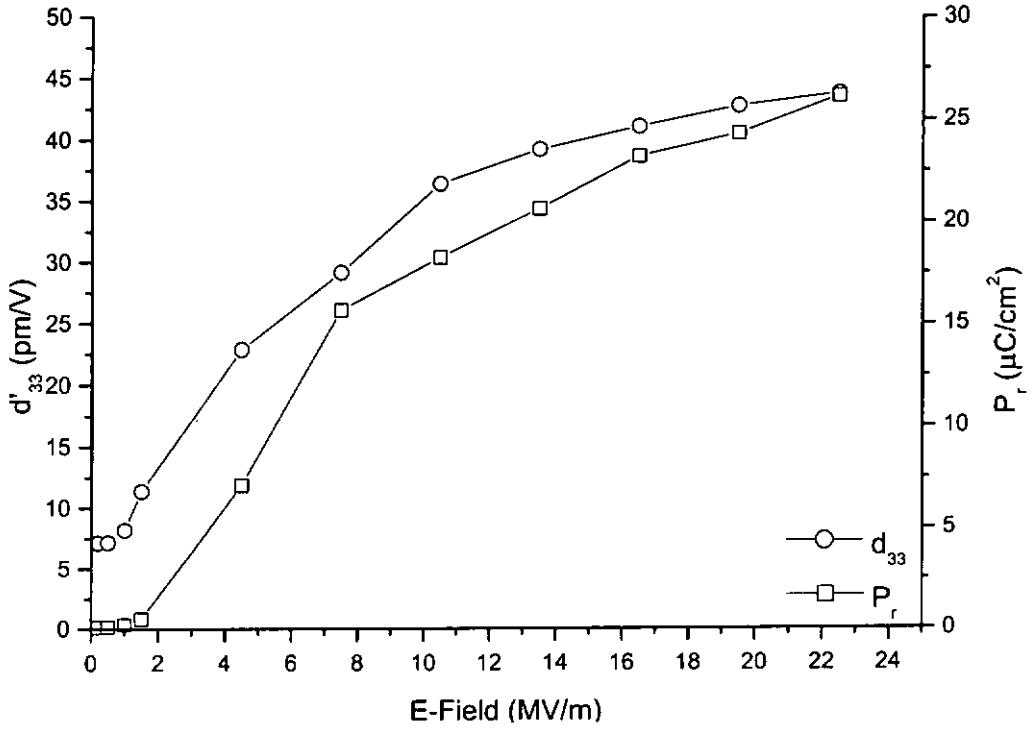

Fig. 4.20 Variations of the observed remanent polarization P_r and longitudinal piezoelectric coefficient $d_{33}^{'}$ of a PZT film with ac field in the depoling process.

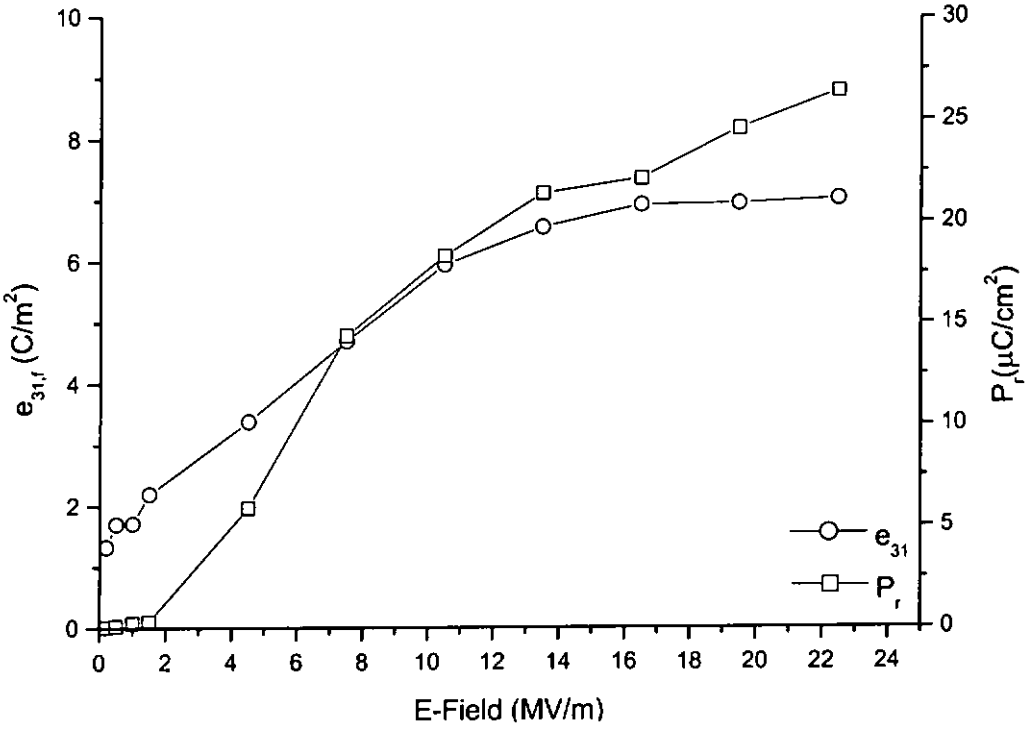

Fig. 4.21 Variations of the observed remanent polarization P_r and transverse piezoelectric coefficient $e_{31,f}$ of a PZT film with ac field in the depoling process.

It is also interesting to note that at a given field amplitude (Figures 4.20 and 4.21), the film has almost the same P_r, d_{33}^{*} and $e_{31,f}$ values in both the poling and depoling processes, implying that the processes are reversible. Figures 4.22-4.23 show the variations of the observed d_{33}^{*} and $e_{31,f}$ values with P_r, respectively, for both the poling and depoling processes. Linear relations between d_{33}^{*} and P_r, $e_{31,f}$ and P_r are observed. This indicates that the piezoelectric properties of a PZT film are linearly dependent on the net polarization of the film.

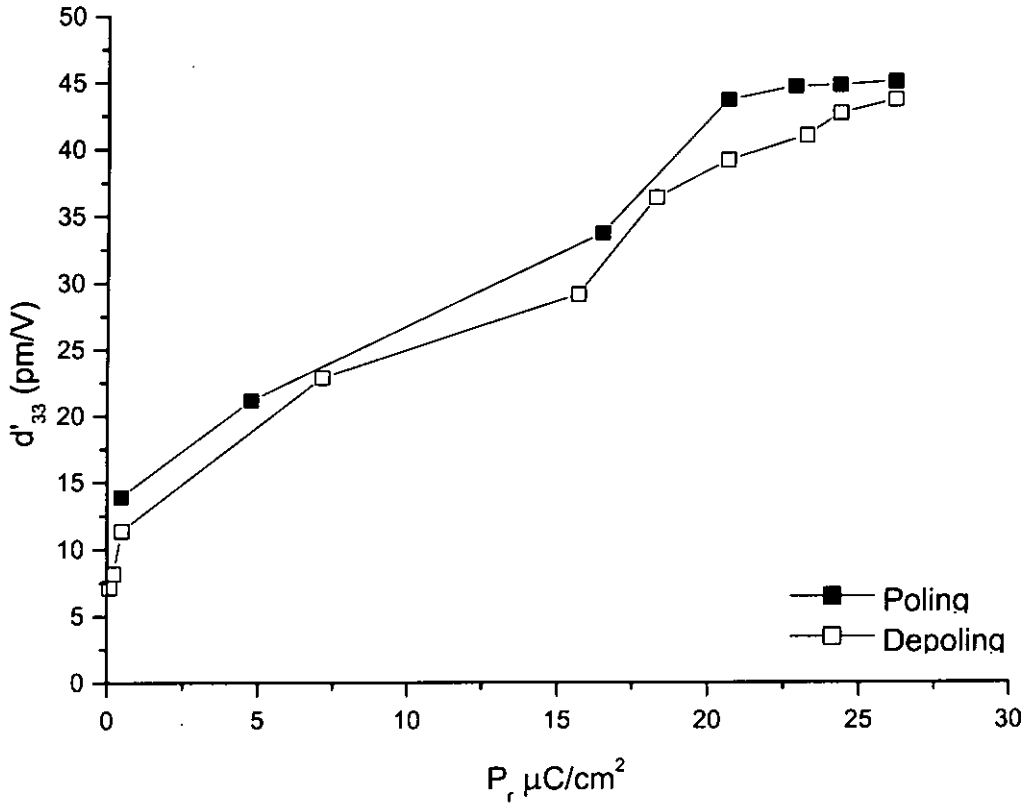

Fig. 4.22 Variations of the observed $d_{33}^{'}$ values of a PZT film with P_r for both the poling (solid symbols) and depoling (open symbols) processes.

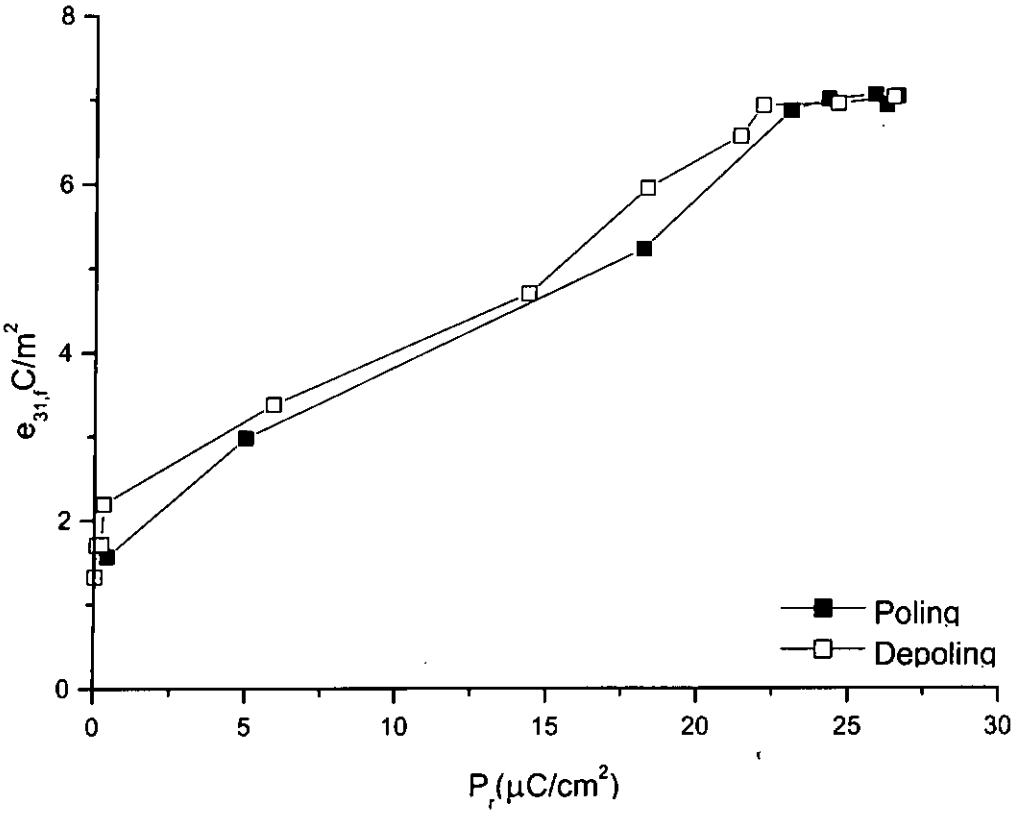

Fig. 4.23 Variations of the observed $e_{31,f}$ values of a PZT film with P_r for both the poling (solid symbols) and depoling (open symbols) processes.

To further confirm the practicability of the depolarization procedure, a "dc-polarized" PZT (with the observed $d_{33}^{'}$ value of 81 pm/V) is depolarized following the similar procedure. The observed P_r and $d_{33}^{'}$ values at each step are shown in Figure 4.24. It is clearly seen that, similar to the "ac-polarized" sample, the observed $d_{33}^{'}$ value is reduced after each step, and the film is quite completely depolarized after the whole process. It is also interesting to note that even for the "dc-polarized" film, linear relation between $d_{33}^{'}$ and P_r is also observed and which is almost the same as those for a

"ac-polarized" samples (Figure 4.22).

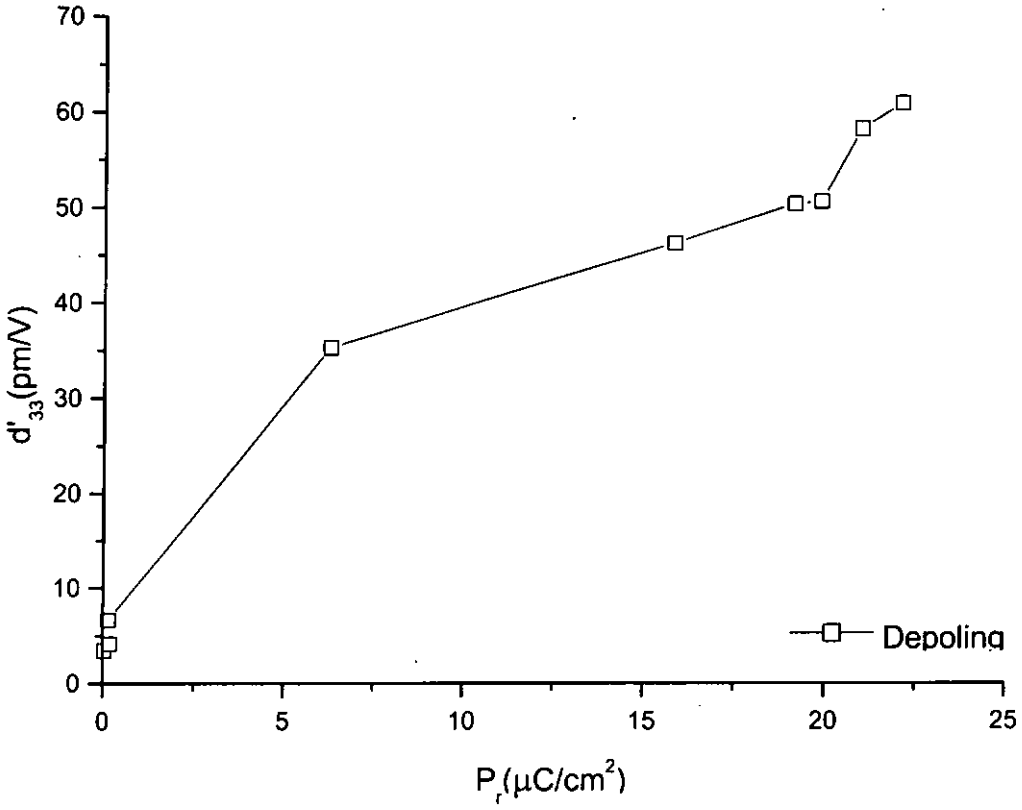

Fig. 4.24 Variations of the observed $d_{33}^{'}$ values with P_r in the depoling process for a "dc-polarized" PZT film.

4.4.4 Explanation of the Depolarization Phenomenon with the Preisach Model

As mentioned, the depoling procedure is basically the reversed procedure of ac poling. Therefore, only the depolarization phenomenon, which is of the greatest interest, is explained here; and the poling process can be easily understood following a similar

mechanism.

Consider a fully polarized PZT film by a full cycle of an ac field of sufficient large amplitude E_o ($E_o > U$ and $-E_o < V$). As the ac field increases from 0 to E_o, all the dipolar units switch up (as $E_o > U$), as depicted in Figure 4.25a. Then they all switch down (as $-E_o < V$) as the field decreases from E_o to $-E_o$ (Figure 4.25b). During the last quarter of the cycle (i.e. E increases from $-E_o$ to 0), the dipolar units with $U < 0$ switch up, resulting in the distribution of the polarization states as depicted in Figure 4.25c.

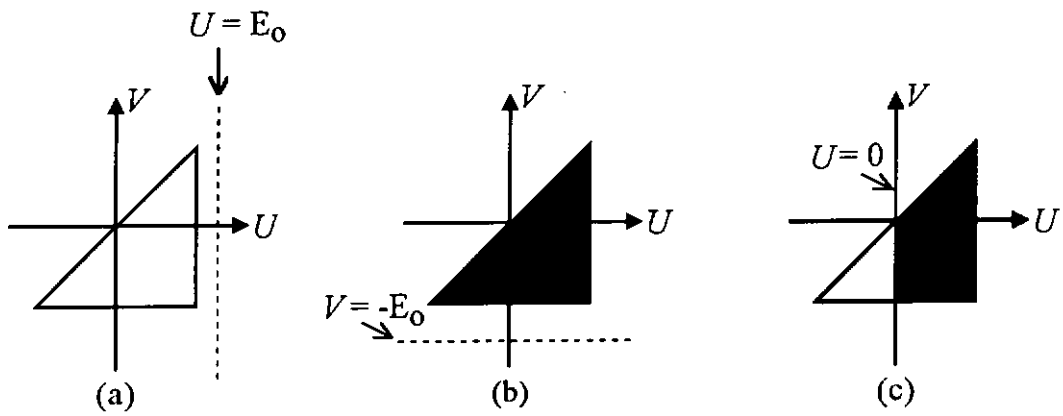

Fig. 4.25 Distributions of the polarization states (dark points: down state; white points: up state) for a ferroelectric film: (a) after the ac field increases from 0 to E_o; (b) after the ac field decreases from E_o to $-E_o$; (c) after the ac field increases from $-E_o$ to 0.

Now, we start the depoling process with the application of an ac field of amplitude E_1 ($E_1 < E_o$) to the film. As the field increases from 0 to E_1, the dipolar units with $U < E_1$ switch up (Figure 4.26a). Then the dipolar units with $V > -E_1$ switch down as the field decreases from E_1 to $-E_1$ (Figure 4.26b). At last, when the field increases from $-E_1$ to 0,

the dipolar units with U < 0 switch up (Fig. 4.26c). It can be seen that after a complete cycle of the ac field, a fraction of the dipolar units changes their state from down to up, thereby leading to a decrease in the net polarization of the film and a decrease in $d_{33}^{'}$ and $e_{31,f}$ values (Figures 4.20 and 4.21). This process continues at each step, ending with the distribution of the polarization states as depicted in Figure 4.27.

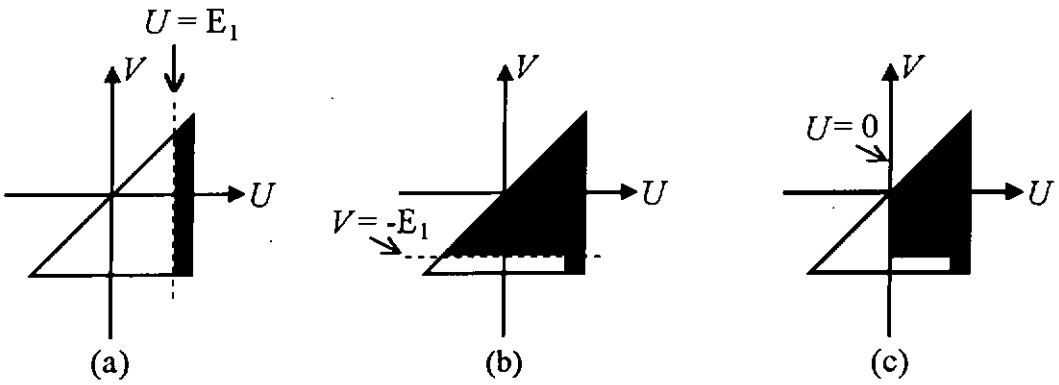

Fig. 4.26 Distributions of the polarization states (dark points: down state; white points: up state) for a ferroelectric film: (a) after the ac field increases from 0 to E_1 ($E_1 < E_o$); (b) after the ac field decreases from E_1 to $-E_1$; (c) after the ac field increases from $-E_1$ to 0.

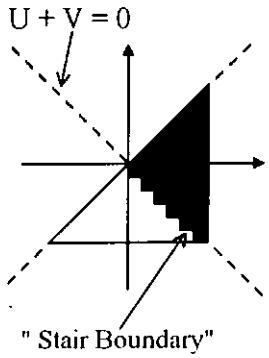

Fig. 4.27 Distribution of the polarization states (dark points: down state; white points: up state) for a ferroelectric film after the application of several cycles of ac field with diminishing amplitude.

As shown in Figure 4.27, the dipolar units have been divided into two groups of similar size by a "stair-boundary". The net polarization is clearly dependent on the number of the dipolar units with different U and V. If the distribution of U and V in the Preisach dipolar units is symmetrical about the line $U+V=0$ in the U-V plane (see Figure 4.27), the net polarization and hence the resulting $d_{33}^{'}$ and $e_{31,f}$ values will be very small, like our results shown in Figures 4.20 and 4.21. It is also clear that the net polarization is dependent on the size of the two groups. It is easily seen that if the amplitude of the ac field is decreased progressively, like the one used by Higgins, the "stair-boundary" will become a "straight-boundary" and the sizes of the two groups will become nearly the same. Nevertheless, one of the groups (down state in our case) is always slightly larger than the other group. It is because the "straight-boundary" is slightly below the line $U+V=0$ on which the dipolar units with $U=-V$ are located. This also implies that if there are only dipolar units with $U=-V$, the polarized film cannot be depolarized by the procedures described above (i.e. by application of a number of ac field steps of diminishing amplitude). In other words, our results reveal that the "local" switch-up and switch-down fields of each dipolar unit are not the same, and on the other, also support the argument in the Preisach model that there is interaction between the dipolar units making the switching fields change.

Chapter Five

Conclusions

The main objectives of the present work are to establish effective techniques for measuring the longitudinal piezoelectric coefficient d_{33} and transverse piezoelectric coefficient e_{31} of lead zirconate titanate (PZT) ceramic films, to study the effects of amount of excess lead, annealing temperature, poling field and poling time on the piezoelectric properties of PZT films, and also to investigate the depolarization phenomenon of the films and explain the phenomenon with the Preisach model.

Sol-gel derived PZT films of thickness 1 μm and 2 μm, have been prepared on Pt/Ti/SiO_2/Si substrate by the multiple-spin-coating technique. The Zr/Ti ratio of the films was 53/47. Various amounts of excess Pb were added in the PZT precursor solution, and the films were annealed at different temperatures. All the films were dense, crack-free, and well crystallized showing single perovskite phase and nontextured polycrystalline structure. With the Au/Cr top electrodes, the PZT films exhibited typical polarization hysteresis loops, showing a remanent polarization of about 20 $\mu C/cm^2$.

Experimental setups for measuring the longitudinal piezoelectric coefficient d_{33} and transverse piezoelectric coefficient e_{31} have been successfully established. The d_{33} measurement was based on the converse piezoelectric effect and the induced surface displacement was measured by using a single beam laser interferometer. The substrate bending has been effectively and completely suppressed by gluing the sample

(film/substrate) on a large and rigid platform (PCB) with mounting wax. The distribution of the surface displacement across the sample as well as the frequency dependence of the surface displacement were inspected, such that the d_{33} measurement was ensured being free from any systematic errors caused by substrate bending and mechanical resonance. The estimated experimental error for $d_{33}^{'}$ was about 7%.

The transverse piezoelectric coefficient $e_{31,f}$ was measured based on the direct piezoelectric effect using a simple experimental setup. In the measurement, a rectangular sample (film/substrate) was bent sinusoidally in such a way that a longitudinal strain was generated along the length of the sample. The induced current was measured using a lock-in amplifier. The measurement was ensured being free from any systematic errors. Linear relation between the induced current and deformation was obtained, and the resulting $e_{31,f}$ value was independent of the position of the top electrode (for the measurement). The estimated experimental error for $e_{31,f}$ was about 10%. This newly established measurement technique is preferable to the others, since it is simple, effective, and does not require any expensive equipment and special techniques for preparing the sample.

The effects of excess lead, annealing temperature, and poling time on the piezoelectric properties of PZT films have been studied. The optimum percentage of excess lead and annealing temperature were found to be 10% and 650°C, respectively. The poling time required for switching the domain was very fast, about 20 seconds, and was almost independent of the poling field. The effect of the poling field on the piezoelectric properties of PZT films has also been studied. The results revealed that

each dipolar unit (micro-domain) in a PZT film had different value of the "local" coercive field (switching field) and the distribution of the dipolar units having the different "local" coercive fields was quite uniform. As the poling field increased to certain values, all the dipolar units were switched and hence the piezoelectric coefficients became saturated. The PZT films of different thicknesses had almost the same (saturated) values of $d_{33}^{'}$ and $e_{31,f}$, but the required poling field for the 1 μm film was larger than that for the 2 μm film (16 MV/m vs 10 MV/m). It was probably due to the non-ferroelectric dead layer at the interface between the film and the electrode. A fully polarized PZT film with 10% excess lead and annealed at 650°C for 1 hour had the observed $d_{33}^{'}$ and $e_{31,f}$ values of 90 pm/V and 8.8 C/m^2, respectively.

A polarized PZT film was completely depolarized by the application of ac fields of diminishing amplitude. The amplitude of the ac fields was decreased from 19.5 MV/m to 0.2 MV/m in 8 steps. The observed $d_{33}^{'}$ and $e_{31,f}$ values of the film decreased after each step, and ended up with almost the same values as an as-deposited film. These results revealed that the magnitudes of the "local" switch-up and switch-down fields of each dipolar unit were different, otherwise the polarized PZT film could not be depolarized using the ac fields. It was believed, based on the Preisach model, that there existed interaction fields between the dipolar units which caused the switch-up and switch-down fields become different from each other. It has also been shown that the ac-poling and ac-depoling processes were reversible, such that no matter a PZT film was polarized or depolarized under the same ac field, it had the same piezoelectric properties.

References

Aggarwal, S., Madhukar, S., Nagaraj, B., Jenkins, I. G., Ramesh, R., Boyer, L., Evans, J. T., "Can Lead Nonstoichiometry Influence Ferroelectric Properties of $Pb(Zr,Ti)O_3$ Thin Films?", *Applied Physics Letters*, Vol. 75 (5), pp. 716-718 (1999).

Aggarwal, S. and Ramesh, R., "Point Defect Chemistry of Metal Oxide Heterostructures", *Annual Review of Materials Science*, Vol. 28, pp. 463-499 (1998).

Amanuma, K., Mori, T., Hase, T., Sakuma, T., Ochi, A. and Miyasaka, Y., "Ferroelectric Properties of Sol-Gel Derived $Pb(Zr, Ti)O_3$ Thin Films", *Japanese Journal of Applied Physics*, Vol. 32 (9B), pp. 4150-4153 (1993).

Auld, B.A., *Acoustic Fields and Waves in Solids* 2nd edition, Vol. 1, Krieger Publishing Co. Malabar, Florida, U. S. A., (1990).

Barrow, D. A., Petroff, T. E., Tandon, R. P. and Sayer, M., "Characterization of Thick Lead Zirconate Titanate Films Fabricated Using a New Sol Gel Based Process", *Journal of Applied Physics* Vol. 81 (2), pp. 876-881 (1997).

Bartic, A. T. Wouters, D. J., Maes, H. E., Rickes, J. T. and Waser, R. M., "Preisach Model for the Simulation of Ferroelectric Capacitors", *Journal of Applied Physics*, Vol. 89, pp. 3420-3425 (2001).

Batthias, B. T. and Hippel, A. von, "Domain Structure and Dielectric Response of Barium Titanate Single Crystals", *Physical Review*, Vol. 73, pp. 1378–1384 (1948).

Berlincourt, D. A., Cmolik, C., and Jaffe, H., *Proc. IRE*, Vol. 48, pp. 220 (1960).

Brantley, W. A., "Calculated Elastic Constants for Stress Problems Associated with Semiconductor Devices", *Journal of Applied Physics*, Vol. 44, pp. 534-535 (1973).

Chen, H. D., Udayakumar, K. R., Gaskey, C. J. and Cross, L. E., "Electrical Properties' Maxima in Thin Films of the Lead Zirconate–Lead Titanate Solid Solution System", *Applied Physics Letters*, Vol. 67, pp. 3411-3413 (1995).

Cheng. J., Meng, Z., "Thickness Dependent Microstructures and Electrical Properties of PZT Films Derived from Sol-Gel Process", *Thin Solid Films*, Vol. 385, pp. 5-10 (2001).

Chung, D. D. L., DeHaven, P. W., Arnold, H. and Ghosh, D., *X-ray Diffeaction at Elevated Temperatures*, VCH Publishers Inc., New York, (1992).

Cillessen, J. F. M., Prins, M. W. J., and Wolf, R. M., "Thickness Dependence of the Switching Voltage in All-Oxide Ferroelectric Thin-Film Capacitors Prepared by Pulsed Laser Deposition", *Journal of Applied Physics*, Vol. 81, pp. 2777-2783 (1997).

Damjanovic, D., "Ferroelectric, Dielectric and Piezoelectric Properties of Ferroelectric Thin Films and Ceramics", *Reports on Progress in Physics*, Vol. 61, pp. 1267–1324 (1998).

Dey, S. K., Budd, K. D., Payne, D. A., "Thin-film Ferroelectrics of PZT by Sol-Gel Processing", *IEEE Transactions on Ultrasonics, Ferroelectrics and Frequency Control*, Vol. 35 (1), pp. 80-81 (1988).

Dubois, M. A., Muralt, P., "Measurement of the Effective Transverse Piezoelectric Coefficient $e_{31,f}$ of AlN and $Pb(Zr_x,Ti_{1-x})O_3$ Thin Films", *Sensors and Actuators*, Vol. 77, pp. 106-112 (1999).

Fujimori, Y., Nakamura, T., Takasu, H., "Low-Temperature Crystallization of Sol-Gel Derived $Pb(Zr,Ti)O_3$ Thin Films", *Japanese Journal of Applied Physics*, Vol. 38 (9B), pp. 5346-5349 (1999).

Gerson, R. and Marshall, T. C., *Journal of Applied Physics*, Vol. 30, pp. 1650 (1959).

Härtl, K. H. and Rau, H., "PbO Vapor Pressure in the $Pb(Zr/Ti)O_3$ System", *Solid State Communications*, Vol. 7, pp. 41-45 (1969).

Hiemenz, P. C., *Principle of Colloid and Surface Chemistry*, Marcel Dekker, New York (1977).

Higgins, M. J., Krishnan, A., Treacy, M. M. J. and Bhattacharya, S., "Depoling a ferroelectric capacitor", *Applied Physics Letters*, Vol. 80, pp. 3373-3375 (2002).

Hughes, D. and Wen, J. T., "Preisach Modeling of Piezoceramic and Shape Memory Alloy Hysteresis", *Smart Materials and Structure*, Vol. 6, pp. 287-300 (1997).

Ikeda, T., *Fundamental of Piezoelectricity* (Oxford) New York (1990).

Ikeda, T., Okano, T. and Watanabe, M., *Japanese Journal of Applied Physics*, Vol. 1, pp. 218, (1962).

Jaffe, B., Cook, W. R. and Jaffe, H., *Piezoelectric Ceramics*, (New York: Academic) (1971).

Jaffe, B., Roth, R. S., and Marzullo, S., *Journal of Applied Physics*, Vol. 25, pp. 809-810 (1954).

Jaffe, B., Roth, R. S., and Marzullo, S., *Journal of Research of the National Bureau of Standards*, Vol. 55, pp. 239-254 (1955).

Karasik, A. Y., Rinkevichius, B. S. and Zubov, V. A., *Laser Interferometry Principles*, Mir Publisher, Moscow, (1994).

Kholkin, A. L., Wutchrich, Ch., Taylor, D.V., and Setter, N., "Interferometric Measurements of Electric Filed Induced Displacements in Piezoelectric Thin Films", *Review of Scientific Instruments*, Vol. 67, pp. 1935-1941 (1996).

Klaus, K. Schuegraf, *Handbook of Thin Film Deposition Processes and Techniques*, Noyes publications, U.S.A. (1988).

Kruger, F. A. and Vink, H. J., *Advances in Research and Applications*, edited by F. Seitz and T. Turnbull, Academic, New York, Vol. 3, 307 (1971).

Kwok, K. W., Wang, B., Chan, H. L. W. and Choy, C. L., "Self-Polarization in PZT Films", *Ferroelectrics*, Vol. 271, pp. 1659-1664 (2002).

Larsen, P. K., Kampschoer, G. L. M., Mark, M. B. van der and Klee, M., "Ultrafast polarization switching of lead zirconate titanate thin films", *Applications of Ferroelectrics, 1992. ISAF '92., Proceedings of the Eighth IEEE International Symposium on Applications in Ferroelectrics*, p. 217-224 (1992).

Lefki, K. and Dormans, G.J.M., "Measurement of Piezoelectric Coefficients of Ferroelectric Thin Films", *Journal of Applied Physics*, Vol. 76, pp. 1764-1767 (1994).

Li, J. F., Moses, P., Viehland, D., "Simple, High Resolution on Interferometer for the Measurement of Frequency-Dependent Complex Piezoelectric Responses in Ferroelectric Ceramics", *Review of Scientific Instruments*, Vol. 66, pp. 215-221 (1995).

Lines, M. E. and Glass, A. M., *Principles and Applications of Ferroelectrics and Related Materials*, Oxford:Clarendon, (1979).

Maiwa, H., Christman, J. A., Kim, S. H., Kim, D. J., Maria, J. P., Chen, B., Streiffer, S. K., Kingon, A. I., "Measurement of Piezoelectric Displacements of Pb(Zr,Ti)O-3 thin Films Using a Double-Beam Interferometer", *Japanese Journal of Applied Physics*, Vol. 38, pp. 5402-5405 Part 1 (1999).

Miyake, S. and Ueda, R., *Journal of Physics Society*, Vol. 1, pp. 32-33 (1946).

Muralt, P., "PZT Thin Film for Microsensors and Actuators: Where Do We Stand? ", *IEEE Transactions on Ultrasonics, Ferroelectrics and Frequency Control*, Vol. 47 (4), pp. 903-915 (2000).

Muralt, P., *Journal of Micromech. Microeng.*, Vol. 10, pp. 136-146 (2000).

Nakra, B. C. and Chaudhry, K. K., *Instrumentation Measurement and Analysis*, Tata McGraw-Hill Publishing Co. Ltd., (1985).

Nye, J. F., *Physical Properties of Crystals*, Oxford: Oxford University Press, (1985).

Pan, W. Y. and Cross, L. E., "A Sensitive Double Beam Laser Interferometer For Studying High-Frequency Piezoelectric and Electrostrictive Strains", *Review of Scientific Instruments*, Vol. 60, pp. 2701-2705 (1989).

Preisach, F., *Z. Phys*, Vol. 94, pp. 277 (1935).

Puyane, R., Gonzalezoliver, C. J. R., "Thin-Film Deposition Using Sol-Gel Technology", *Proceedings of the Society of Photo-Optical Instrumentation Engineers*, Vol. 401, pp. 307-311, (1983).

Ren, W., Zhou, H. -J., Wu, X. -Q., Zhang, L. Y. and Yao, X., "Measurement of Piezoelectric Coefficient of PZT Thin Film by Normal Load Method Using a Composite Tip", *Materials Letters*, Vol. 31, pp. 185-188 (1997).

Royer, D. and Kmetik, V., " Measurement of Piezoelectric Constants Using an Optical Heterodyne Interferometer", *Electronics Letters*, Vol. 28, pp. 1828-1830 (1992).

Sawyer, C. B. and Tower, C. H., "Rochelle Salt as a Dielectric", *Phys. Rev.*, Vol. 35, pp. 269-273 (1930).

Seyferth, D., Wiseman, G. H., *Ultrastructure Processing of Ceramics, Glasses and Composites*, edited by Hench L. L. and Ulrich D. R., Wiley, New York 265-271 (1984).

Shepard, J. F., Chu, F., Kanno, I., Trolier-McKinstry S., "Characterization and Aging Response of the d_{31} Piezoelectric Coefficient of Lead Zirconate Titanate Thin Films", *Journal of Applied Physics*, Vol. 85, pp. 6711-6716 (1999).

Sirotin, Y. I. and Shaskolskaya, M. P., *Fundamentals of Crystal Physics*, Mir Publisher, Moscow (1982).

Smith, D. L., *Thin-film Deposition (Principles & Practice)*, McGraw-Hill, New York (1995).

Suzuki, H., Othman, M. B., Murakami, K., Kaneko, S. and Hayashi, T., "Low-Temperature Processing of Ferroelectric $Pb(Zr_{0.53}/Ti_{0.47})O_3$ Thin Film from Molecular-Designed Alkoxide Precursor Solution", *Japanese Journal of Applied Physics*, Vol. 35 (9B), pp. 4896-4899 (1996).

Tanaka, K., Yoko, T., Atarashi, M., Kamiya, K., "Preparation of Fe_3O_4 Thin-Film by the Sol-Gel Method and its Magnetic Properties", *Journal of Materials Science Letters*, Vol. 8 (1), pp. 83-85 (1989).

Timoshenko, S. P., Goodier, J. N., *Theory of Elasticity*, Third edition McGraw-Hill, Kogakusha, Tokyo, (1970).

Tsang, C. H., Ploss, B. (Beatrix), Ploss, B. (Bernd) and Shin, F.G., "Simulation of the Poling of P(VDF-TrFE) with Ferroelectric Electrodes based on the Preisach Model", *Ferroelectrics*, Vol. 259, pp. 139-144 (2001).

Turik, A. V., *Soviet Physics-Solid State*, Vol.5, pp.885 (1963).

Wainer, E. and Salomon, A. N., *Electrical Report*, Vol. 8 (1942).

Wainer, E. and Salomon, A. N., *Electrical Report*, Vol. 9 (1943).

Wul, B. M. and Goldman, I. M., *Dokl. Akad. Nauk. SSSR*, Vol. 49, pp. 179-182 (1945).

Wul, B. M. and Goldman, I. M., *Compt. Rend. CAD. Sci. URSS*, Vol. 49, pp. 177-180 (1945).

Xu, F., Chu, F., and Trolier-McKinstry, S., "Longitudinal Piezoelectric Coefficient Measurement for Bulk Ceramics and Thin Films Using Pneumatic Pressure Rig", *Journal of Applied Physics*, Vol. 86, pp. 588-594 (1999).

Xu, F., Trolier-McKinstry, S., Ren, W., Xu, B., Xie, Z.-L. and Hemker, K. J., "Domain Wall Motion And its Contribution to the Dielectric and Piezoelectric Properties of Lead Zirconate Titanate Films", *Journal of Applied Physics*, Vol. 89, pp. 1336-1348 (2001).

Xu, Y., *Ferroelectric Materials and their Applications*, North-Holland, New York, (1991).

Yang, J. K., Kim, W. S., Park, H. H., "Effect of Grain Size of $Pb(Zr_{0.4},Ti_{0.6})O_3$Sol-Gel Derived Thin Films on the Ferroelectric Properties", *Applied Surface Science*, Vol. 169-170, pp. 544-548 (2001).

Zhou, Q. F., Chan, H. W. L. and Choy, C. L., "Nanocrystalline Powder and Fibres of Lead Zirconate Titanate Prepared by the Sol-Gel Process", *Journal of Materials Processing Technology*, Vol. 63, pp. 281-285 (1997).

List of Publications

Conference Paper

Tsang, R. C. W., Kwok, K. W., Chan, H. L. W. and Choy, C. L., "Piezoelectric Coefficients of PZT Thin Films", *The Proceedings for the 14th International Symposium on Integrated Ferroelectric*, Nara, Japan, 28 May – 1 June, 2002 (in press).

Journal Paper

Kwok, K. W., Tsang, C. W., Shin, F. G., Chan, H. L. W. and Choy, C. L., "Depolarizing a Ferroelectric Film by AC Fields of Diminishing Amplitude", submitted to Applied Physics A.